TOPONIUM PHYSICS AT LEP

W. Buchmüller, A. Martin

CERN, Geneva, Switzerland

J.H. Kühn

Max-Planck-Institut für Physik und Astrophysik

8000 München, Fed.Rep.Germany

F. Richard, P. Roudeau

LAL, Orsay, France

G. Coignet

LAPP, Annecy, France

L. Rolandi

University of Trieste, Italy

CONTENTS

1. **INTRODUCTION**

Since the discovery of the J/ψ [1] more than a decade ago, heavy quarkonia have played a central role in particle physics. The ψ and Y families [1, 2] of the (c$\bar{c}$) and (b$\bar{b}$) bound states have become the 'hydrogen atoms' of strong interactions: their spectroscopies provide direct evidence of the quark structure of hadrons, their decay patterns support the quark-gluon picture of perturbative quantum chromodynamics (QCD), and from some of their properties one can even obtain a quantitative determination of the QCD scale parameter Λ.

The standard gauge theory of strong and electroweak interactions predicts the existence of the t-quark, a sixth heavy quark, which should complete the third quark-lepton family. So far the search for the corresponding (t$\bar{t}$) spectroscopy at PETRA and PEP has not been successful, and the present lower bound on the mass of the (t$\bar{t}$) ground state has reached 46 GeV [3]. Present UA1 results [4] indicate a mass range from 60 GeV to 100 GeV for toponium states which will be accessible in the near future at SLC and LEP.

Toponium physics at e^+e^- colliders has been extensively discussed in the literature. Earlier work can be found in Refs. [5] to [11]; interesting recent developments have been reviewed in Refs. [12] to [14]. Contrary to the ψ and Y spectroscopies, in the (t$\bar{t}$) system the weak interactions will play a major role. Production and annihilation decays of toponium states are strongly affected by the Z boson, and furthermore the β-decay of the t-quark becomes increasingly important for t-quark masses above 30 GeV. On the experimental side, compared to quarkonium physics at SPEAR, DORIS, and CESR, the main challenge is the large spread in beam energy which decreases the height of the resonance peaks. As we will see, however, this problem is less severe than one may naïvely expect, and toponium physics at LEP energies appears to be very promising.

In this paper we study in detail to what extent toponium physics will be experimentally feasible at LEP. In Section 2 we recall the theoretical expectations for the (t$\bar{t}$) system and give a collection of formulae on which calculations in the following sections are based. Section 3 deals with the scan for the toponium ground state and the spectroscopy of (t$\bar{t}$) S-states (θ) and P-states (χ_t). In Section 4 we examine the feasibility of measuring angular and polarization asymmetries in the vicinity of (t$\bar{t}$) resonances, and in Section 5 we discuss the prospects for finding Higgs particles in toponium decays. Section 6 is devoted to supersymmetric decay modes of (t$\bar{t}$) resonances, and in Section 7 we describe how the toponium physics program could be extended if the energy spread of the machine could be decreased. The summary and conclusions of our study are presented in Section 8. In the appendix radiative corrections to some of the formulae of Section 2 are listed.

2.   QUARKONIUM PHYSICS AT LEP ENERGIES

The starting point of quantitative quarkonium spectroscopy is the choice of a quark-antiquark potential. The properties of the ψ and Y families are well described by 'QCD-like' potential models which incorporate the QCD predictions of a Coulomb singularity at short distances and linear confinement at long distances. The simplest example is the Cornell model [15] which is simply the sum of a linear term and a Coulomb term with constant α_s. More sophisticated versions include the dominant one-loop radiative corrections [16, 17] to the short-distance part which lead to a running coupling $\alpha_s(r)$. A particularly simple and successful potential of this kind was suggested by Richardson [16]:

$$V(r) = - \frac{4}{3} \frac{16\pi^2}{b_0} \int \frac{d^3q}{(2\pi)^3} e^{i\vec{q}\vec{x}} \frac{1}{q^2 \ln [1 + (q^2/\Lambda^2)]} , \qquad (2.1)$$

where

$$r = |\vec{x}| , \quad q = |\vec{q}| , \quad b_0 = 11 - \frac{2}{3} n_f ,$$

and n_f is the number of effective flavours. In order to relate the short-distance behaviour of the potential to a well-defined QCD scale parameter, e.g. $\Lambda_{\overline{MS}}$, one has to incorporate the complete next-to-leading-order QCD corrections [18]:

$$V(r) \sim - \frac{4}{3} \frac{1}{r} \frac{4\pi}{b_0 \ln (1/r^2\Lambda^2_{\overline{MS}})} \left[1 - \frac{b_1}{b_0^2} \frac{\ln [\ln (1/r^2\Lambda^2_{\overline{MS}})]}{\ln (1/r^2\Lambda^2_{\overline{MS}})} \right.$$

$$\left. + C \frac{1}{\ln (1/r^2\Lambda^2_{\overline{MS}})} + O \left[\frac{1}{\ln^2 (1/r^2\Lambda^2_{\overline{MS}})} \right] \right] , (2.2)$$

$$b_1 = 102 - \frac{38}{3} n_f , \quad C = \frac{1}{360} \left(31 - \frac{10}{3} n_f \right) + 2\gamma_E ,$$

where $\gamma_E = 0.5772...$ is Euler's constant. Contrary to the ψ and Y spectroscopies, the toponium system will probe the $(Q\bar{Q})$ potential at distances where it is expected to be described by the perturbative QCD expression (2.2).

Within the theoretical uncertainties, potential models with no resemblance to QCD, such as the logarithmic potential [19] or Martin's power potential [20],

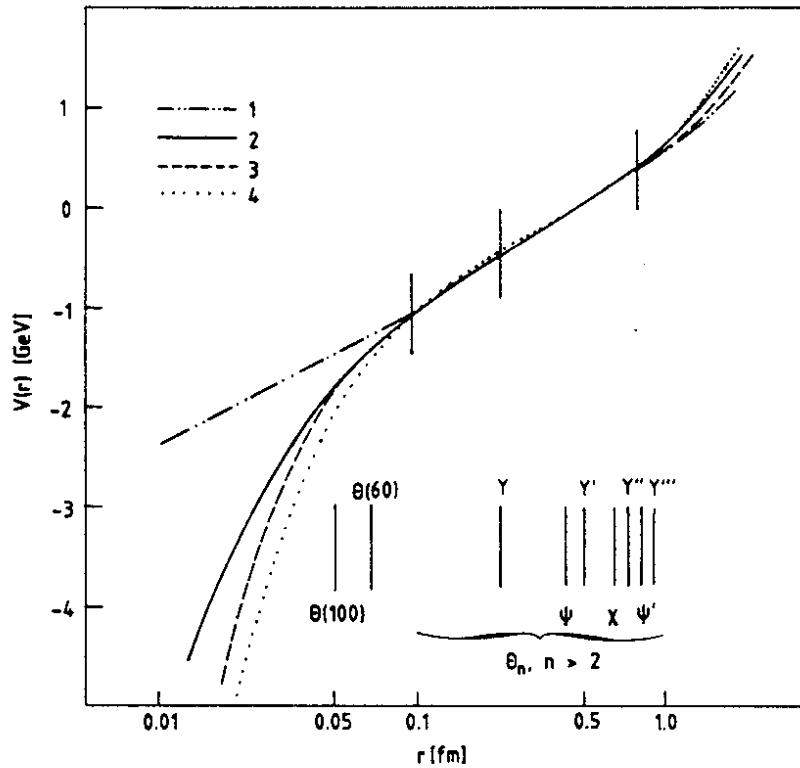$$V(r) = A + B r^{0.1} , \qquad (2.3)$$

Fig. 2.1 Comparison of the power.law potential Eq. (2.3) (1 = Ref. [20]) with different QCD-like potentials (2 = Ref. [18], 3 = Ref. [22], 4 = Ref. [15]). The error bars denote the uncertainty in absolute normalization. Some states of the ψ and Y families and the toponium ground state θ for $2m_t$ = 60 and $2m_t$ = 100 GeV are displayed at their mean square radii (cf. ref. [21]).

work equally well as QCD-like models. The reason is that in the region of r probed by the ψ and Y spectroscopies, all potentials agree numerically (see Fig. 2.1). The determination of the $(Q\bar{Q})$ potential at distances r < 0.1 fm requires heavier quarkonia; the determination of the behaviour at distances beyond 1 fm may be possible by means of resonances above threshold. Indications in favour of QCD-like models with running coupling α_s are their successful predictions of the centre-of-gravity mass of the Y 1P-states [16] and the Y leptonic width [18, 21], but unequivocal evidence of a Coulomb-like short-distance behaviour can only come from the $(t\bar{t})$ system.

The number of various toponium S-states below the threshold for pair production of T $(t\bar{q})$ mesons has been predicted as [23]

$$n_0 \approx 2(m_t/m_c)^{1/2} . \tag{2.4}$$

The position of the continuum threshold can be estimated, based on the charm and bottom spectroscopy and quark-mass differences which are independent of the normalization of the $(Q\bar{Q})$ potential [24]:

$$2m_T = m_{\psi'} + 2(m_t - m_c) + 120 \text{ MeV} , \qquad (2.5a)$$

$$2m_T = m_{\gamma'} + 2(m_t - m_b) + 225 \text{ MeV} . \qquad (2.5b)$$

From Eq. (2.4) we expect ten S-states below threshold for a t-quark with 40 GeV mass. Owing to its confining part the $(Q\bar{Q})$ potential is steeper than the Coulomb potential. Therefore the total number of narrow resonances n_t is bounded from below by the corresponding number for the Coulomb potential,

$$n_t \geq 2 n_0 + 4 \sum_{l=1}^{n_0-1} (n_0 - l) = 2n_0^2 , \qquad (2.6)$$

where energy levels with $l = 0$ ($l > 0$) contribute 2 (4) states with total angular momentum 0 and 1 (l-1, l, l, l+1).

For a 40 GeV t-quark there will be more than 200 resonances with a total width of less than 100 keV and angular momenta up to at least $l = 9$, a fantastic spectroscopy! Unfortunately, because of the large spread in beam energy, only the lowest few S-states and the 1P states appear to be experimentally accessible. This is different from the ψ and Y spectroscopies, where seven of the predicted eight narrow $(c\bar{c})$ states and nine of the predicted thirty narrow $(b\bar{b})$ states have been found up to now.

Figure 2.2 shows the size of the lowest $(t\bar{t})$ resonances as a function of $2m_t$. It is obvious that mass predictions of different potential models will
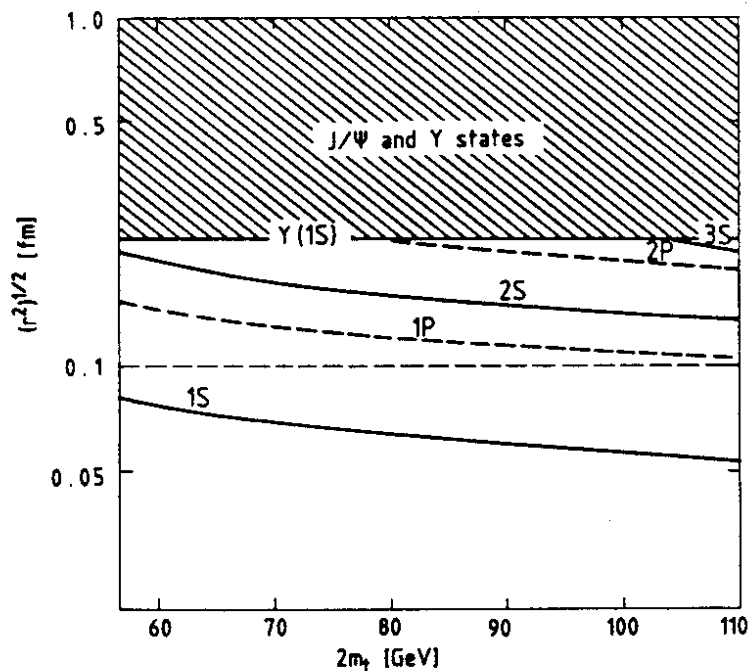

Fig. 2.2 The sizes of the lowest toponium states as functions of $2m_t$

differ only for the 1S-, 2S-, and 1P-states. Extensive tables of mass predictions can be found in Refs. [12], [17], [21], [24], and [25]. The sensitivity of the first two S-states with respect to the behaviour of the potential $V(r)$ at distances below 0.1 fm can be inferred from Figs. 2.4 and 2.5, where the 1S-2S mass difference $E_2 - E_1$ and the leptonic width of the ground state are plotted for Martin's potential and two QCD-like potentials (see Fig. 2.3) with a short-distance behaviour corresponding to the QCD scale parameters $\Lambda_{\overline{MS}} = 200$ MeV and $\Lambda_{\overline{MS}} = 500$ MeV [see Eq. (2.2)]. The differences are large. For $2m_t > 60$ GeV the predictions for $E_2 - E_1$ differ by more than 100 MeV. Even more sensitive is the leptonic width of the ground state [for the effect of the Z boson, see Eq. (2.14)],

$$\Gamma_0(\theta) = \frac{64\pi\alpha_{em}}{9m_\theta^2}\left[1 - \frac{16}{3\pi}\alpha_s(m_\theta)\right]|\psi_\theta(0)|^2 , \qquad (2.7)$$

which varies from the power potential to the QCD model with $\Lambda_{\overline{MS}} = 500$ MeV by more than a factor of 3! Therefore, we expect that the toponium system will determine the $(Q\bar{Q})$ potential down to distances of at least 0.04 fm. This should provide direct evidence of asymptotic freedom, i.e. Coulomb behaviour of the potential at short distances with a running coupling strength $\alpha_s(r)$.

Figures 2.4 and 2.5 for the 1S-2S mass difference and the 1S leptonic width suggest that the $(t\bar{t})$ system may provide an accurate determination of the QCD scale parameter $\Lambda_{\overline{MS}}$ (see Ref. [26]) via the $(Q\bar{Q})$ potential. As emphasized in Ref. [21], the quantitative dependence of these quantities on $\Lambda_{\overline{MS}}$ has to be considered with caution. It is obtained by assuming that the absolute normalization of the QCD potential at short distances is known theoretically, and that also the c-, b-, and t-quark masses--and therefore the absolute normalization of the empirical $(Q\bar{Q})$ potential--are known. Given the normalization of the short-distance QCD potential, the quark masses are very sensitive to $\Lambda_{\overline{MS}}$. It has been estimated [21], for instance, that for a 60 GeV toponium system a measurement of the three-gluon partial width with an accuracy of 20% could determine the quark masses up to ±150 MeV. We thus hope that after the discovery of toponium the combined analysis of the $(Q\bar{Q})$ potential and $(t\bar{t})$ decays will lead to a quantitative test of QCD.

The 1S, 1P, and 2S $(t\bar{t})$ states will determine the $(Q\bar{Q})$ potential at distances below 0.1 fm. Also important is the test of flavour independence of the potential, which will result from the measurement of masses and leptonic widths of higher radial excitations. The existence of a flavour-independent potential describing the $(c\bar{c})$, $(b\bar{b})$, and $(t\bar{t})$ spectroscopies would justify a *posteriori* the validity of potential models [27] for the ψ and Y systems which has been seriously questioned in connection with the QCD sum-rule approach.

Fig. 2.4 1S-2S mass difference as a function of $2m_t$ for the three potentials of Fig. 2.3. From Ref. [21].

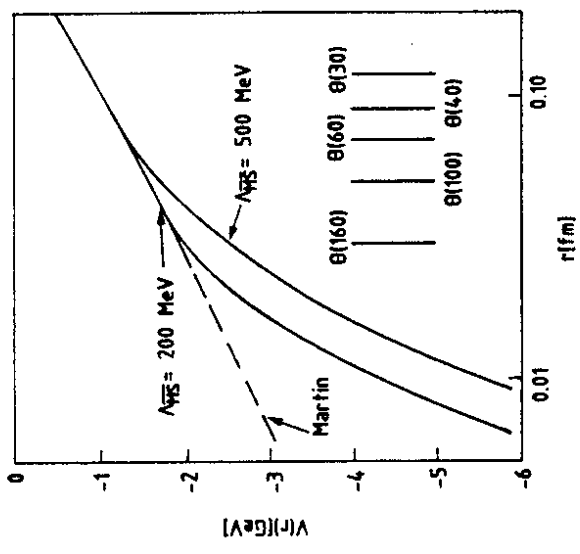Fig. 2.3 Martin's power law potential and two QCD-like potentials with $\Lambda_{\overline{MS}}$ = 200 MeV and $\Lambda_{\overline{MS}}$ = 500 MeV at short distances. The mean square radius of the toponium ground state is shown for different values of $2m_t$. From Ref. [21].
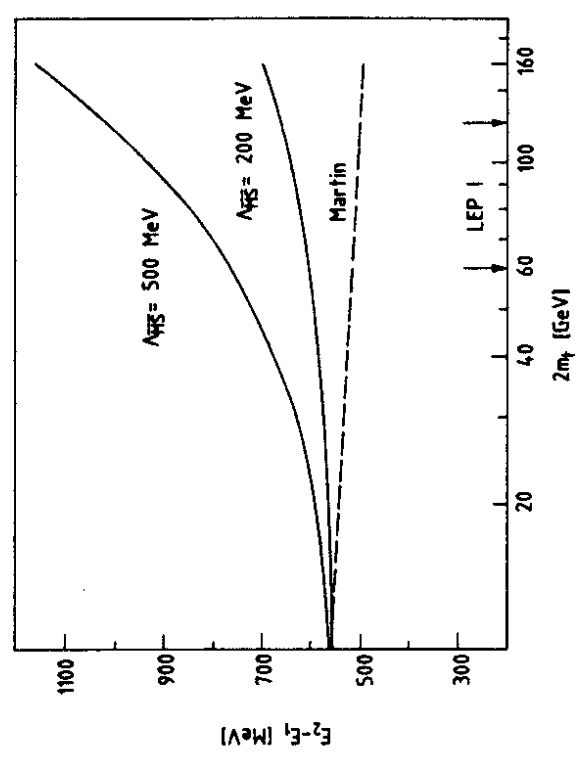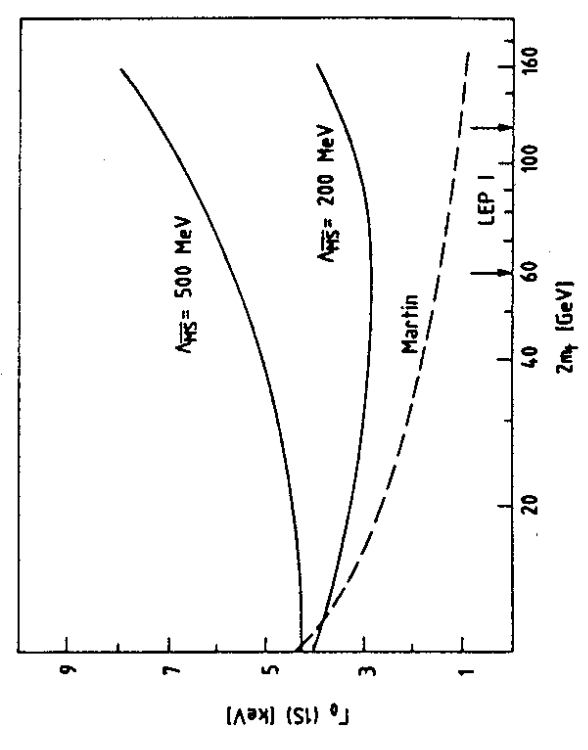
Fig. 2.5 The leptonic width of the ground state (without Z^0 contribution) as a function of $2m_t$ for the three potentials of Fig. 2.3. From Ref. [21].

The splitting of toponium energy levels caused by spin-dependent forces is a relativistic effect and is therefore expected to be small. The total fine-structure splitting (fs) of the $1P$-states,

$$\Delta m_{fs} = m(1P, J=2) - m(1P, J=0) ,$$ (2.8)

scales from the $(c\bar{c})$ to the $(b\bar{b})$ system like the square of the quark velocity in the ground state,

$$\frac{\Delta m_{fs}^b}{\Delta m_{fs}^c} \approx \frac{(v^2/c^2)_b}{(v^2/c^2)_c} ,$$ (2.9)

where $\Delta m_{fs}^c \approx 141$ MeV, $\Delta m_{fs}^b \approx 42$ MeV, $\langle v^2/c^2 \rangle_c \approx 0.23$, and $\langle v^2/c^2 \rangle_b \approx 0.08$. With $(v^2/c^2)_t|_{m_t=40 \text{ GeV}} = 0.01, \ldots, 0.02$, one obtains for the size of the toponium fine structure

$$\Delta m_{fs}^t \approx (5-10) \text{ MeV} ,$$ (2.10)

which seems to be impossible to resolve. The hyperfine splitting (hfs) of the toponium ground state is related to the leptons width,

$$\Delta m_{hfs}(\theta) = \frac{8}{9} \frac{\alpha_s}{e_t^2 \alpha_{em}^2} \Gamma_0(\theta) ,$$ (2.11)

from which one obtains

$$\Delta m_{hfs}(\theta) \approx (10-30) \text{ MeV} .$$ (2.12)

A more detailed discussion can be found in Refs. [13] and [17].

Quarkonium decays can proceed as annihilation decays (Figs. 2.6a to 2.6e), single-quark decays (Figs. 2.6f and 2.6g), and hadronic and radiative transitions (Fig. 2.7). In the following we will normalize the partial decay width to a final state F relative to the leptonic width (2.7) (without neutral-current effects), i.e. we will consider the ratios

$$r_F = \frac{\Gamma_F}{\Gamma_0} .$$ (2.13)

The QCD radiative corrections, which have been calculated for most quarkonium decays [26, 28] will be neglected because they are unknown for the important
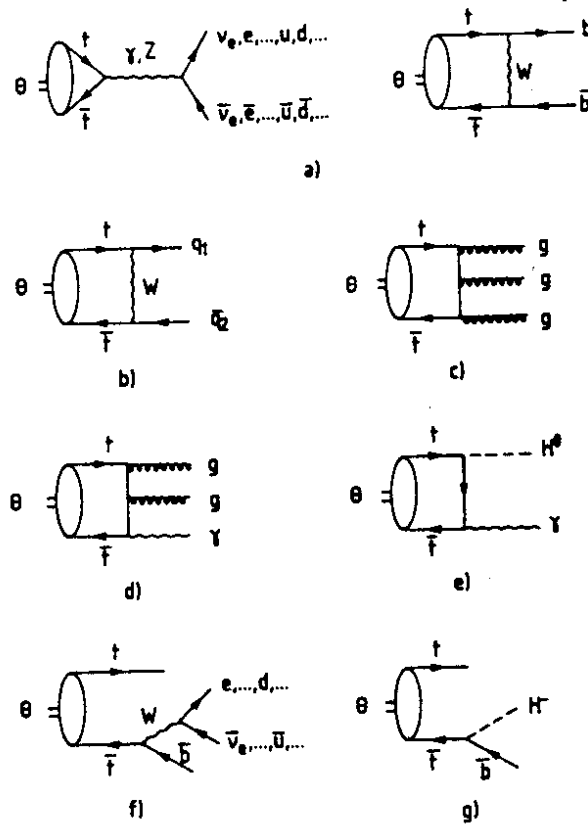
Fig. 2.6 Annihilation decay modes (a - e) and single-quark decay modes (f, g) of toponium

Fig. 2.7 a) Hadronic and b) electromagnetic transitions between ($t\bar{t}$) resonances

single-quark decay (SQD). A thorough discussion of quarkonium decays can be found in Refs. [5], [6], [8], [28], and [29].

The most frequent final state of toponium decays below 110 GeV is a fermion-antifermion pair (Fig. 2.6a). The corresponding ratio r reads,

$$r_{f\bar{f}} = \frac{c_f}{e_t^2} \left\{ e_t^2\, e_f^2 + 2\,\frac{e_t e_f v_t v_f}{y^2}\, \mathrm{Re}\, \chi_Z + \frac{v_t^2(v_f^2 + 1)}{y^4}\, |\chi_Z|^2 \right.$$

$$\left. + \delta_{f,b} \left[\frac{v_t(1 - v_f)}{3xy^2}\, \chi_W\, \mathrm{Re}\, \chi_Z - \frac{e_t e_f}{3x}\, \chi_W + \frac{1}{18x^2}\, \chi_W^2 \right] \right\} \quad . \tag{2.14}$$

where

$$x = 4 \sin^2 \theta_W , \quad y = 4 \sin \theta_W \cos \theta_W ,$$

$$\chi_Z = \frac{m^2}{m^2 - m_Z^2 + i\Gamma_Z m_Z} , \quad \chi_W = \frac{m^2}{m_W^2} \frac{m_W^2 + (m^2/8)}{m_W^2 + (m^2/4)} ,$$

$$c_f = \begin{cases} 3 , & \text{quarks} \\ 1 , & \text{leptons} \end{cases} , \quad \delta_{f,b} = \begin{cases} 1 , & f = b \\ 0 , & f \neq b \end{cases} ,$$

$$e_u = e_c = e_t = \frac{2}{3} , \quad e_d = e_s = e_b = -\frac{1}{3} ,$$

$$e_{\nu_e} = e_{\nu_\mu} = e_{\nu_\tau} = 0 , \quad e_e = e_\mu = e_\tau = -1 ,$$

$$v_u = v_c = v_t = 1 - \frac{2}{3} x , \quad v_d = v_s = v_b = -1 + \frac{1}{3} x ,$$

$$v_{\nu_e} = v_{\nu_\mu} = v_{\nu_\tau} = 1 , \quad v_e = v_\mu = v_\tau = -1 + x .$$

Except for the $b\bar{b}$ final state, we have neglected in (2.10) the charged-current contributions which are Cabibbo-suppressed. The W exchange can also give rise to flavour non-diagonal quark-antiquark decay modes (Fig. 2.6b):

$$r_{q_1 q_2} = \frac{1}{\Gamma_0(\theta)} \left[\Gamma(\theta \to \bar{q}_1 q_2) + \Gamma(\theta \to \bar{q}_2 q_1) \right]$$

$$= \frac{|V_{tq_1} V_{tq_2}|^2}{3x^2 e_t^2} \chi_W^2 . \tag{2.15}$$

These branching ratios are, however, very small because the Kobayashi-Maskawa (KM) matrix elements V_{tq_i} are known to obey the bounds [30] $V_{ts} < 0.069$, $V_{td} < 0.024$. For the familiar decay modes into three gluons, two gluons and a photon, and Higgs scalar and a photon (Figs. 26 c, d, e), one has

$$r_{ggg} = \frac{10 \ (\pi^2 - 9)}{81\pi} \frac{\alpha_s^3}{\alpha_{em}^2 e_t^2} , \tag{2.16}$$

$$r_{gg\gamma} = \frac{8(\pi^2 - 9)}{9\pi} \frac{\alpha_s^2}{\alpha_{em}} , \tag{2.17}$$

$$r_{H^0\gamma} = \frac{G_F m_\theta^2}{4\sqrt{2}\pi\alpha_{em}} \left(1 - \frac{m_{H^0}^2}{m_\theta^2}\right) = \frac{1}{2x} \frac{m_\theta^2}{m_W^2} \left(1 - \frac{m_{H^0}^2}{m_\theta^2}\right) . \tag{2.18}$$

Very important for toponium physics is the β-decay of the t-quark (SQD) (Fig. 2.6f), which is given by [$\Gamma_0(\theta) = 5$ keV]:

$$r_{SQD} = \frac{1}{\Gamma_0(\theta)} \left[\Gamma(\theta \to t\bar{b}W^-) + \Gamma(\theta \to b\bar{t}W^+)\right]$$

$$= \frac{18}{192\pi^3} \frac{G_F^2 m_t^5}{\Gamma_0(\theta)} f\left(\frac{m_t^2}{m_W^2}, \frac{m_b^2}{m_t^2}\right)$$

$$\approx 8.4 \left(\frac{m_t}{40 \text{ GeV}}\right)^5 f\left(\frac{m_t^2}{m_W^2}, \frac{m_b^2}{m_t^2}\right) , \tag{2.19}$$

with

$$f(\varrho, \mu) = 2 \int_0^{(1-\sqrt{\mu})^2} du \frac{1}{(1-u\varrho)^2} \left[(1-\mu)^2+u(1+\mu)-2u^2\right]\left[1+\mu^2+u^2-2(\mu u+\mu+u)\right]^{1/2}$$

$$= \begin{cases} (1-\mu^2)(1-8\mu+\mu^2) - 12\mu^2 \ln \mu , & \varrho = 0 \\ \frac{2}{\varrho^4} \left(6[\varrho+(1-\varrho) \ln (1-\varrho)] - 3\varrho^2 - \varrho^3 \right) , & \mu = 0 , \end{cases}$$

$$f(\varrho, \mu) = f(\varrho, 0) f(0, \mu) + O(10^{-2}) ,$$

$$0.9 < f\left(\frac{m_t^2}{m_W^2}, \frac{m_b^2}{m_t^2}\right) < 1.3 \quad \text{for} \quad 30 \text{ GeV} < m_t < 55 \text{ GeV} .$$

A second important 'single-quark decay' is the two-body decay into a b-quark and a charged Higgs scalar (Fig. 2.6g), which in some models is predicted with a mass smaller than $m_t - m_b$. The corresponding ratio $r_{bH^\pm}$ reads [$m_b \ll m_t$, $\Gamma_0(\theta) = 5$ keV]:

$$r_{bH^\pm} = \frac{1}{\Gamma_0(\theta)} \left[\Gamma(\theta \to t\bar{b}H^-) + \Gamma(\theta \to \bar{t}bH^+)\right]$$

$$\approx \frac{G_F}{4\sqrt{2}\pi} |\tilde{V}_{tb}|^2 \frac{m_t^3}{\Gamma_0(\theta)} \left(1 - \frac{m_{H^\pm}^2}{m_t^2}\right)^2$$

$$\approx 0.8 \times 10^4 |\tilde{V}_{tb}|^2 \left(\frac{m_t}{40 \text{ GeV}}\right)^3 . \tag{2.20}$$

Unless the KM-type matrix element $\tilde{V}_{tb}$ is very small, this process will clearly dominate toponium decays! For superheavy t-quarks with $m_t > m_W + m_d$, where d is a quark with electric charge -1/3, the two-body decay into d and a real W proceeds with the branching ratio [6]:

$$\Gamma_{dW} = \frac{G_F |V_{td}|^2}{4\pi\sqrt{2}\,\Gamma_0(\theta)}\, m_t^3 \left(1 + 2\,\frac{m_W^2}{m_t^2}\right) \left(1 - \frac{m_W^2}{m_t^2}\right)^2 . \tag{2.21}$$

Hadronic transitions (Fig. 2.7a), which are very important in the ψ family and also in the Υ family, are expected to be much suppressed in the $(t\bar{t})$ system. For the mass range 30 GeV $< m_t <$ 50 GeV, Kuang and Yan have estimated [31]

$$\Gamma(\theta' \to \theta\pi\pi) \approx 0.5 \text{ keV} . \tag{2.22}$$

Partial widths for electromagnetic dipole transitions (Fig. 2.7b) between S- and P-states are given by

$$\Gamma_{if} = \frac{4}{3}\, e_t^2\, \alpha_{em}\, k^3\, (2J_f + 1) \int_0^\infty dr\, R_i(r)\, R_f(r) , \tag{2.23}$$

where k, J_f, and R_{if} are the photon momentum, the total angular momentum of the final state, and the radial wave functions of the initial and final states, respectively. Rates for the toponium system have been calculated in Ref. [25].

The most important ingredients in a calculation of decay widths of toponium states are the wave functions at the origin or, equivalently, the leptonic widths Γ_0. According to Fig. 2.5, a reasonable estimate for the ground state is

$$\Gamma_0(\theta) = 5 \text{ keV} . \tag{2.24}$$

Furthermore, we choose as input

$$\Gamma_0(\theta') = \frac{1}{3}\, \Gamma_0(\theta) , \qquad \Gamma(\theta' \to \gamma\chi_t) = 1.2 \times \left(\frac{40 \text{ GeV}}{m_t}\right)^{1.25} \text{ keV} ,$$

$$m_W = 83.2 \text{ GeV} , \qquad m_Z = 94.0 \text{ GeV} ,$$

$$\Gamma_Z = 2.5 \text{ GeV} , \qquad \sin^2\theta_W = 0.217 ; \tag{2.25}$$

$$\alpha_s(m) = \frac{12\pi}{23 \ln\left(\frac{m}{100 \text{ MeV}}\right)^2} \qquad (n_f = 5) .$$

We emphasize that the input parameters (2.24) and (2.25) represent only an 'educated guess' based on QCD-like potential models. The leptonic widths could be larger or smaller by a factor of 2, and the dipole transition rate is even more model-dependent (see Ref. [25]).

From Eqs. (2.13) to (2.25) we can calculate the various toponium decay widths. Figure 2.8 shows the total and leptonic widths for the energy range of LEP I, i.e. 60 GeV < $\sqrt{s}$ < 110 GeV, and in Fig. 2.9 the partial widths $\Gamma_{f\bar{f}}$, Γ_{3g}, and Γ_{SQD} are compared. The striking feature, which distinguishes toponium physics from ψ and Υ physics, is the dominance of the weak interactions over electromagnetic and strong interactions:

$$BR_{weak} (W^*, Z^*) > BR_{em} (\gamma^*) > BR_{strong} (ggg) . \qquad (2.26)$$

Branching ratios into various final states are plotted in Figs. 2.10 and 2.11 for the 1S- and 2S-state as functions of $2m_t$. Owing to the interplay between the single-quark decays and the annihilation decays, which are strongly affected by the Z boson, the branching ratios vary drastically with m_t and lead to decay patterns which are qualitatively different for $2m_t$ = 70, 80, 90, and 100 GeV! In the vicinity of the Z pole, branching ratios into fermion-antifermion final states dominate. The branching ratio into neutrino pairs is remarkably large. It reaches 10% at $m_\theta \approx$ 80 GeV, which, however, is not sufficient to allow for a neutrino counting which could compete with the Z^0 width determination [25]. From Fig. 2.11 we also conclude that the search for P-states in radiative θ' decays appears to be feasible only for toponium masses below 90 GeV.

A special region for toponium physics is the mass range

$$m_Z - 2\Gamma_Z < m_\theta < m_Z + 2\Gamma_Z , \qquad (2.27)$$

where the toponium-Z interference has to be taken into account [32]. One of the most striking features of this interference is that in the case of degenerate masses, $m_\theta = m_Z$, toponium manifests itself as a *dip* in R rather than an enhancement of the Z peak, a phenomenon first observed by Kühn and Zerwas [33].

In order to understand this, let us consider the contribution of toponium to the $e^+e^- \to \mu^+\mu^-$ cross-section. In the case $m_\theta \ll m_Z$, one has (see Fig. 2.12a) for the amplitude at $W = m_\theta$:

$$A(m_\theta) \sim \frac{1}{m_\theta^2} + \frac{1}{m_\theta^2} \frac{g_{\theta\gamma}^2}{im_\theta\Gamma_\theta} \frac{1}{m_\theta^2} \equiv A_{B,\gamma} - i A_\theta , \qquad (2.28)$$

which implies that the θ term enhances the photon background term:

$$|A|^2 \sim A_{B,\gamma}^2 + A_\theta^2 . \qquad (2.29)$$

Fig. 2.9 Partial widths for the total fermion-antifermion, three-gluon, and single-quark decay modes of the toponium ground state as functions of $2m_t$
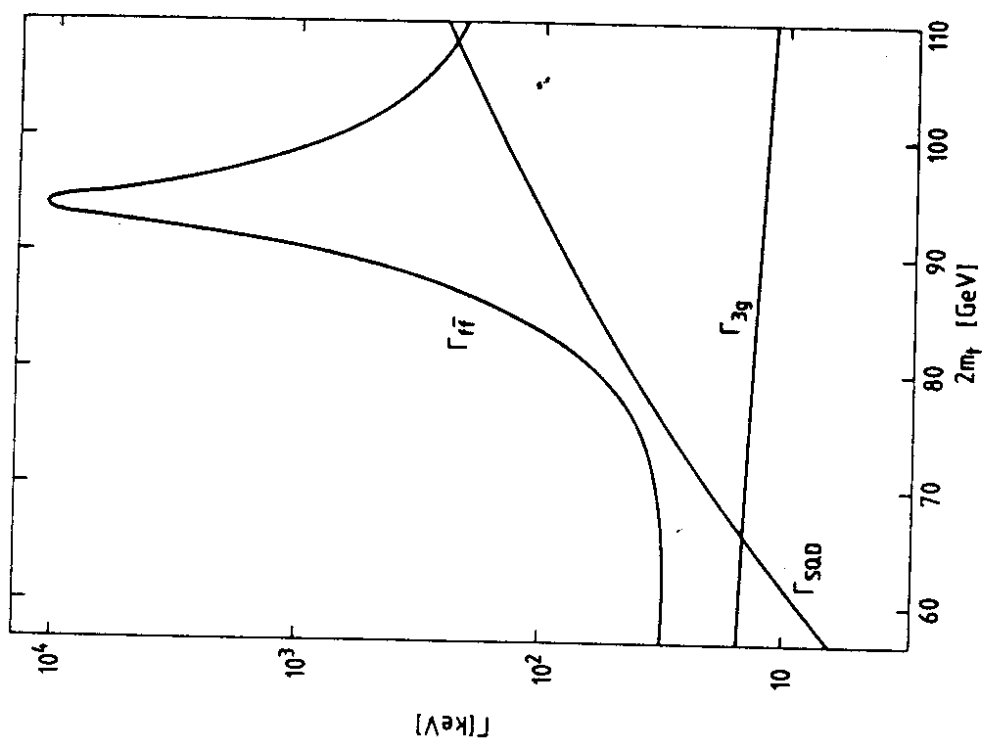
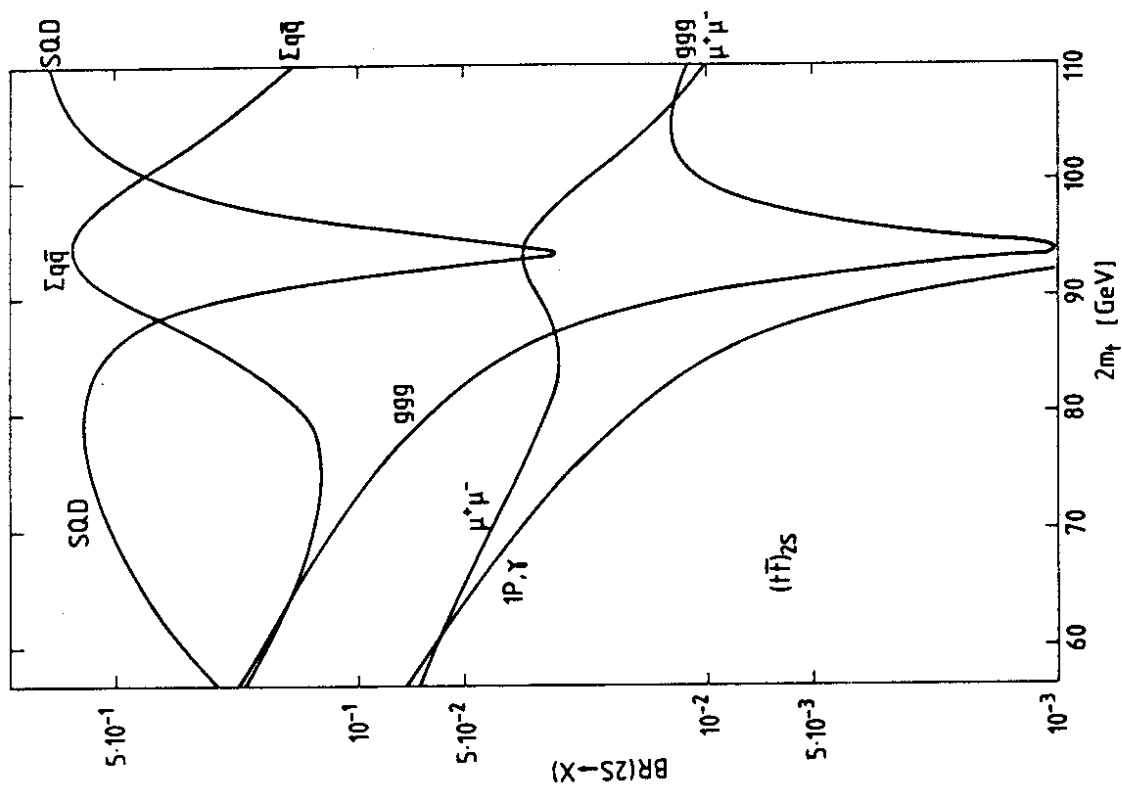Fig. 2.8 Total width and leptonic width of the toponium ground state as functions of $2m_t$

Fig. 2.11 Branching ratios for $\theta = (t\bar{t})_{2S}$ decays as functions of $2m_t$
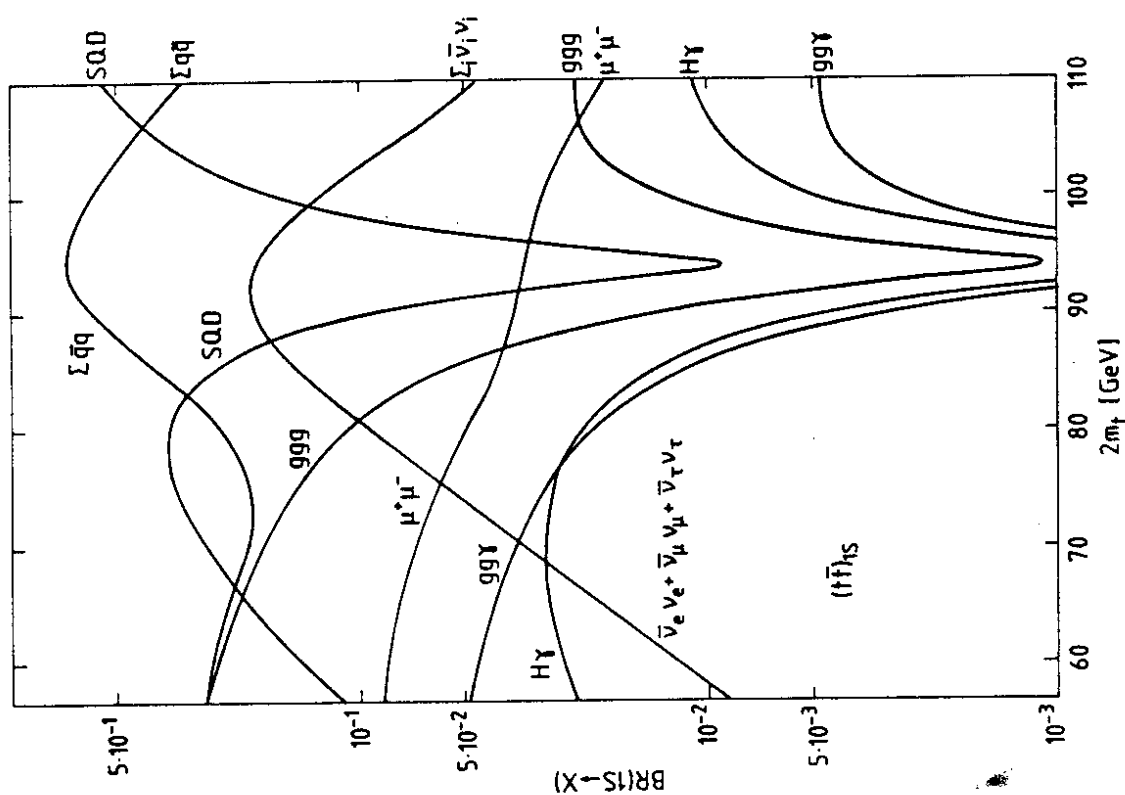

Fig. 2.10 Branching ratios for $\theta = (t\bar{t})_{1S}$ decays as functions of $2m_t$

Fig. 2.12 a) γ-θ interference and b) Z-θ interference in the process $e^+e^- \to \mu^+\mu^-$.

On the other hand, for $m_\theta = m_Z$ (see Fig. 2.12b) one obtains

$$A(m_\theta) \sim \frac{1}{im_Z\Gamma_Z} + \frac{1}{im_Z\Gamma_Z}\,\frac{g^2_{\theta Z}}{im_\theta\Gamma_\theta}\,\frac{1}{im_Z\Gamma_Z} \equiv -i\,A_{B,Z} + i\,A_\theta \; . \qquad (2.30)$$

The interference with the imaginary Z background term produces a dip

$$|A|^2 \sim (A_{B,Z} - A_\theta)^2 = 0 \; , \qquad (2.31)$$

where the vanishing of the cross-section follows from

$$\Gamma_\theta = \frac{g^2_{\theta Z}}{m_Z^2\Gamma_Z^2}\,\Gamma_Z \; . \qquad (2.32)$$

If the energy resolution of the machine is larger than the width of the toponium resonance, the effect is weakened. For $\delta W = 50$ MeV, for instance, the cross-section at $W = m_Z$ is decreased by about 10% (see Fig. 2.13). The complete pattern [24, 33-36] for a toponium system inside the Z^0 peak is shown in Figs. 2.14 and 2.15 for $\delta W = 0$ and $\delta W = 48$ MeV, respectively.

The amplitude for the process $f_i\bar{f}_i \to f_j\bar{f}_j$, where f_i represents leptons or quarks, can be obtained directly from S-matrix theory by imposing analyticity, unitarity, and certain smoothness assumptions. For a set of N toponium resonances with $\Gamma_m \ll m_m - m_n < \Gamma_Z$, m, $n = 1, \ldots, N$, one finds for the T-matrix [36],

$$T_{ij}(W) = \alpha_i\alpha_j t(W) \; , \qquad (2.33)$$

with

$$t(W) = \frac{1}{2i}\left[\;\prod_{m=1}^{N}\;(\frac{W - m_m - i\Gamma_m/2}{W - m_m + i\Gamma_m/2})\,(\frac{W - m_Z - i\Gamma_Z/2}{W - m_Z + i\Gamma_Z/2}) - 1\right] \; ,$$

$$\sum_i |\alpha_i|^2 = 1 \; ,$$

from which one can easily understand the structure of Figs. 2.14 and 2.15.
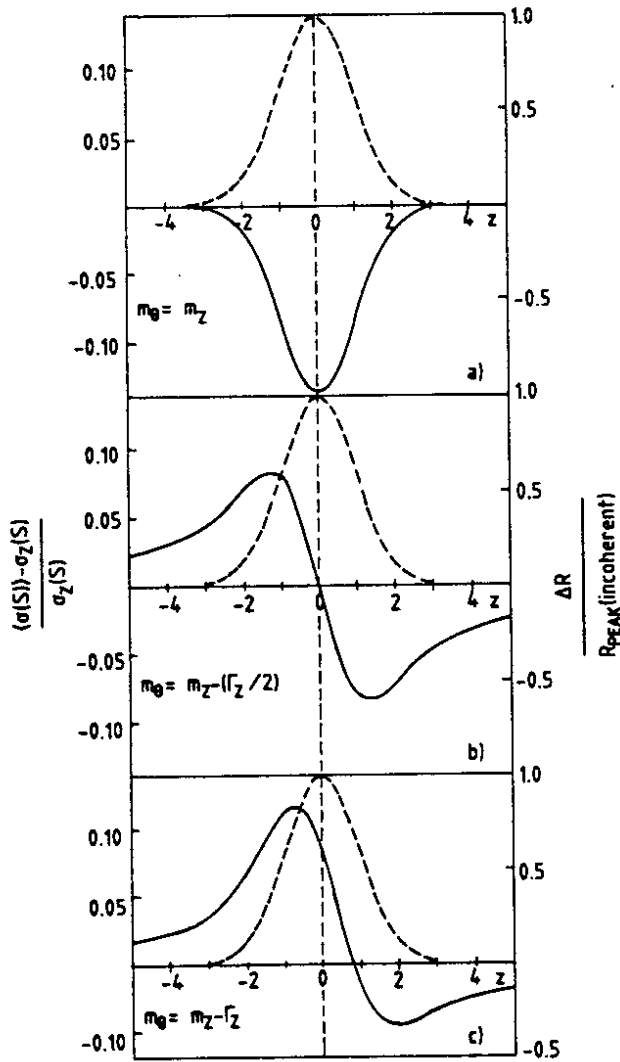
Fig. 2.13 Energy dependence of the
resonance excitation cross-section
for a toponium mass a) $m_\theta = m_Z$,
b) $m_\theta = m_Z - \Gamma_Z/2$, and c) $m_\theta \cong m_Z - \Gamma_Z$.
The dashed line shows the cross-section
without interference terms taken into
account; $z_\theta = (W-m_\theta)/\delta W$, $\delta W = 50$ MeV.
From Ref. [33].
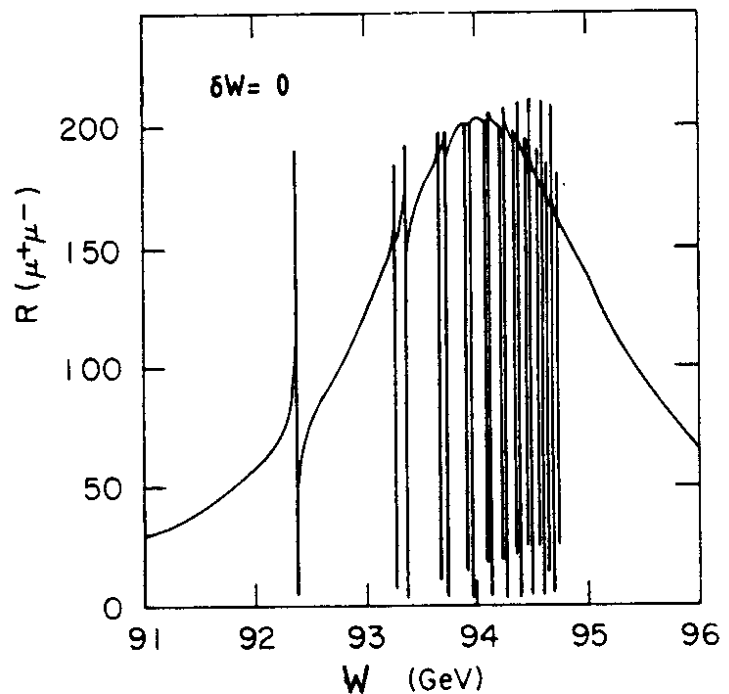
Fig. 2.14 $R(\mu^+\mu^-)$ for a t-quark
mass of 47 GeV without average
over the beam profile. From
Ref. [24].
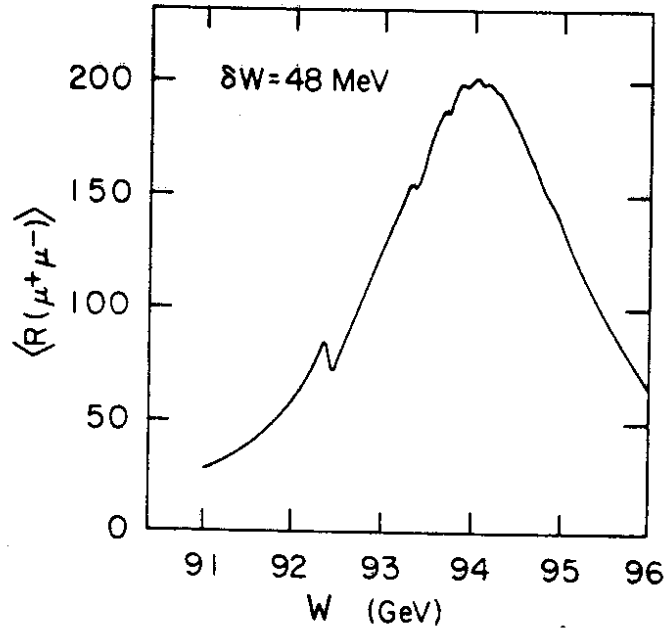
Fig. 2.15 $R(\mu^+\mu^-)$ for a t-quark mass of 47 GeV averaged over the beam profile. From Ref. [24].

A toponium system with $m_Z - 2\Gamma_Z < m_\theta < m_Z + 2\Gamma_Z$ would lead to an interesting interference pattern and would obviously greatly facilitate the determination of the $(t\bar{t})$ resonances. On the other hand, this would complicate the planned precision tests of the standard model on the Z^0 and imply the suppression of interesting toponium decay modes.

Finally, let us estimate the event rates for toponium production at LEP. In Fig. 2.16 we have plotted the contributions to

$$R^\theta = \frac{1}{\sigma_{pt}} \sigma(e^+e^- \rightarrow \text{hadrons}) , \qquad (2.34)$$

$$\sigma_{pt} = \sigma(e^+e^- \xrightarrow{\gamma^*} \mu^+\mu^-) ,$$

from the continuum $(R^{\gamma,Z})$, the toponium ground state (R^θ), and the single-quark decays of the toponium ground state (R^θ_{SQD}). Radiative corrections have been incorporated as [37]

$$R^\theta = R^{(0)} \left[\left(\frac{2\delta W}{m_\theta}\right)^t + \epsilon \right] ,$$

$$\epsilon = \frac{2\alpha_{em}}{\pi} \left(\frac{\pi^2}{6} - \frac{17}{36}\right) + \frac{13}{12} t , \qquad (2.35a)$$

$$t = 2 \frac{\alpha_{em}}{\pi} \left(\ln \frac{m_\theta^2}{m_e^2} - 1\right) ,$$

$$R^{(0)} = \frac{9\pi}{2\alpha_{em}^2 \sqrt{2\pi}} \frac{\Gamma_0(\theta)}{\delta W} \Gamma_{e^+e^-} BR(\theta \to had) \,, \qquad (2.35b)$$

where $R^{(0)}$ is the uncorrected value of R [see Eqs. (2.7) and (2.14)], m_e is the electron mass, and δW is the design energy spread [38],

$$\delta W \text{ (MeV)} = \frac{4.43 \times 10^{-3} \text{ W}^2 \text{ (GeV}^2)}{\left[1 - 0.41 \times 10^{-6} \text{ W}^3 \text{ (GeV}^3)\right]^{1/2}} \,. \qquad (2.36)$$

In the calculation for Fig. 2.16 the invariant mass of fermion-antifermion pairs in fermion-antifermion-photon final states has been restricted to more than 10 GeV [*].
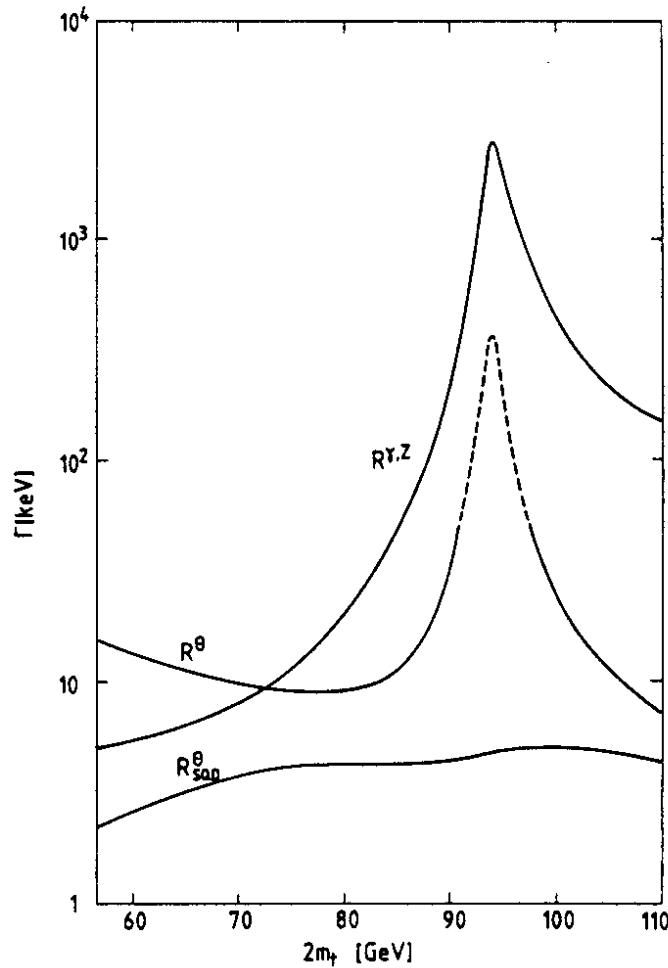
Fig. 2.16. Different contributions to R as functions of $2m_t$: $R^{\gamma,Z} = (1/\sigma_{pt})$ $\sigma(e^+e^- \xrightarrow{\gamma,Z} had)$, $R^\theta = (1/\sigma_{pt})\sigma(e^+e^- \xrightarrow{\theta} had)$, $R^\theta_{SQD} = R^\theta \cdot BR(SQD)/BR(had)$. Interference effects modify R^θ significantly in the dashed region. Radiative corrections are taken into account.

---

[*] We thank R. Kleiss for supplying the computer program for performing the radiative correction to the continuum cross-section (see Ref. [39]).

The rates of hadronic events from θ-decays and continuum production are given by

$$N_{had}^{\theta} = \sigma_{pt} \ R^{\theta} \ L \ T \quad , \tag{2.37a}$$

$$N_{had}^{C} = \sigma_{pt} \ R^{\gamma,Z} \ L \ T \ , \tag{2.37b}$$

where L and T are the luminosity and the running time. The reference cross-section σ_{pt} is given by

$$\sigma_{pt} = \frac{86.8 \ nb}{[W \ (GeV)]^2} \ . \tag{2.38}$$

As an example, let us consider the case $W = m_{\theta} = 80$ GeV, where one has (see Ref. [38] and Fig. 2.16)

$$L \equiv L_0 = 1.1 \times 10^{31} \ cm^{-2} \ s^{-1} \ , \ \delta W \equiv \delta W_0 = 32 \ MeV \ ,$$

$$\sigma_{pt} \equiv \sigma_0 = 13.6 \ pb; \tag{2.39}$$

$$R^{\theta} = 9 \ , \quad R^{\gamma,Z} = 20 \ .$$

With the conventions

$$1(TH) \ 'day' = 24 \ h \ ,$$

$$1(EXP) \ 'year' = 2800 \ h \approx 10^7 \ s \ , \tag{2.40}$$

one obtains from Eqs. (2.37) and (2.39) the event numbers listed in Table 2.1. Although the background is more than twice as large as the signal, the event rates are large enough to make toponium physics at LEP possible.

The main theoretical uncertainty in the estimate of the toponium production cross-section is the unknown wave function at the origin (see Fig. 2.5). The number of hadronic events N_{had}^{θ} could be larger or smaller by a *factor of 2* compared to the values given in Table 2.1. The expected event rates in the whole LEP energy range are plotted in Fig. 2.17.

In this section we have discussed the theoretical expectations for toponium physics at LEP. Heavy quark-antiquark bound states in the mass range from 60 to 110 GeV are an ideal testing ground for the standard model: their spectroscopy should provide direct evidence for asymptotic freedom and their decays are governed by weak, electromagnetic, and strong interactions which in the above

Table 2.1

Number of hadronic events for signal (N^{θ}_{had}) and
background (N^{C}_{had}) at $W = m_{\theta} = 80$ GeV

Running time T	$\int L\, dt$ (pb^{-1})	N^{C}_{had}	N^{θ}_{had}
1 'day'	0.95	260	118
1 'year'	111	30,000	14,000
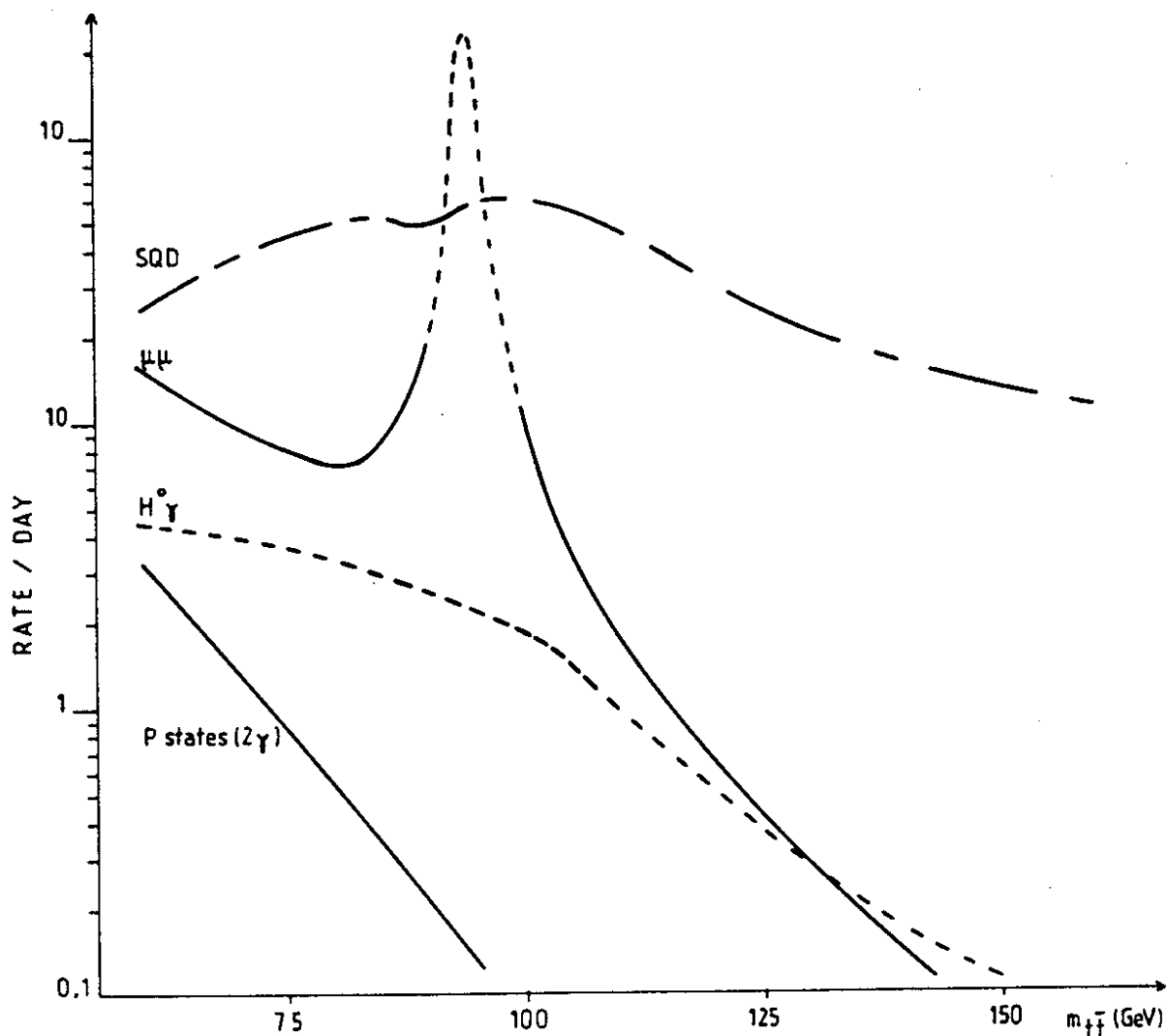
Fig. 2.17 Expected counting rates per day (24 h) for the decay modes $\theta \rightarrow$ SQD, $\mu^{+}\mu^{-}$, $H^{0}\gamma$, and $\theta' \rightarrow \chi_{t} + \gamma$ as functions of $2m_{t}$

mass range are of comparable strength. In the following sections we will study the experimental feasibility of various aspects of toponium physics in more detail: in Section 3 toponium scan and spectroscopy; in Sections 4 and 5 electroweak physics, i.e. asymmetry measurements and the search for Higgs particles; and in Section 6 the possible effects of supersymmetry on toponium decays. After a discussion of the role of the energy spread in Section 7, we will summarize our results in Section 8. In this paper we have not discussed the question of QCD tests through toponium decays, such as $\theta \to 3g$, $\theta \to \gamma 2g$, etc. An analysis of these decay modes will be treated by the study group of A. Ali et al. on QCD and $\gamma\gamma$ scattering [40].

3. TOPONIUM SEARCH AND SPECTROSCOPY

The search for the toponium S-states is performed in two steps, as follows:

i) The scanning region is reduced to a range of about 2 GeV through a rough measurement of the top (t) quark mass.

ii) This region is then scanned in steps of $2\delta W$ (δW denotes the spread in the centre-of-mass energy W), looking for a signal in the total hadronic cross-section--eventually applying additional topological cuts as discussed below.

The strategy for limiting the scanning region to 2 GeV is very different for toponium above or below the Z^0 mass. If t-quarks are light enough, a large number of T mesons can be produced at the Z^0 resonance in e^+e^- reactions, and the t-quark mass can then be determined. If toponium is above the Z^0, it will be more efficient to search for the top threshold, as discussed later.

3.1 Top-quark mass determination

Three methods are now described which make it possible to estimate the t mass in Z^0 decays and thus predict the scanning region for the toponium search.

3.1.1 Threshold effect

The rate of $t\bar{t}$ events at Z^0, when normalized to $\mu^+\mu^-$, shows a simple threshold dependence:

$$R_t = \frac{\Gamma(Z \to t\bar{t})}{\Gamma(Z \to \mu^+\mu^-)} = \frac{3\beta \left[(3-\beta^2)/2 \ (1 - 8/3 \ \sin^2 \theta_w)^2 + \beta^2\right]}{(1 - 4 \sin^2 \theta_w)^2 + 1} , \qquad (3.1)$$

where

$$\beta^2 = 1 - \frac{4m_t^2}{m_Z^2} .$$

Life becomes more complicated when first-order QCD corrections are included [41]:

$$R_t = \frac{3\beta \; [A + V \; (1 - 8/3 \; \sin^2 \theta_w)^2]}{(1 - 4 \; \sin^2 \theta_w)^2 + 1} \; , \qquad (3.2)$$

where

$$V = \frac{3 - \beta^2}{2} \left\{ 1 + \frac{4}{3} \; \alpha_s \left[\frac{\pi}{2\beta} - \frac{(3 + \beta)}{4} \left(\frac{\pi}{2} - \frac{3}{4\pi} \right) \right] \right\} \; ,$$

$$A = \beta^2 \left\{ 1 + \frac{4}{3} \; \alpha_s \left[\frac{\pi}{2\beta} - \left(\frac{19}{10} - \frac{22}{5} \; \beta + \frac{7}{2} \; \beta^2 \right) \left(\frac{\pi}{2} - \frac{3}{4\pi} \right) \right] \right\} \; ,$$

$$\alpha_s = \frac{12\pi}{25 \; \log \left(\frac{\beta m_t}{\sqrt{1-\beta^2}} / 200 \; \text{MeV} \right)} \; .$$

Figure 3.1 shows how R_t depends on m_t with and without QCD corrections; m_t can be deduced from R_t with some uncertainties, both theoretical and experimental.
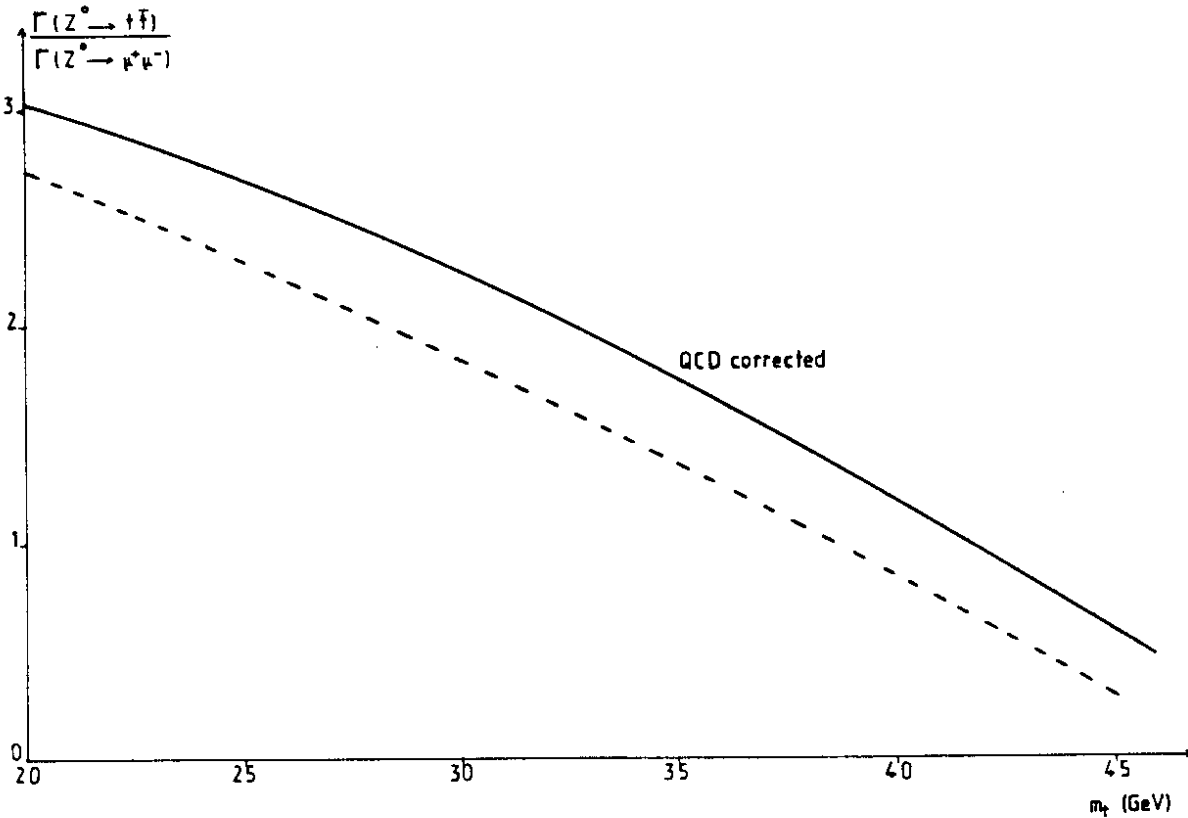
Fig. 3.1   Decay rate of Z^0 into top quarks normalized to $\mu^+\mu^-$.   The dashed line indicates the rate without QCD corrections.   From Ref. [41].

a)   Experiment

The t$\bar{\text{t}}$ sample can be isolated using topological cuts (see discussion below) which usually keep more than F_1 = 90% of t$\bar{\text{t}}$ with less than F_2 = 10% contamination (mass-dependent concept). With such figures it seems reasonable to assume a 5% systematic uncertainty on the number of t$\bar{\text{t}}$. When m_t increases, the signal-to-background ratio decreases while the topological separation improves. With this coarse estimate, one can thus neglect the mass dependence of the systematic error.

b)   Theory

If m_t = 40 GeV, the QCD correction term amounts to about 40%. With an error on α_s of order 10% we can see that the theoretical uncertainty is of the same order as the experimental one.

One might hope that the potentially large higher-order corrections sum up to modify the leading term by only a factor $[1 - \exp(- 2\pi \alpha_s/3\beta)]$ similar to the result in QED (see Ref. [42]). However, one cannot rigorously exclude some sizeable effect of higher-order corrections.

To conclude, such an approach should give an error on m_t of ~ 1.5 GeV for m_t ~ 40 GeV.

3.1.2 Semileptonic decays

a) Rest system distribution

In units of $m_t/2$, the μ (e) energy spectrum in the rest system is given by [43]:

$$\frac{1}{\Gamma} \frac{d\Gamma}{dx} = 12 \frac{x^2 (1 - x - \epsilon^2)^2}{1 - x} , \qquad (3.3a)$$

where

$$\epsilon = \frac{m_b}{m_t} , \qquad x = \frac{2E_{e(\mu)}}{m_t} .$$

This formula is valid at the quark level and for $0^- \rightarrow 0^-$ transitions. For $0^- \rightarrow 1^-$ transitions one gets [43]:

$$\frac{1}{\Gamma} \frac{d\Gamma}{dx} = 12 x^2 \frac{(1 - x - \epsilon^2)^2}{(1 - x)^2} (1 + 2\epsilon^2 - x) . \qquad (3.3b)$$

At ϵ = 0 all these formulae coincide; ϵ^2 is indeed known to be very small: $\epsilon^2 < 1/20$.
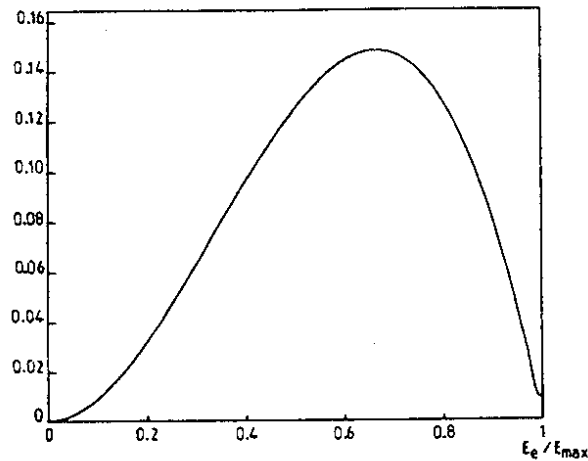
Fig. 3.2   Energy spectrum of the e (μ) in the top rest system

From Fig. 3.2 we see that this type of spectrum allows a very accurate determination of m_t through the end-point.

b)   *Laboratory system*

At Z^0, top particles are not produced at rest. Even if it is assumed that they are elastically produced (no fragmentation effect), their decay products cannot be well separated and thus their direction cannot be determined precisely. Therefore it does not seem possible to define the semileptonic decay distribution in the top rest frame.

Assuming an isotropic angular distribution of the lepton in the rest frame, the energy distribution in the lab. system can be generated. The result is shown in Fig. 3.3 in the elastic case, for m_t = 40 GeV. The end-point is difficult to determine. However, it is possible to try a global fit of the data (keeping out the low-energy region to avoid background from secondary leptons).
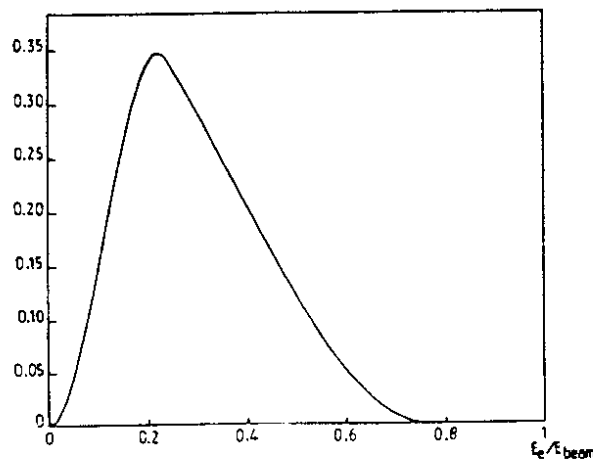
Fig. 3.3   Energy spectrum of direct e (μ) from T decays in the lab. system at Z^0 with m_t = 40 GeV

This fit was tried at m_t = 30 and 40 GeV and gave back the right mass to better than 200 MeV (with a sensitivity corresponding to about 10^6 Z^0).

c) *Polarization effects*

The standard model tells us that, at Z^0, t-quarks are polarized with

$$\langle\lambda_t\rangle = - \frac{2a_t\, v_t}{a_t^2 + v_t^2} \approx -0.74 \; , \tag{3.4}$$

where

$$a_t = 1 \; , \quad v_t = 1 - \frac{8}{3}\sin^2\theta_w \; .$$

This formula is only approximative since it neglects the mass of the t-quark. Using formulae given in Ref. [44], the average longitudinal polarization (at the Z^0 pole) can be computed:

$$\langle\lambda_t\rangle = \frac{-2a_t\, v_t\, \beta}{3/4\;(v_t^2 - a_t^2)/\gamma^2 + (3/4 + \beta^2/4)\;(v_t^2 + a_t^2)} \; . \tag{3.5}$$

For light t-quarks, $\beta \approx 1$, and one recovers the previous formula. For m_t = 40 GeV, $\langle\lambda_t\rangle$ = -0.85, which means that the polarization is still large and mostly longitudinal.

The averaged transverse polarization is given by

$$\langle P_T\rangle = \frac{\pi}{2\gamma}\frac{\sqrt{\beta^2\,(\Gamma_Z/m_Z)^2 + 4v_e^2\, v_t^2}}{(1 + \beta^2/3)(v_t^2 + a_t^2) + (v_t^2 - a_t^2)/\gamma^2} \; . \tag{3.6}$$

For m_t = 40 GeV, $\langle P_T\rangle$ = 0.087, which confirms our expectation that the polarization is mostly longitudinal. In the following calculations, we only take into account the longitudinal polarization as given by the previous formula.

Vector top mesons T^* will also be polarized, and since the usual cascade $T^* \rightarrow T + \gamma$ is negligible with respect to the weak decay, the process

$$T^* \rightarrow ev B$$

will act as an analyser of polarization:

$$\frac{d\sigma}{d\cos\theta} = (1 + P\cos\theta) \; . \tag{3.7}$$
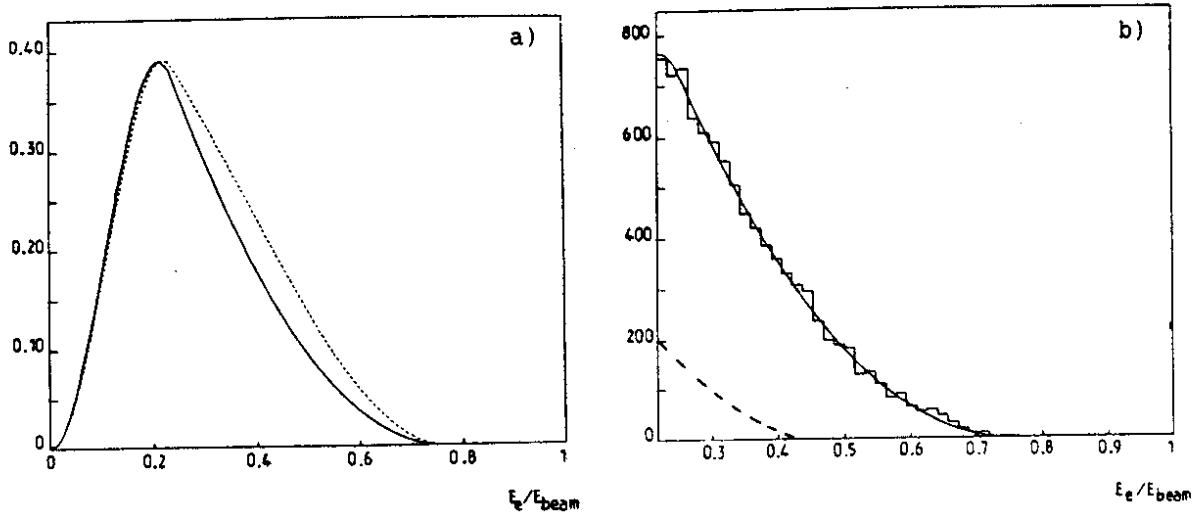
Fig. 3.4 a) Energy spectrum in the lab. system assuming an effective longitudinal polarization of -0.40 and m_t = 40 GeV (dotted curve corresponds to no polarization). b) Fit to the data (15,000 semileptonic decays generated). The dashed line corresponds to the expected background from secondary (charm, beauty) leptonic decays from t$\bar{\text{t}}$ events.

Assuming $T^*/T = 3$ and remembering that only two helicity states contribute, we can write [45],

$$P = \frac{1}{2} \langle \lambda_t \rangle ,$$ (3.8)

and we arrive at the lepton distribution shown in Fig. 3.4a for m_t = 40 GeV.

A total of 15,000 semileptonic decay events have been generated at m_t = 40 GeV using previous formulae for the angular distribution of the leptons and the quark-decay formula (3.3) for the energy spectrum.

The resulting distribution is fitted using the formula (see also [45])

$$\frac{d\Gamma}{dy} \propto (y - y_{max})^2 \left[2y + y_{max} + \frac{P}{\beta} (6yy_{max} - 2y - y_{max}) \right] ,$$ (3.9)

where

$$y = E_e/E_{beam} ,$$

$$y_{max} = \frac{1 + \beta}{2} ,$$

$$\beta = \sqrt{1 - \frac{4m_t^2}{m_Z^2}} .$$

This formula is valid when

$$\frac{1 - \beta}{2} < y < \frac{1 + \beta}{2} \,,$$

and has been derived in the approximation $\epsilon = 0$ [see Eq. (3.3)].

Starting from $m_t = 40$ GeV in the Monte Carlo generation, the fit gives (Fig. 3.4b)

$$m_t = 40.3 \pm 0.1 \text{ GeV} \,.$$

d)   Fragmentation effects

Fragmentation introduces a further complexity into the problem. At present, several models seem to describe the charm and beauty data [46]. Although they all give quasi-elastic events, the deformation which they introduce into the spectra is noticeable at the χ^2 level when the fit given in the previous paragraph is performed. The resulting value for m_t is not changed by more than 500 MeV.

To summarize:
- a precise determination of the top mass from Z^0 events requires an understanding of the shape of the lepton spectrum in the lab system;
- this shape is affected by fragmentation and polarization effects;
- if these effects are reasonably well understood, we can hope to reach a precision of 500 MeV on m_t using this method.

3.1.3 Top-mass determination using multijet final states

The non-leptonic weak decays of the top particles produce final states containing three jets for each meson decay with, in addition, a few low energetic particles coming from the spectator quarks. Using a cluster algorithm, for instance the standard subroutine LUCLUS from the Lund Monte Carlo program, we can reconstruct some of these jets. In the following we have considered events containing five or six identified jets, and the top mass will be obtained by considering subsamples of two or three jets. If hadrons are produced in addition to top particles, the mass of the selected jet sample will be incorrect and the proportion of correct combinations will decrease.

a)   Lund generation

The standard Lund Monte Carlo program generates only a $T\overline{T}$ system. This is due to the very high peaking of the fragmentation function at high z values.

We have selected, for each event, the jet subsample which has its energy closest to the beam energy, and the mass of these systems is shown in Fig. 3.5 for different choices of the t-quark mass. The measured mass has been rescaled
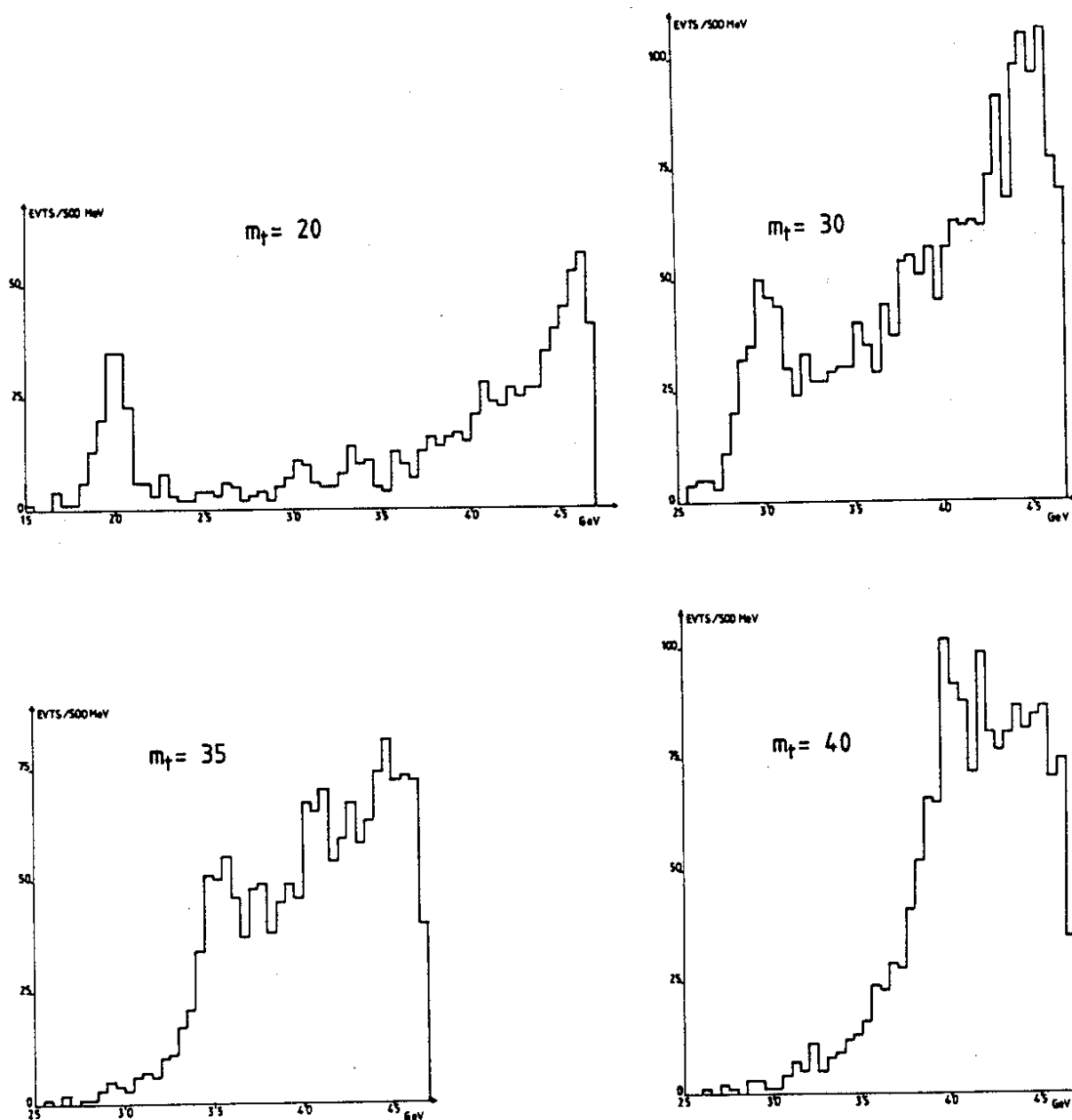
Fig. 3.5 Top-mass reconstruction using jets for m_t = 20, 30, 35, and 40 GeV.
The statistics corresponds to 3000 TT pairs.

by the ratio E_{beam}/E_{jet} to correct for particle losses. A simplified simulation
of the DELPHI apparatus has been used, which incorporates dead regions, expected
accuracies on energy and angle reconstruction, and photon conversions. A mini-
mum energy of 500 MeV is needed to accept a photon, and at least 1 GeV is re-
quired for a neutral hadron (K_L^0, n).

In one year of running at the Z^0 resonance (10^6 hadronic events), clear
mass peaks can be obtained, allowing a determination of the top mass with a
negligible statistical uncertainty. The systematic uncertainty depends mainly

on the relation between the t-quark and the T-meson masses; it can be minimized by the use of a Monte Carlo program and a reasonable theoretica input. An accuracy of better than 200 MeV seems possible up to 40 GeV.

b) Peterson-like generation

If we use a different fragmentation function for the t-quarks, one of the main effects is to recover $t\bar{t}g$ events. Using the same method we observe a peak around the initial t-quark mass; its height is decreased by about a factor of 3 in comparison with the result obtained with the Lund scheme, and its mean value is shifted towards higher masses because of the rescaling procedure which overestimates the energy of the T-meson.

The systematic uncertainty comes mainly from the shape of the t-quark fragmentation function. However, changing this function from Lund to Peterson recipes, we have observed a displacement of the peak of less than 500 MeV. (As already mentioned in the previous section, the semileptonic decays can be used to reduce the uncertainty on the fragmentation function.)

In conclusion, we believe that our method can give m_t to better than 500 MeV.[*]

3.1.4 Toponium above the z^0 mass

If toponium lies in the region above the z^0 mass, one could in principle run at the highest energy, identify top mesons, and measure their mass just as before. An alternative method consists in making a direct search for open-top threshold in the following way: The rise of R above threshold is very sharp [41]. For simplicity we ignore the threshold suppression completely. The topology of open-top events [48] is strikingly different from that of two-jet ($q\bar{q}$) and three-jet ($q\bar{q}g$) events. The cuts to be discussed below for the selection of SQDs of toponium allow 95% of the continuum cross-section to be rejected, whilst nearly 90% of the signal is retained. Similar numbers apply also in the case of open-top production.

At each energy we take an integrated luminosity corresponding to at least ten events of open-top production (if above threshold); this will take 30 hours in the worst case.

Depending on the observation of the open-top production at the current energy, we increase or decrease the centre-of-mass energy by half of the previous energy step. This procedure converges quickly, and the threshold of open-top production can be measured with an error of about 2 GeV in six steps which correspond to a total of about ten days of data-taking.

---

*) For a related discussion, see also Ref. [47].

3.2 S-states

3.2.1 Scan

We assume that an energy interval of 2 GeV will be scanned in steps of $2\delta W$ (centre-of-mass energy spread), requiring a signal of n standard deviations in the total cross-section. For each step we need an integrated luminosity LT,

$$LT = n^2 \frac{\sigma_S + \sigma_B}{\sigma_S^2} , \qquad (3.10)$$

where σ_S is the 1S toponium effective cross-section at the peak and σ_B is the background cross-section.

The total integrated luminosity needed to scan the full 2 GeV interval is

$$LT(total) = n^2 \frac{\sigma_S + \sigma_B}{\sigma_S^2} \frac{2 \text{ GeV}}{2\delta W} \qquad (3.11)$$

(σ_S is proportional to the inverse of δW). When $\sigma_S \ll \sigma_B$ (as happens above 80 GeV), the total integrated luminosity is proportional to δW and can be reduced by decreasing the energy spread of the beam.

As already stated, the topology of the toponium SQD is very different from the background topology. If this decay mode is important, it may be more convenient to search for a signal in the cross-section of 'spherical' events using topological cuts to reduce continuum events [48].

Figure 3.6a shows a plot of thrust (T) [49] versus oblateness (O) [50] for SQD events from a toponium state with a mass of 100 GeV. Figure 3.6b shows the same plot for $q\bar{q}$ and $q\bar{q}g$ events at the same energy. (For the continuum events, we used the Lund Monte Carlo; for SQD events we also used the Lund Monte Carlo simulating open $t\bar{t}$ production at threshold.) The SQD events are localized mainly in the region of small thrust and oblateness,

$$O < 2(1-T) - 2h,$$

where h is an adjustable parameter than can be optimized. The efficiency of the cut for various choices of h is displayed in Table 3.1. The optimum is achieved for h = 0.05, where we can retain 87% of the signal and reject 95% of the background. The cut is not sensitive to the centre-of-mass energy, and we therefore regard these numbers as being constant in the full energy range that we consider.
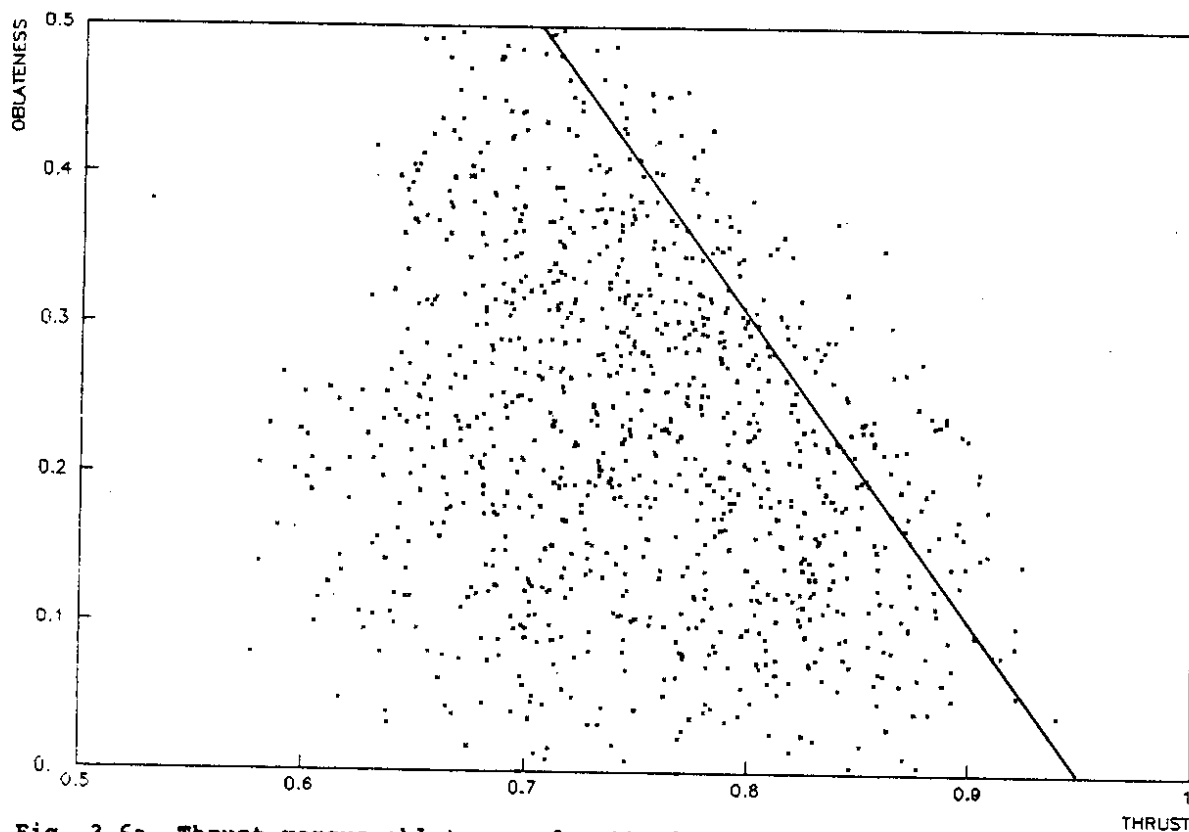
Fig. 3.6a Thrust versus oblateness for SQD decay for a toponium with a mass of
100 GeV. The line shows the cut described in the text.
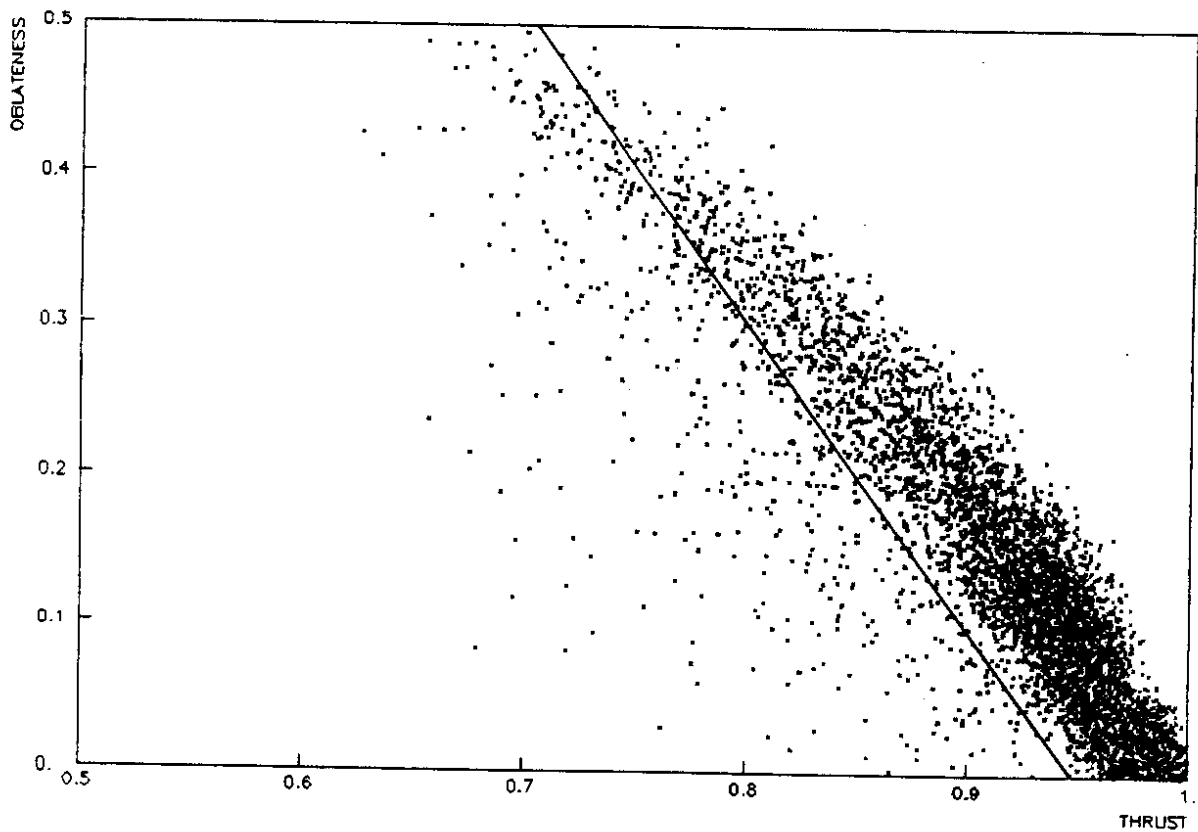
Fig. 3.6b Thrust versus oblateness for $q\bar{q}$ and $q\bar{q}g$ events at 100 GeV
centre-of-mass energy. The line shows the cut described in the text.

<u>Table 3.1</u>

The percentage of SQD events and background events

that pass the cut for various values of h

h	0	0.01	0.03	0.05	0.07	0.09
SQD	95	97	98	87	76	64
Background	79	48	12	5	3	2
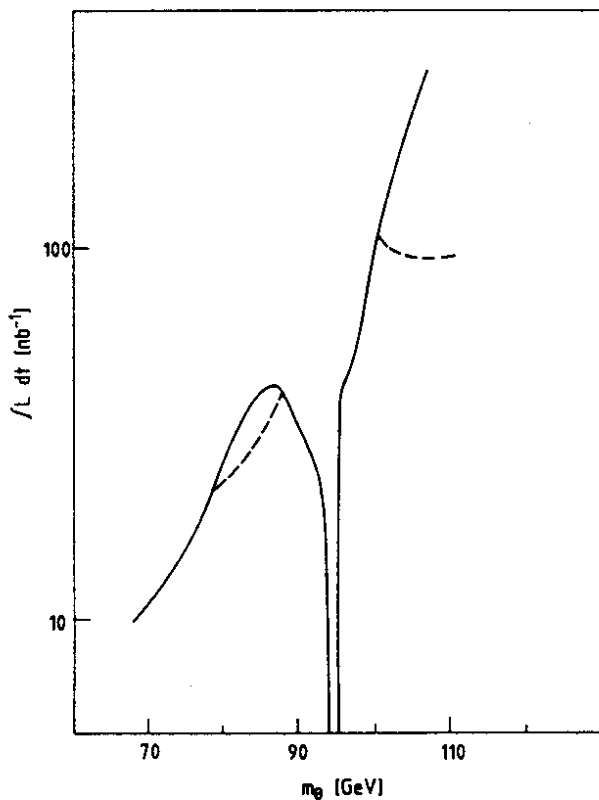
Fig. 3.7a Integrated luminosity needed
to achieve a signal of 1 st. dev. in one
step of the scanning as function of the
toponium mass
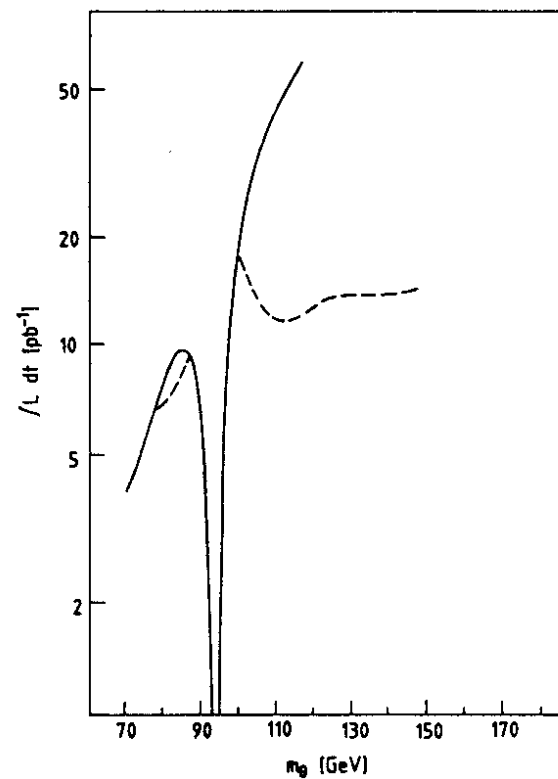
Fig. 3.7b Integrated luminosity needed
for the full scanning of a 2 GeV mass
interval asking for a signal of 3 st.
dev. as function of the toponium mass

Figure 3.7a shows the integrated luminosity needed to achieve 1 st. dev.
signal in one step of the scanning as a function of the toponium mass. The
dotted line indicates the region where the topological cut is applied.

Figure 3.7b shows the total integrated luminosity needed for scanning the
2 GeV region as a function of the toponium mass with a 3 st. dev. signal. We
see that up to a toponium mass of 150 GeV the total integrated luminosity needed
for the full scan is less than 20 pb^{-1}, which corresponds to 20 days of full
luminosity or to 2 real months.

Furthermore, it is evident from this figure that these cuts would be of crucial importance if toponium were to have a mass above 100 GeV. In the region quite above that of the Z^0, one might eliminate the radiative tail of the Z^0 by appropriate cuts on missing energy and momentum, but we have not studied this possibility in detail.

3.2.2 Measurement of m_θ and $\Gamma_{ee}(\theta)$

We assume that the shape of the background in the resonance region is known. To measure the toponium mass and Γ_{ee} we can fit a Gaussian plus the known background to the total cross-section:

$$\sigma(W) = \sigma_{pt} R^\theta \, e^{-(m-W)^2/2\delta W^2} + \text{Background} , \qquad (3.12)$$

where R^θ has been defined in Eq. (2.35).

Table 3.2 gives the statistical accuracy on the toponium mass, assuming that we take 0.4 pb^{-1} at nine different energies in the resonance region. The absolute measurement of the mass has a systematic error of about 100 MeV owing to the systematic error on the energy of the beams, although this could be reduced if the beams were transversely polarized. This error is not relevant for the measurement of the mass difference between the 1S- and 2S-states.

Table 3.2
Accuracy on the toponium mass and leptonic width

Mass (GeV)	70	80	90	100	110	120
δm_θ (MeV)	10	20	15	20	30	40
$\delta\Gamma_{ee}/\Gamma_{ee}$ (%)	10	10	10	15	20	25

If the toponium mass is in the region of 80 GeV, its branching ratio to neutrinos can reach the 10% level. In this case the branching ratio $\Gamma_{vis}/\Gamma_{tot}$ is considerably different from 1, and the measurement of Γ_{ee} must be corrected to take this effect into account. The error on the correction is, in any case, negligible compared to the statistical error.

If toponium should be found in the immediate neighbourhood of the Z^0, both the line shape and height of the resonance are affected by interference with the continuum, and a more complicated analysis has to be performed (see Section 2).

3.2.3 Search for radial excitations

Owing to the low signal-to-background ratio, the search for the other S-states (apart from the 2S-state) is possible only if toponium is below the Z^0 mass; we thus concentrate on a single case: the toponium mass at 80 GeV.

Figures 3.8a and 3.8b give a possible scenario if the toponium mass is in this region. Figure 3.8a is a plot of R, and Fig. 3.8b is a plot of R for the events that pass the topological cut described earlier. As input we used the values for Γ_0 and binding energies listed in Table 3.3, as calculated [24] for the Richardson potential. The comparison of these figures shows that it is easier to find the resonances using the topological cut.

Once the 1S-state has been found, we restrict the scanning region for the 2S-state to about 400 MeV. To scan this region we need five steps of 0.7 pb^{-1} per point to get a 3 st. dev. signal. This figure corresponds to about four days of data-taking at full luminosity. In the resonance region, we then need about nine points, of 0.8 pb^{-1} each, to measure the mass with a statistical error lower than 10 MeV and a relative accuracy on Γ_{ee} of 20%. This figure corresponds to about seven days at full luminosity.
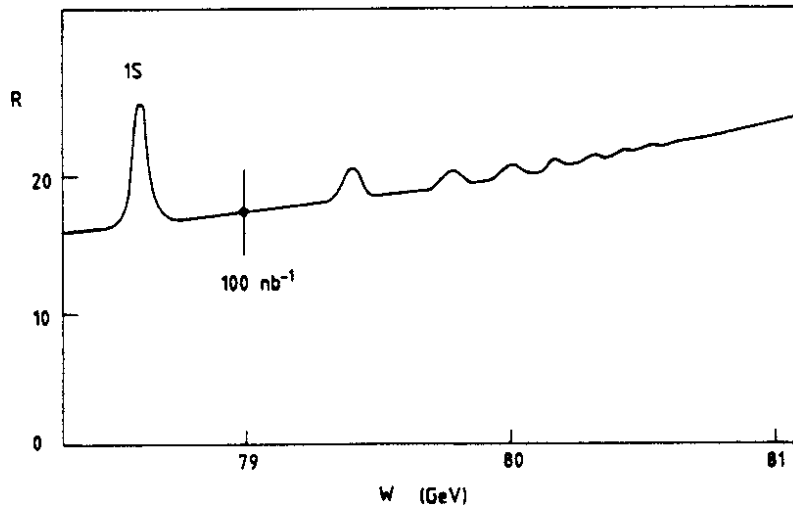
Fig. 3.8a R as a function of the centre-of-mass energy assuming m_t = 40 GeV
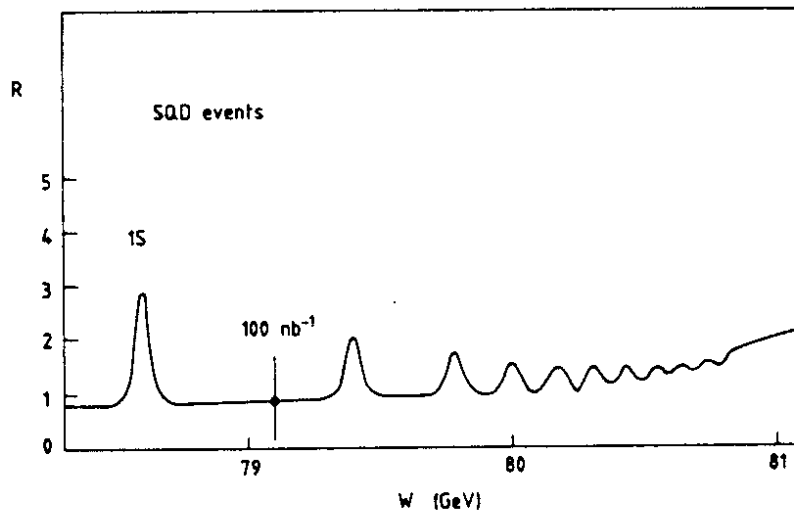
Fig. 3.8b R for the events that pass the topological cut (see text) as a function of the centre-of-mass energy assuming m_t = 40 GeV

Table 3.3

Model parameters as calculated for the Richardson potential ($m_t = 40$ GeV)

n	1	2	3	4	5	6	7	8	9	10
Γ_0 (keV)	7.34	1.97	1.08	0.77	0.61	0.52	0.46	0.42	0.39	0.37
E_B (MeV)	-1.485	-572	-218	4	172	310	431	539	638	731

Assuming that we again scan a region of 400 MeV asking for a 3 st. dev. signal for the 3S-state, it will require about 7 pb^{-1} for the full scanning.

The scan for the other states is much more difficult, as is evident for the rapidly decreasing resonance enhancement due to the decreasing Γ_0 and the decreasing spacing between the levels listed in Table 3.3. However, once the first three states have been found and their masses have been measured, the masses of the other states should be fixed by the potential models with an error smaller than the centre-of-mass energy spread (32 MeV in this region). Assuming that the experimental width of each resonance is defined by the energy spread of the beams, and assuming that one knows the background below each resonance, the mass of any state can be measured, in principle, taking data at only two energies, one below and one above the foreseen position of the resonance at a distance of the order of the centre-of-mass energy spread. As an example for this method, the mass of the 5S-state can be measured with a precision of 10 MeV in about seven days of data-taking, but more than twenty days are required in which to achieve the same precision on the mass of the 7S-state.

All these figures could be substantially improved if the centre-of-mass energy spread could be reduced.

3.3 P-states[*]

As already mentioned in the Introduction, after the discovery of the 1S- and 2S-states the determination of the P-wave χ_t mass will be important in order to check the behaviour of the quark-antiquark potential at distances below 0.1 fm.

As for lighter quarkonium states [$(c\bar{c})$ and $(b\bar{b})$], the method used to investigate the $(t\bar{t})$ P-states will consist in detecting the photons emitted by E1 transitions in the reaction:

$$\theta' \rightarrow \gamma_1 \chi_t$$
$$\llcorner\!\!\rightarrow \gamma_2 \theta \ . \tag{3.13}$$

---

[*] D. Boutigny (LAPP) has contributed significantly to the work presented in this subsection.

Contrary to the ψ and Y spectroscopies the branching ratio for the dipole transition $\chi_t \rightarrow \gamma_2\theta$ is larger than 50% for toponia in the mass range from 60 to 80 GeV [25]. The inclusive photon spectrum of θ' decays will therefore contain two sharp lines of comparable height, which in principle facilitates the search for the χ_t states.

Owing to the anticipated large t-quark mass, SQD channels are open for both S- and P-states and, as can be seen from Fig. 2.11, branching ratios for radiative decays decrease steeply when the top mass m_t increases. In addition, the energy level differences between states are mass-dependent and also model-dependent. For example, if $m_{\theta'}$ = 80 GeV, the following energy ranges are expected (Section 2):

$$E_{\gamma_1} = 100\text{-}150 \text{ MeV},$$

$$E_{\gamma_2} = 370\text{-}850 \text{ MeV}, \tag{3.14}$$

$$\Delta m_{FS}^t = 5\text{-}10 \text{ MeV} .$$

In order to estimate the integrated luminosity necessary to determine the centre of gravity of the P-states, we have simulated the signal produced in reaction (3.13) as well as the associated background. To do this, the θ' production rates have been computed assuming that $R_{\theta'} = 1/3 \ R_\theta$ with R_θ taken from Fig. 2.16 and using the LEP 13 (3 mA) luminosity and beam-spread conditions [38]. The assumed θ, θ', and P-states properties are shown in Fig. 3.9 for
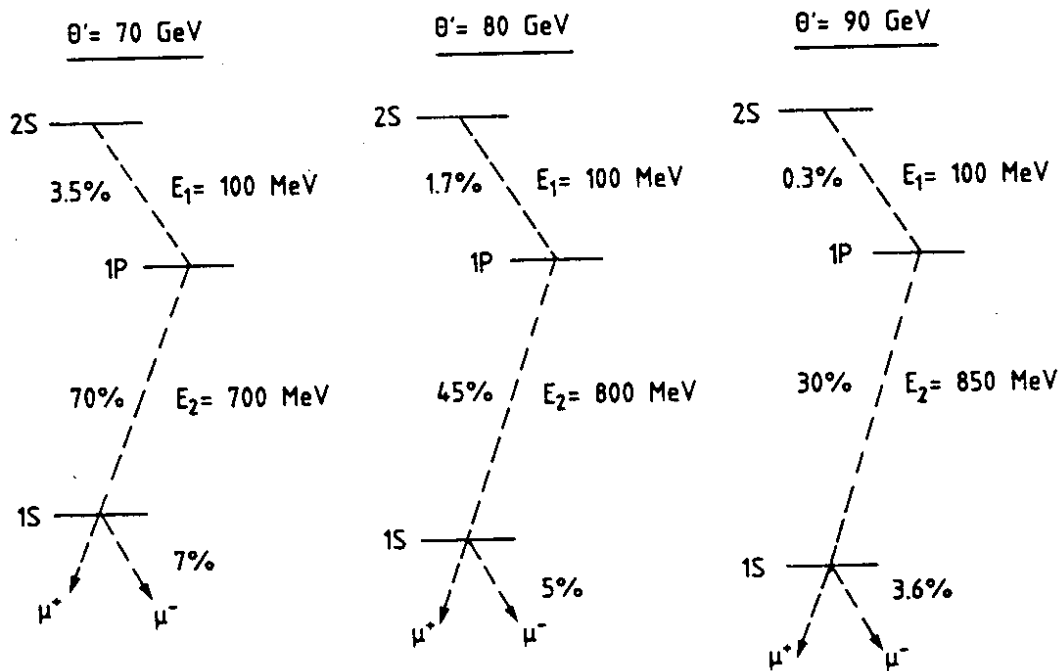
Fig. 3.9 Input parameters for radiative transitions
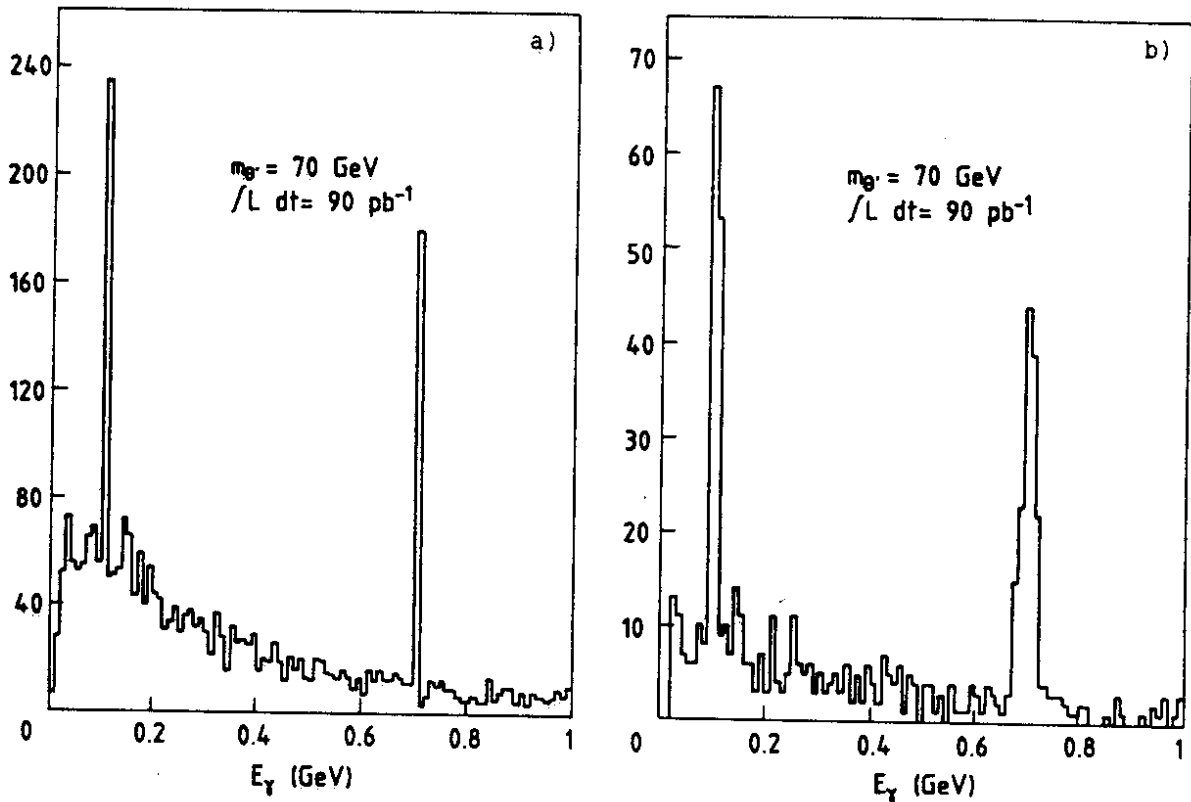
Fig. 3.10 Photon energy spectrum from the cascade decay $\theta' \to \gamma_1 \gamma_2 \theta$, including photons from θ decay products ($W = m_{\theta'} = 70$ GeV); a) generated; b) after π^0, η^0 reconstruction and energy smearing.

distinct θ' masses of 70, 80, and 90 GeV. They have been estimated on the basis of QCD-like potential models [see Eq. (2.25), Ref. 25].

The energy spectrum of the photons emitted in reaction (3.13), including the photons from all θ-decay products, has been computed for the corresponding θ' mass values. As an example, Fig. 3.10a shows the 0 to 1 GeV photon spectrum obtained at $m_{\theta'} = 70$ GeV for an integrated luminosity of 90 pb^{-1} corresponding to approximately one year of operation.

The associated background photons have also been computed for the following contributions:

- the continuum, with values of $R^{\gamma,Z}$ as shown in Fig. 2.16, generated according to the Lund model;
- the various hadronic decay products of the θ' (see Fig. 2.11);
- the hadronic decay products of the χ_t states [see Ref. (25)].

A $|\cos \theta_\gamma| < 0.98$ cut was applied in order to essentially eliminate photons from initial-state radiation.

Figure 3.11 shows, for $m_{\theta'} = 70$ GeV and $\int L\, dt = 90$ pb^{-1} (corresponding to 1.8×10^4 events), the number of background photons per bin 10 MeV.
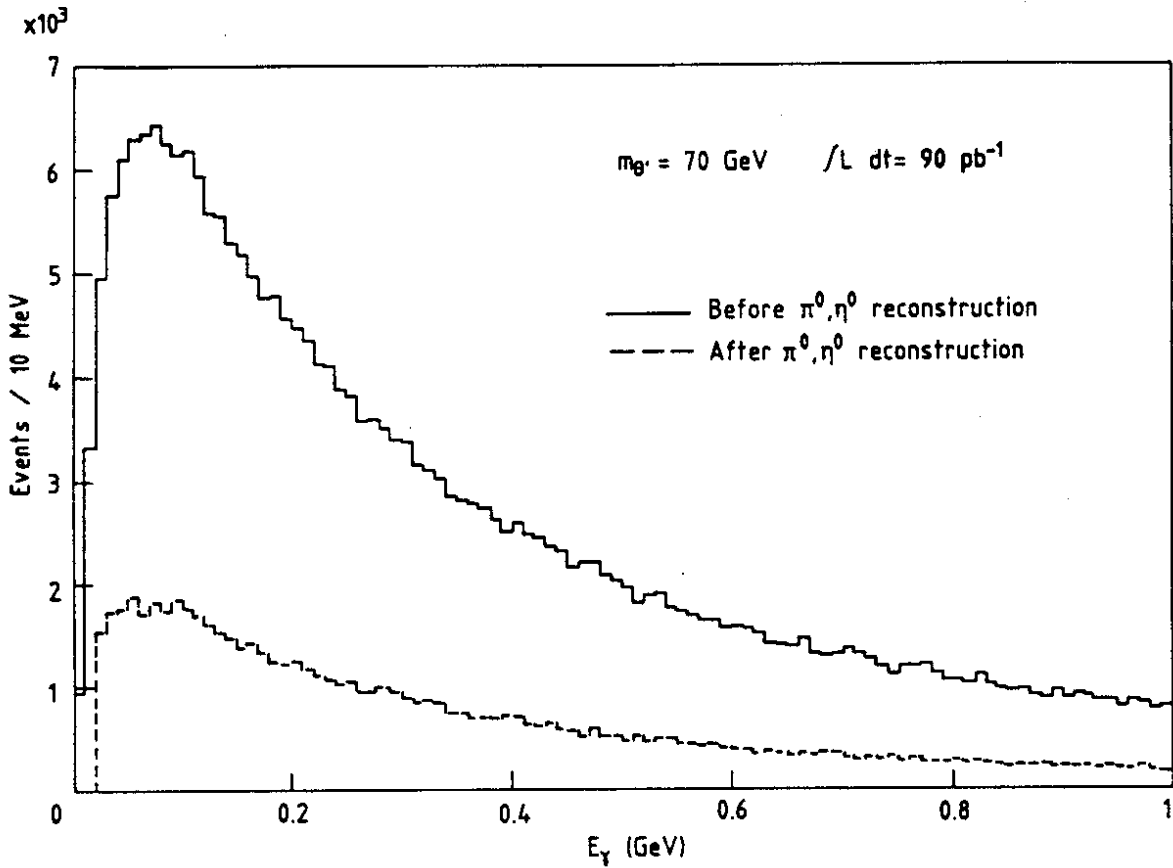
Fig. 3.11 Energy spectrum of background photons coming from processes other than $\theta' \rightarrow \gamma_1 \gamma_2 \theta$ ($\rightarrow$ anything) (W = $m_{\theta'}$ = 70 GeV). The plot is based on 1.8×10^4 Monte Carlo events.

The probability per hadronic event to find a background photon of energy E_γ is given by

$$P(E_\gamma) = \frac{dN}{dE_\gamma}(E_\gamma) \cdot \Delta E_\gamma \cdot F(E_\gamma) \quad , \tag{3.15}$$

where dN/dE_γ can be obtained from Fig. 3.11, multiplying the number of photons per 10 MeV bin by $(N_{evts} \times 10 \text{ MeV})^{-1}$; ΔE_γ is determined by the energy resolution of the detector; F denotes the fraction of photons that remain after π^0 and η^0 rejection. The evidence of P-state production can be obtained searching for a signal in the single-photon spectrum or by studying the double-photon cascade. As an illustration, we consider the case of a BGO detector with an energy resolution

$$\sigma_E = 1.65\%/\sqrt{E} \quad , \quad \text{for } 0.02 \text{ GeV} < E < 2.7 \text{ GeV} \quad ,$$

$$\tag{3.16}$$

$$\sigma_E = 1\% \ E \quad , \quad \text{for } E > 2.7 \text{ GeV} \quad ,$$

and a spatial resolution $\sigma_{x,y}$ varying between 1 and 6 mm, depending on E. Using specific pattern-recognition algorithms for photon isolation, π^0 and η^0 reconstruction has been attempted [51]. Figure 3.10b and the dashed line of Fig. 3.11 show the spectra of photons that remain after the assumed reconstruction.

For distinct θ' mass values and integrated luminosities, the number of detected photons with energy E_1 or E_2 and the number of events where both photons are detected in coincidence in a $\pm 2\sigma_E$ window are given in Table 3.4 for the signal and for the background. The results given in Table 3.4 can probably be slightly improved by reduction of systematic errors on energy resolution and optimization of pattern-recognition algorithms.

In any case, owing to the fast increase of $R^{\gamma,Z}/R^{\theta'}$ combined with the decrease of radiative transition rates when the toponium mass increases, this two-photon coincidence method of searching for χ_t states seems to be limited to toponium masses lower than 80 GeV.

<u>Table 3.4</u>

Energies of γ_1 and γ_2, number of signal and background photons
in the inclusive spectrum, and number of events requiring $\gamma_1\gamma_2$ coincidence

$m_{\theta'}$ (GeV)	70		80
$\int L\, dt$ (hours) $\int L\, dt$ (pb^{-1})	1000 32	2800 90	2800 110
	$\theta' \rightarrow \gamma_1 \chi_t$		
E_{γ_1} (MeV)	100 ± 10	100 ± 10	100 ± 10
Signal S_1	63	177	74
Background B_1	1254	3540	6210
S_1/B_1 (σ)	1.8	3.0	0.9
	$\chi_t \rightarrow \gamma_2 \theta$		
E_{γ_2} (MeV)	700 ± 25	700 ± 25	800 ± 30
Signal S_2	53	147	38
Background B_2	675	1834	2920
S_2/B_2 (σ)	2.0	3.4	0.7
	$\gamma_1\gamma_2$ coincidence		
Signal $S_{1,2}$	33	93	29
Background $B_{1,2}$	113	315	398
$S_{1,2}/B_{1,2}$ (σ)	3.1	5.2	1.5

Table 3.5

Counting rates in the exclusive channel $\theta' \rightarrow \gamma_1 \gamma_2 l^+ l^-$

$m_{\theta'}$ (GeV)	$\int L\, dt$ (hours)	$\int L\, dt$ (pb^{-1})	$\gamma_1 \gamma_2 l^+ l^-$
70	1000	32	14
	2800	90	40
75	1000	36	6.5
	2800	100	18
80	1000	39	3
	2800	110	9
85	2800	125	4
90	2800	136	2.5

As an alternative, we have also considered the possibility of using the exclusive reaction

$$\theta' \rightarrow \gamma_1 \gamma_2 \theta \quad\quad (3.17)$$
$$ \hookrightarrow l^+ l^- ,$$

which gives the signal event rates shown in Table 3.5 when summing over the three charged-lepton types: e^+e^-, $\mu^+\mu^-$, $\tau^+\tau^-$. In this case the background is due to radiation in initial and final states, which produces photons mainly collinear to the beam or to the final leptons. With an angular cut of 10° and neglecting interferences between initial and final radiation, one finds

$$\tilde{P}(E_\gamma) = 4.5 \times 10^{-2} \frac{\Delta E_\gamma}{E_\gamma} \quad\quad (3.18)$$

for the number of photons radiated per event, in a certain energy interval ΔE_γ.

The probability per event to contribute as background to the double-cascade process is given by

$$\tilde{P}(E_{\gamma_1}, E_{\gamma_2}) = (4.5 \times 10^{-2})^2 \cdot \frac{\Delta E_{\gamma_1}}{E_{\gamma_1}} \cdot \frac{\Delta E_{\gamma_2}}{E_{\gamma_2}} . \quad\quad (3.19)$$

The requirements (as previously proposed in Ref. [52]), that the two leptons have an acollinearity < 10° in the e^+e^- or $\mu^+\mu^-$ case or that there be a number of charged tracks ≤ 3 for each back-to-back τ decay and a total measured energy

$E_{vis} > 0.4 \sqrt{s}$, lead us to estimate that the background is smaller than the signal up to $m_{\theta'} \simeq 85\text{-}90$ GeV, in the case of a BGO detector.

With a gaseous electromagnetic detector, for which we assume that the detection of photons down to 100 MeV is feasible with $\sigma_E/E = 15\%/\sqrt{E}$, we estimate that the background becomes as large as the signal near $m_{\theta'} \simeq 80$ GeV.

It should be noted that with such a gaseous detector it will not be possible to determine the 1P-state position with precision, but the event rate could put constraints on the model, through the measurement of the dipole transition rate. With a BGO detector a more precise determination of the χ_t mass will be possible.

To summarize: Based on the predictions of the present models, the χ_t energy-level determination seems feasible for toponium masses in the low-energy range of LEP I.

Using the reaction

$$\theta' \rightarrow \gamma_1 \gamma_2 \theta \ ,$$

the inclusive one-photon or semi-inclusive two-photon methods appear to be limited to toponium masses of less than 80 GeV. The exclusive method, with the associated detection of $\mu^+\mu^-$, e^+e^-, or $\tau^+\tau^-$, seems to be more promising for pushing this limit up to toponium masses of 85-90 GeV.

It is worth recalling here that the toponium production rates are uncertain within a factor of 2. On the other hand, the knowledge of the θ and θ' energy levels will constrain the expected counting rates as well as the photon energy ranges to be scanned.

4. ANGULAR AND POLARIZATION ASYMMETRIES

As discussed in Section 2, neutral-current effects and W exchange will play an important role in toponium decays. Indeed, toponium seems to be an ideal place for determining the coupling of the neutral current to top quarks. The measurement of asymmetries on toponium determines the relative strength of the neutral-current coupling g_t^V and the electromagnetic coupling e_t quite unambiguously, in contrast with open-top production, which has to cope with uncertainties from QCD corrections and quark-mass effects, and which involves a mixture of vector and axial-vector contributions.

We shall base the following discussion mainly on the theoretical formalism developed in Refs. [29] and [24] and on earlier works referred to in those papers. We shall treat four different asymmetry measurements. These are all (apart from those with $b\bar{b}$ as the final state) dependent on g_t^V/e_t or its square, although from an experimental view-point they are rather different. The ratio g_t^V/e_t is of course determined in the standard model by $\sin^2 \theta_w$. Nevertheless it

is desirable to measure this quantity, which is also necessary for deducing the wave function at the origin from Γ_{ee}, in a model-independent way. Furthermore, this allows an independent determination of quark charge and isospin.

In the analysis presented below, we have always taken an incoherent sum of the resonance and the γ-Z continuum. In the neighbourhood of Z ($|m_\theta - m_Z| \lesssim 2\Gamma_Z$) a more involved formalism is required (see Refs. [24] and [33]). Here we are only interested in the experimental accuracy that can be expected and in a comparison of the different methods proposed, and for this the simplified treatment is adequate. To determine g_t^V/e_t, one could make use of longitudinal beam polarization, or measure the τ polarization; or one could directly measure the toponium polarization through semileptonic SQDs; $(g_t^V/e_t)^2$ can also be measured through the difference in the forward-backward asymmetries of lepton pairs on and off resonance. We shall now discuss these possibilities in turn, and list the integrated luminosity in pb^{-1} ($\approx$ 24 hours at $L = 10^{31}$ cm^{-2} s^{-1}) which is required in order to achieve a specified accuracy in the detection of the asymmetry.

4.1 Polarization asymmetry

Longitudinally polarized beams will not be available in the first round of LEP experiments. We nevertheless start with the polarization asymmetry α_{RL}, which can be expressed in terms of the coupling constants in a particularly simple way. Other asymmetries which can be measured with unpolarized beams are then conveniently expressed in terms of α_{RL} and may thus also serve to measure this quantity.

If longitudinally polarized beams are available, one expects a difference in the production cross-section for right-handed versus left-handed polarization owing to neutral-current effects [53, 54, 29, 24]. The polarization asymmetry defined by

$$\alpha_{RL} = \frac{\sigma_R - \sigma_L}{\sigma_R + \sigma_L} , \tag{4.1}$$

is in general different on and off resonance. Ignoring the aforementioned interference between resonance and continuum, and taking the effects of beam energy smearing into account, α_{RL} on top of the resonance is given by

$$\langle \alpha_{RL} \rangle = \frac{\alpha_{RL}^{on} + \alpha_{RL}^{off} \eta}{1 + \eta} , \tag{4.2}$$

where $\eta = R^{cont}/R_\theta$ parametrizes the 'contamination' of the resonance by the continuum background. The asymmetries from resonance and continuum are given by

$$\alpha_{RL}^{on} = -2 \; \frac{Re \; (\lambda_e^* \lambda_e')}{|\lambda_e|^2 + |\lambda_e'|^2} \; , \tag{4.3}$$

$$\alpha_{RL}^{off} = \frac{\displaystyle\sum_{h_f, h_e} h_e |F^C(h_f, h_e)|^2}{\displaystyle\sum_{h_f, h_e} |F^C(h_f, h_e)|^2} \; , \tag{4.4}$$

where

$$\lambda_f = \frac{e^2}{s} \; e_f e_t + \left(\frac{e}{y}\right)^2 \frac{v_f v_t}{s - m_Z^2 + i m_Z \Gamma_Z} \; , \tag{4.5}$$

$$\lambda_f' = \left(\frac{e}{y}\right)^2 \frac{a_f v_t}{s - m_Z^2 + i m_Z \Gamma_Z} \; , \tag{4.6}$$

$$y = 2 \sin 2\theta_w \; ,$$

$$F^C(h_f, h_e) = \frac{e^2 e_f e_e}{s} + \left(\frac{e}{y}\right)^2 \frac{(v_f - h_f a_f)(e_e - h_e a_e)}{s - m_Z^2 + i m_Z \Gamma_Z} \; , \tag{4.7}$$

and

$$a_u = a_v = 1 \; , \quad a_d = a_e = -1 \; ;$$

v_f has been defined in Eq. (2.14).

The asymmetries α_{RL}^{on} and α_{RL}^{off} (for μ pairs) are shown in Fig. 4.1 as a function of m_θ. (Note that α_{RL}^{on} is independent of the final state, but not α_{RL}^{off}.)
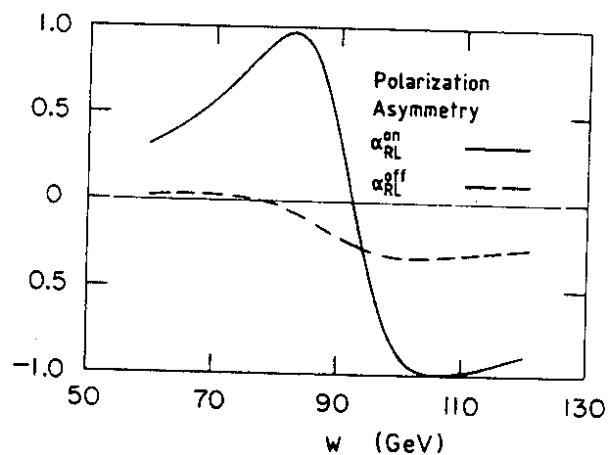
Fig. 4.1 The polarization asymmetry α_{RL}^{on} on top of an S-wave toponium resonance as a function of the toponium mass, compared with the corresponding value of the $\mu^+\mu^-$ continuum. From Ref. [24].
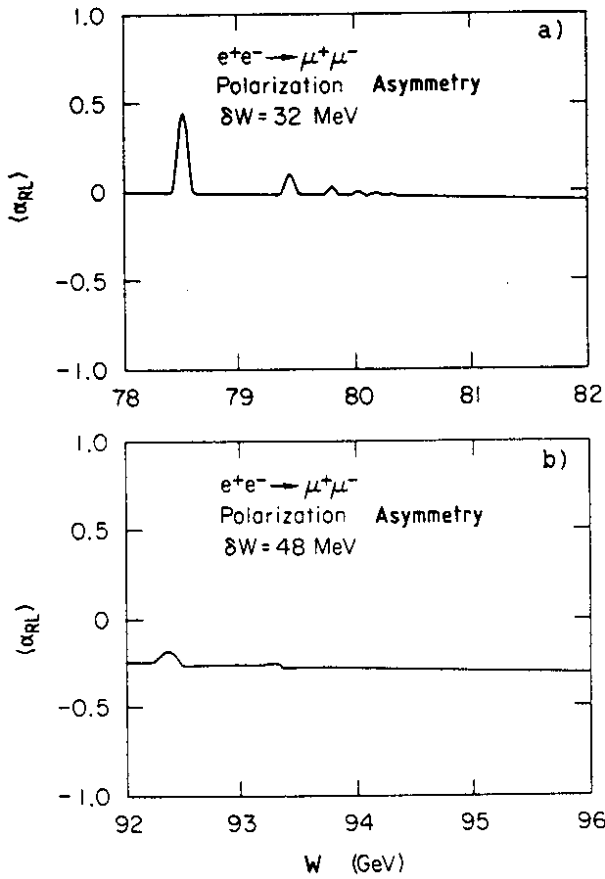
Fig. 4.2 Polarization asymmetry $\langle \alpha_{RL} \rangle$ in μ-pair production averaged over the beam profile for top quark masses of a) 40 GeV and b) 47 GeV (radiative corrections are not taken into account). From Ref. [24].

As an illustration, we show in Fig. 4.2 the variation of $\langle \alpha_{RL} \rangle$ for the μ-pair final state--assuming that toponium is located in the 80 GeV region.

For the realistic case where both the electron and the positron beams are only partially polarized, of degree P_- and P_+, the relative difference in the cross-section is given by $\alpha_{RL} \cdot P_{eff}$, where

$$P_{eff} \equiv \frac{P_- - P_+}{1 - P_+ P_-} = \frac{2P_-}{1 + P_-^2} \ . \tag{4.8}$$

The statistical error expected for this measurement is given by

$$\Delta\sigma_{RL}^{on} = \frac{(1+\eta)}{\sqrt{N}} \sqrt{\left(\frac{1}{P_{eff}^2} - \langle \alpha_{RL} \rangle^2 \right) + \eta^2 (\langle \alpha_{RL} \rangle - \alpha_{RL}^{off})^2} \ . \tag{4.9}$$

In addition, one has to take into account the systematic error from the uncertainty in the beam polarization:

$$\Delta\alpha_{RL}^{on}(sys.) = \alpha_{RL}^{on} \frac{\Delta P_{eff}}{P_{eff}} = \alpha_{RL}^{on} \frac{(1-P_-^2)}{(1+P_-^2)} \frac{\Delta P_-}{P_-} \ . \tag{4.10}$$

Table 4.1

Polarization asymmetry α_{RL}^{on} for different values of m_θ, the ratio η, the required statistical error $\Delta\alpha_{RL}^{on}$, and the continuum and resonance contributions to R. The number of events and the integrated luminosity needed to achieve 0.1 statistical error on α_{RL}^{on} for 100% and 50% beam polarization are listed, together with the systematic error on α_{RL}^{on}, assuming $\Delta P_{beam} = \pm0.05$

m_θ (GeV)	60	70	80	83	90	100	110
α_{RL}^{on}	0.32	0.55	0.92	0.99	0.48	-0.90	-0.97
η(hadron events)	0.4	0.77	2.2	3.3	6.4	18	20
$\Delta\alpha_{RL}^{on}$	0.1	0.1	0.1	0.1	0.1	0.1	0.1
$R^{off} + R^{res}$ (hadron events)	19	18	29	44	250	440	140
100% polarization							
N_{evts}	187	297	1349	2838	6851	49951	65345
L (pb^{-1})	0.2	0.4	1.7	2.5	1.2	6.5	32.5
50% polarization							
N_{evts}	298	474	1925	3878	9931	70257	90152
L (pb^{-1})	0.5	1.2	3.9	5.6	2.9	14.7	71.8
Syst. error ($\Delta P/P = 0.1$)	0.02	0.03	0.06	0.06	0.02	0.05	0.06

In Table 4.1 we have listed the number of hadronic events needed to achieve $\Delta\alpha_{RL}^{on} = 0.1$, together with the required integrated luminosity and the systematic error. The dilution of α_{RL}^{on} by the continuum is reduced for some masses (particularly above ~ 100-110 GeV) if we base this measurement on final states from SQDs. We have shown in subsection 3.2 that topological cuts will allow 95% of the hadronic continuum to be rejected, whilst 87% of the SQDs are retained.

Table 4.2

The integrated luminosity required in order to achieve $\Delta\alpha_{RL}^{on} = \pm 0.1$ with
longitudinally polarized beams: a) selecting SQD events through topological
cuts; b) selecting semileptonic SQD events. The underlined numbers indicate
cases where these cuts lead to an improvement

a) SQD events (87% signal, 5% background)

m_θ (GeV)	60	70	80	83	90	100	110
η	0.13	0.13	0.27	0.47	2.89	5.2	1.7
$R^{off} + R^{res}$	2.39	3.6	4.6	5.3	14.8	26.2	11.1
N_{evts}	190	169	173	259	2691	6954	1138
L (pb^{-1})	2.6	2.1	2.2	3.1	13.3	29.9	11.4

b) Semileptonic SQD events (no background!!)

m_θ (GeV)	60	70	80	83	90	100	110
η	0	0	0	0	0	0	0
R^{res}	1.1	1.7	1.9	1.9	2.0	2.2	2.1
N_{evts}	147	125	71	56	133	75	62
L (pb^{-1})	4.4	3.3	2.2	1.8	4.9	3.1	3.2

The resulting requirements on the counting rate for a statistical error of 0.1
are listed in Table 4.2. This also contains the numbers if we select the almost
background-free semileptonic SQDs.

In the early stages of LEP operation, longitudinally polarized beams will
not be available. However, for toponium there are a number of other possibilities
for determining α_{RL}, which we will now discuss.

4.2 Polarization of τ leptons

Assuming identical neutral-current couplings of electrons, muons, and τ
leptons, the longitudinal polarization of outgoing muons and τ's is given by

α_{RL} as defined in Eqs. (4.2) to (4.4). The polarization of τ's can be observed through the momentum distribution of their decay products[*]. For example, for the energy distribution of π's or ϱ's from τ decay [55, 56] one finds

$$\frac{dN}{dz} = \frac{1}{(1-r_h^2)} \left\{ 1 + \alpha_{RL} \frac{C_h}{1-r_h^2} \left[2z - (1 + r_h^2) \right] \right\} , \tag{4.11}$$

$$r_h^2 < z < 1 ,$$

where

$$r_h = m_{\pi,\varrho}/m_\tau ,$$

$$C_h = \begin{cases} 1 & , \quad \text{for } h = \pi \\ \dfrac{m_\tau^2 - 2 m_\varrho^2}{m_\tau^2 + 2 m_\varrho^2} & , \quad \text{for } h = \varrho . \end{cases}$$

For τ pair production in the continuum, this technique is discussed in more detail in the report of Altarelli et al. on precision studies [57]. Considering the small combined branching ratio on toponium, the expected statistical error will be large. Nevertheless, this piece of information could be used to resolve the sign ambiguity inherent in the determination of g_t^V/e_t through the forward-backward asymmetry.

4.3 Forward-backward asymmetry

Neutral-current effects and W exchange will also lead to a marked difference of the forward-backward asymmetry on and off resonance. The angular distribution for an arbitrary fermion-antifermion final state is given by

$$\frac{dN}{d \cos \theta} \propto 1 + \cos^2 \theta + 2\alpha_{FB} \cos \theta , \tag{4.12}$$

and a non-vanishing α_{FB} leads to a forward-backward asymmetry,

$$\frac{N_F - N_B}{N_F + N_B} = \frac{3}{4} \alpha_{FB} . \tag{4.13}$$

---

[*] The use of τ leptons to study weak effects on quarkonia was first emphasized in Refs. [55, 56].

As before, the measurement of α_{FB} for $W = m_\theta$ will be affected by the resonance and the continuum asymmetry. Ignoring interference between the two contributions, which is legitimate for $|m_\theta - m_Z| \gtrsim 2\Gamma_Z$,

$$|\alpha_{FB}| = \frac{\alpha_{FB}^{on} + \alpha_{FB}^{off}\eta}{1 + \eta} , \qquad (4.14)$$

where η again parametrizes the relative strength of continuum versus resonance. Under the same assumptions as before, α_{FB}^{on} is related to the polarization asymmetry (4.3) in a rather simple way [58]:

$$\alpha_{FB}^{on} = \alpha_{RL}^2 , \qquad (4.15)$$

and a similar relation can be derived also for quark-antiquark final states [58]:

$$\alpha_{FB}^{on}(q) = \alpha_{RL}\alpha_{RL}(q) , \qquad (4.16)$$

where $\alpha_{RL}(q)$ is defined analogously to $\alpha_{RL} = \alpha_{RL}(e)$ in Eq. (4.3).

The statistical error in the determination of α_{FB}^{on} for a sample of N lepton pairs is given by

$$\Delta\alpha_{FB}^{on} = \frac{1+\eta}{\sqrt{N}} \sqrt{(C - \langle\alpha_{FB}\rangle^2) + \eta^2(\langle\alpha_{FB}\rangle - \alpha_{FB}^{off})^2} , \qquad (4.17)$$

with $C = 16/9$ if we use only the forward-backward asymmetry

$$\frac{N_F - N_B}{N_F + N_B} = \frac{3}{4}\langle\alpha_{FB}\rangle , \qquad (4.18)$$

and $C = 8/5$ if we use the full shape of the distribution and evaluate $\overline{\langle\cos\theta\rangle}$ using

$$\overline{\langle\cos\theta\rangle} = \frac{1}{2}\langle\alpha_{FB}\rangle \quad \text{and} \quad \Delta\langle\alpha_{FB}\rangle = \frac{2}{\sqrt{N}}\sqrt{\frac{2}{5} - \left(\frac{\langle\alpha_{FB}\rangle}{2}\right)^2} . \qquad (4.19)$$

The asymmetry off resonance is given by

$$\alpha_{FB}^{off} = \frac{\sum\limits_{h_f, h_e} h_f h_e |F^C(h_f, h_e)|^2}{\sum\limits_{h_f, h_e} |F^C(h_f, h_e)|^2} . \qquad (4.20)$$
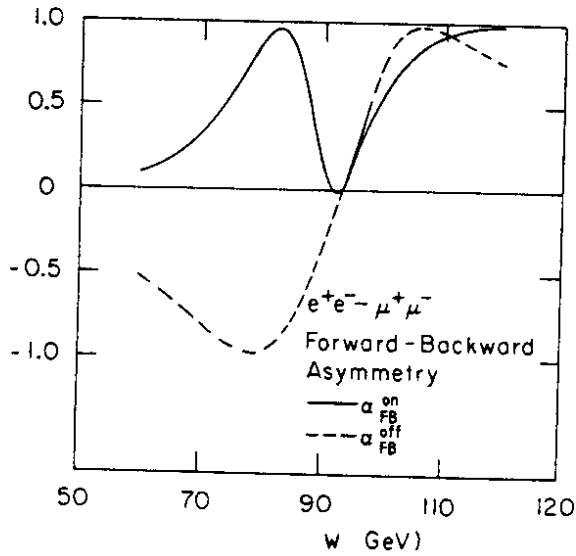
Fig. 4.3 The μ^- forward-backward asymmetry α_{FB}^{on} on top of an S-wave toponium resonance decaying into $\mu^+\mu^-$, compared with the continuum. From Ref. [24].
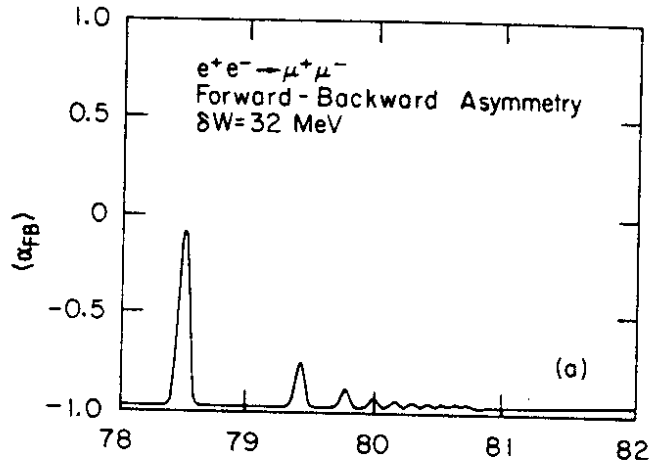
Fig. 4.4 μ^- forward-backward asymmetry $\langle\alpha_{FB}\rangle$ averaged over the beam profile for top-quark masses of a) 40 GeV and b) 47 GeV (radiative corrections are not taken into account). From Ref. [24].
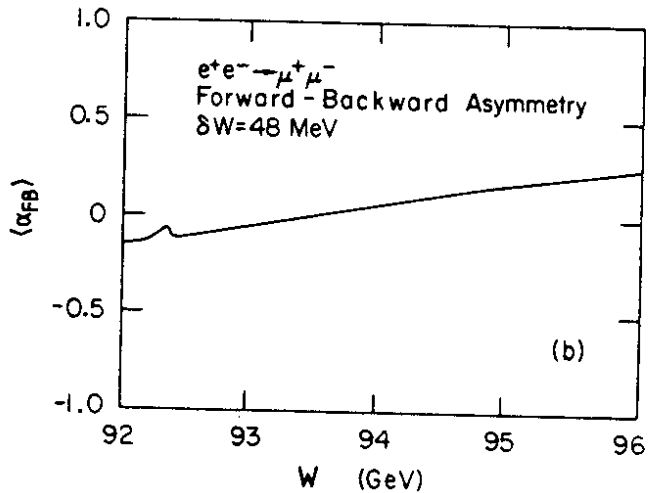
The asymmetries α_{FB}^{on} and α_{FB}^{off} for μ pairs are shown in Fig. 4.3 as a function of m_θ. Figure 4.4 shows the variation of $\langle\alpha_{FB}\rangle$ for the μ-pair final state with $m_t = 40$ GeV. In Table 4.3 we have listed the number of lepton pairs required to achieve either 10% statistical error on α_{FB}^{on}, or alternatively 10% error on $|\alpha_{RL}^{on}| = \int\alpha_{FB}^{on}$. The estimated integrated luminosity is based on μ pairs only. The inclusion of some or all of the τ-pair final states would reduce the luminosity requirements accordingly.

Toponium annihilation into $b\bar{b}$ and the resulting asymmetries [29] may give important information on the strength of the W exchange amplitude. The relative importance of this channel is strongly mass-dependent; furthermore, the possibility to tag B mesons will depend on the B-meson lifetime. In spite of these uncertainties it is worth while keeping this possibility in mind.

In passing we note that also azimuthal distributions might be different on and off resonance, if transversely polarized beams are available. The relevant formulae are given elsewhere [24].

Table 4.3

The integrated luminosity required in order to achieve $\Delta\alpha_{FB}^{on} = 0.1$ and, alternatively, $\Delta|\alpha_{RL}^{on}| = 0.1$, through a measurement of the μ-pair asymmetry. For $m_\theta = 100$ and 110 GeV the upper (lower) values are without (with) radiative corrections applied to the continuum. The other energies are always with radiative corrections

m_θ (GeV)	60	70	80	83	90	100	110
α_{RL}^{on}	0.10	0.30	0.84	0.97	0.23	0.81	0.93
α_{FB}^{off}	-0.51	-0.75	-0.98	-0.90	-0.46	0.55	0.94
$\eta_{\mu\mu}$	1.13	1.63	3.3	4.4	7.1	$\frac{12.3}{24.8}$	$\frac{18.8}{51.2}$
$\langle\alpha_{FB}\rangle$	-0.22	-0.34	-0.34	-0.55	-0.37	$\frac{0.57}{0.56}$	0.94
$R^{off} + R^{res}$	2.37	2.27	2.6	3.2	13.8	$\frac{11.9}{23.0}$	$\frac{3.12}{8.36}$
$\Delta|\alpha_{RL}^{on}|$	0.1	0.1	0.1	0.1	0.1	0.1	0.1
$\Delta\alpha_{FB}^{on}$	0.06	0.10	0.18	0.20	0.10	0.18	0.19
$N_{\mu\mu}$	2085	1321	1863	2694	12052	$\frac{7300}{28000}$	$\frac{7500}{54000}$
L (pb^{-1})	36	33	53	67	81	$\frac{71}{139}$	$\frac{337}{901}$
$\Delta|\alpha_{RL}^{on}|$	0.1	0.1	0.1	0.1	0.1	0.1	0.1
$N_{\mu\mu}$	728	1321	6037	10778	12052	$\frac{23652}{40000}$	$\frac{27000}{195000}$
L (pb^{-1})	12	33	171	276	81	$\frac{228}{415}$	$\frac{1217}{3255}$

4.4 Polarization measurements
through semileptonic single-quark decays

A convenient method of determining the polarization asymmetry is based on the analysis of leptons from SQDs [59]. The polarization asymmetry leads to a longitudinal polarization of toponium even for unpolarized beams:

$$\langle\vec{S}\cdot\vec{n}_e\rangle = \alpha_{RL}^{on} \ . \tag{4.21}$$

The parity-violating SQDs provide a convenient tool for analysing the spin of
toponium. Since t and t̄ are in a spin triplet S-wave state, their polarization
is also given by Eq. (4.21). The angular distribution of leptons from the decay
of a top quark is correlated with the top spin through

$$dN \propto (1 + \vec{n} \cdot \vec{s}) \, d\Omega \ . \tag{4.22}$$

The remaining t (or t̄) quark is converted into a top-meson T or T*, and the
T and T* both decay weakly [60]. For leptons from this second step this leads
to a partial depolarization by a factor of 1/2. The angular distribution of
positive leptons from t decay is finally given by

$$dN \propto \left(1 + \frac{3}{4} \, \alpha_{RL} \cos \theta\right) d \cos \theta \ , \tag{4.23}$$

and for negative leptons from t̄ decay the sign is obviously reversed.

Events from semileptonic SQDs can be discriminated against the background
through their characteristic topology and their hard isolated lepton. The
statistical error on the measurement of α_{RL} through this method is

$$\Delta\alpha_{RL} = \frac{1}{\sqrt{N}} \sqrt{C_{SQD} - \langle\alpha_{RL}\rangle^2} \simeq \frac{8}{3} \frac{1}{\sqrt{N}} \ , \tag{4.24}$$

and $C_{SQD} \simeq 64/9$ or 16/3 depending on whether we base the analysis on the forward-
backward asymmetry or on $\langle\cos\theta\rangle$. The requirements for the counting rate and
running time to achieve $\Delta\alpha_{RL} = 0.1$ are listed in Table 4.4.

<div align="center">Table 4.4</div>

The integrated luminosity required in order to achieve $\Delta\alpha_{RL}^{on} = 0.1$ through a
measurement of lepton asymmetries in semileptonic SQDs

m_θ (GeV)	60	70	80	83	90	100	110
α_{RL}^{on}	0.30	0.55	0.92	1.0	0.48	-0.9	-0.97
$\Delta\alpha_{RL}^{on}$	0.1	0.1	0.1	0.1	0.1	0.1	0.1
4/9 R_{SQD}	1.1	1.7	1.9	1.9	2.0	2.2	2.1
N_{evts}	524	503	448	433	510	452	4394
L (pb^{-1})	19.7	16.7	17.4	18.1	23.8	23.7	29.1

The advantage of this method is twofold: first, the branching ratio for semileptonic SQDs is larger than the μ-pair rate, apart from a narrow mass range very close to m_Z; secondly, there are no continuum events which feed into this channel, so that a smaller sample leads to a relatively smaller statistical error.

4.5 Summary

In Table 4.5 we have compared the requirements on the integrated luminosity in units of pb^{-1} ($\simeq$ 24 hours at L = 10^{31} cm^{-2} s^{-1}). It is apparently quite possible to achieve $\Delta\alpha_{RL}$ = 0.1 through the lepton-pair asymmetry within the first year of toponium physics. Longitudinally polarized beams reduce the time requirement by a sizeable amount, and the systematic error from ΔP/P would dominate relatively quickly in this case. However, for the method based on semileptonic single-quark decays, the luminosity requirements are also modest.

Table 4.5

Comparison of the various methods in terms of integrated luminosities (pb^{-1}) required in order to achieve a statistical error of 0.1 on α_{RL}^{on}

m_θ (GeV)	60	70	80	83	90	100	110
Polarized beams (P = 0.5)							
Hadron events	0.5	1.2	3.9	5.6	2.9	14.7	71.8
SQDs	2.6	2.1	2.2	3.1	13.3	29.9	11.4
Semileptonic SQDs	4.4	3.3	2.2	1.8	4.9	3.1	3.2
Unpolarized beams							
FB	36	33	53	67	81	$\frac{71}{139}$	$\frac{337}{901}$
Semileptonic SQDs	19.7	16.7	17.4	18.1	23.8	23.7	29.1

A statistical error below 0.1 is easily attainable in this case, and the main limitations will be set by the systematic error. A measurement of α_{RL} to an accuracy of 0.05 would be sensitive to radiative corrections within the standard model. Depending on the toponium mass, this might lead to an independent determination of $\sin^2 \theta_w$ with an accuracy of up to 4 x 10^{-3} [61].

5.   SEARCH FOR HIGGS PARTICLES

Higgs particles are an inescapable ingredient of present gauge theories of the electroweak interactions. They are the vestige of symmetry breaking and they are responsible for mass generation of the known particles. Their experimental investigation is, then, of the highest importance [62, 63].

In the minimal Weinberg-Glashow-Salam model, one neutral Higgs particle H^0 is needed. In extensions of the standard model (e.g. SUSY, technicolour, etc.) many charged and neutral Higgs-like scalars are expected: H_1^0, H_2^0, ...; H_1^+, H_2^+, ...

In both cases, the masses of these particles are almost completely undetermined; on the other hand, the fermion-Higgs couplings g_{fH} are usually assumed to be proportional to the fermion (quark or lepton) masses. This immediately suggests that toponium is an interesting source of Higgs particles with masses $m_H < m_\theta$.

5.1 Charged Higgs scalars

The detection of charged Higgs particles with masses less than the top-quark mass m_t will certainly be easy since, in this case, the heavy quark (antiquark) of the bound state will predominantly decay into an H^+ (H^-) and a b ($\bar{b}$) quark (Fig. 2.6g): The amplitude for this decay is proportional to $\xi_{Htb}(m_t/v)$, where ξ_{Htb} represents an unknown (t, b) mixing angle and v is the Higgs vacuum expectation value. The relative widths for toponium decays into charged Higgs scalars and SQD are connected by the relation [8]

$$\Gamma_{H^\pm}/\Gamma_{SQD} \simeq \xi_{Htb}^2 \frac{10^2}{[m_t (100 \text{ GeV})]^2} .$$ (5.1)

It can be seen from this formula that, with the prejudiced value $\xi_{Htb} = 1$, the $H^\pm$ decay becomes the dominant one, and consequently the decay branching ratios indicated in Fig. 2.10 will be very much suppressed. Even if ξ_{Htb} is reduced by more than one order of magnitude, the toponium decay into charged Higgs scalars will still be sizeable, the preferred decay modes of a $H^\pm$ being $H^+ \to \bar{b}c$, and then $H^\pm \to \tau^+ v$.

It is worth noticing that the UA1 data [4] interpreted as the manifestation of a t-quark with $m_t \simeq 40$ GeV, would exclude a maximally coupled charged Higgs scalar with $m_{H^\pm} < m_t$.

5.2 Neutral Higgs scalars

The importance of the heavy vector-meson decay into $H^0 + \gamma$ (Fig. 2.6e) was first recognized by Wilczek [64]. For toponium--neglecting radiative corrections and QCD corrections [65, 66]--the decay width for this channel can be written [cf. (2.18)],

$$\Gamma(\theta \to H^0\gamma) = \frac{1}{8 \sin^2 \theta_w} \frac{m_\theta^2}{m_W^2} \left(1 - \frac{m_{H^0}^2}{m_\theta^2}\right) \Gamma_0(\theta) \ . \tag{5.2}$$

For m_{H^0} not too close to m_θ and using the parameters given in (2.24) and (2.25), we obtain $\theta \to H^0\gamma$ branching ratios in the 1-3% range for θ masses in the LEP energy domain (cf. Fig. 2.10). This has to be compared with the equivalent bottomonium branching ratio, which is smaller by two orders of magnitude.

This reaction has a clean signature characterized by a monochromatic photon, the Higgs mass being determined by the missing-mass technique.

In order to estimate roughly the sensitivity needed to discover an eventual neutral Higgs scalar particle, we have first estimated (Table 5.1) the production rates of θ and of continuum events for three θ masses, 70, 90, and 110 GeV, using the R^θ and $R^{\gamma,Z}$ values shown in Fig. 2.16. The corresponding event numbers obtained for 1000 hours of running time under LEP 13 (3 mA) conditions are given in Table 5.2 for different m_{H^0} values. One notices from this table that the event rates are quite high, even for large Higgs masses.

<u>Table 5.1</u>

Number of events from the continuum
and from the resonance per 1000 hours

W (GeV)	70	90	110
$N^{\gamma,Z}$	4 700	114 000	68 000
N^θ	7 500	26 800	3 600

<u>Table 5.2</u>

Number of $\theta \to H^0 + \gamma$ events per 1000 hours
for different choices of m_{H^0}

m_θ (GeV) [∫ L dt (pb^{-1})] \ m_{H^0} (GeV)	10	30	50	60	70	80	85	90	100
70 [32]	202	160	102	52					
90 [49]	107	95	75	60	43	22	12		
110 [65]	39	36	31	28	25	19	16	13	7

We have then computed the inclusive photon background originating from
- the γ and Z contribution generated according to the Lund model;
- the contribution due to competing θ decays, weighted with their relative
  branching ratios as indicated in Fig. 2.10.

In each case, a $|\cos \theta_\gamma| \leq 0.98$ cut, which virtually does not affect the
signal, was applied to essentially eliminate photons from initial-state radiation.

5.2.1 Hadronic background

The inclusive spectra originating from the various background reactions are
shown in Figs. 5.1, 5.2, and 5.3 for m_θ = 70, 90, and 110 GeV, respectively.
They have been arbitrarily normalized to 10^5 Lund (γ, Z) events. The corres-
ponding rates of monochromatic photons from the $\theta \to H^0 \gamma$ reaction are also indi-
cated for various Higgs masses.

From these curves, summing up the various inclusive contributions to obtain
the final background spectrum at each energy, it is possible to estimate the
integrated luminosity needed to detect a H^0 particle. As an example, Fig. 5.4
shows the typical integrated luminosities needed to detect a 3σ effect with a 4π
acceptance BGO detector. With a gaseous detector the energy resolution is about
five times worse, whilst the granularity in position allows π^0's up to 20 GeV to
be identified with ~ 90% probability. In other words, in the high-mass region,
because of these compensating factors the gaseous detectors will show similar
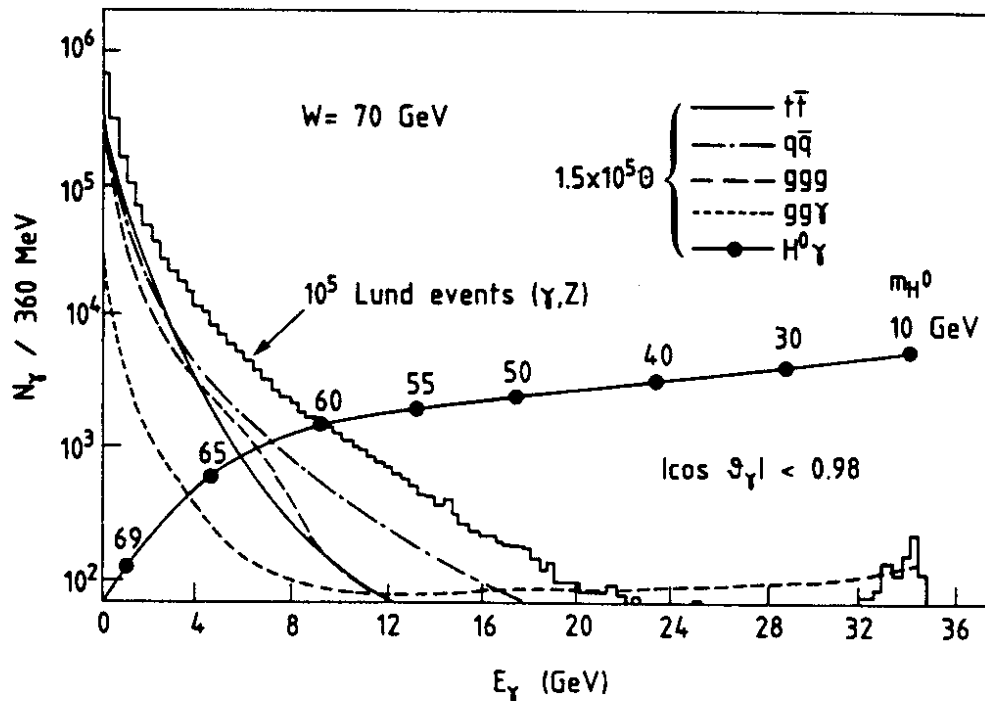
Fig. 5.1 Complete inclusive photon spectrum for different Higgs masses at
$W = m_\theta$ = 70 GeV, normalized to 10^5 continuum Lund events
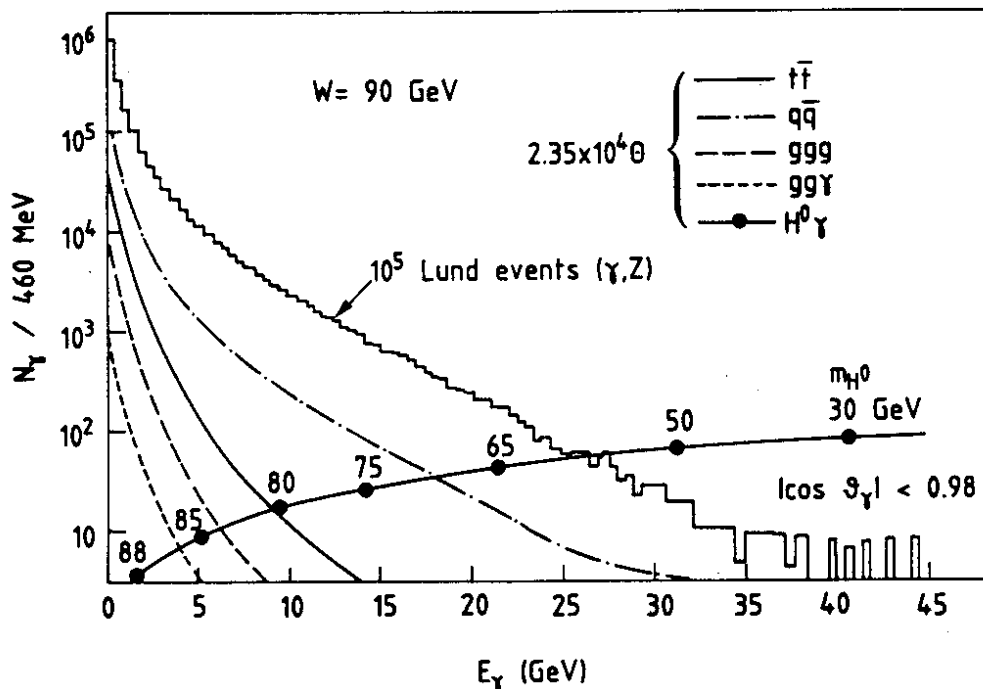
Fig. 5.2 Complete inclusive photon spectrum for different Higgs masses at
$W = m_\theta$ = 90 GeV, normalized to 10^5 continuum Lund events
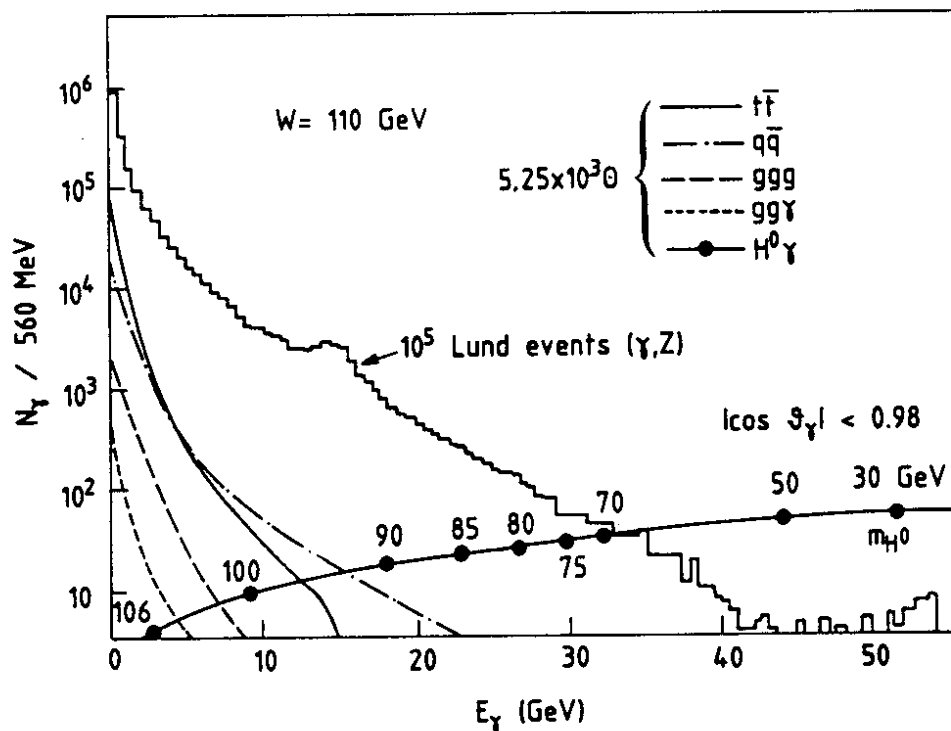
Fig. 5.3 Complete inclusive photon spectrum for different Higgs masses at
$W = m_\theta$ = 110 GeV, normalized to 10^5 continuum Lund events

$m_\theta = 70$ GeV $m_\theta = 90$ GeV $m_\theta = 110$ GeV

150   150   150

100   100

$\int L\, dt$ (pb^{-1})

50   50   50

50   50

10

0   0   0

50 60 70   50 60 70 80   50 60 70 80

$m_H{}^0$ (GeV)
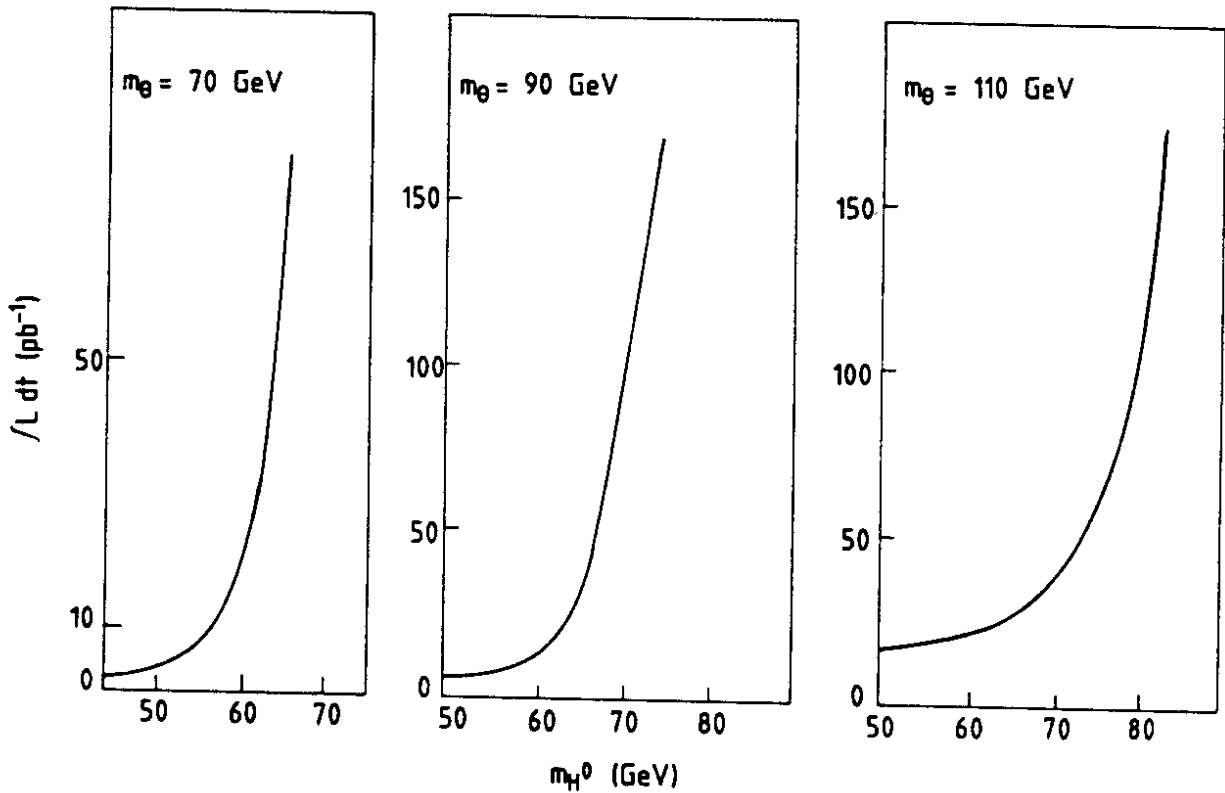
Fig. 5.4 Integrated luminosity required to detect a Higgs particle as a 3σ
effect with a 4π detector by means of the inclusive photon spectrum

signal-to-background ratios, and thus Fig. 5.4 also essentially applies. It can
be seen that, without any special requirement on the final-state topology, the
detection of inclusive photons will allow Higgs mass values such as $m_H{}^0 \leq$
$(0.7-0.8)m_\theta$ to be reached quite easily.

On the other hand, as shown in Fig. 5.3 the inclusive γ background due to
hadron jets can be very severe when $m_\theta \sim m_Z{}^0$ for large Higgs masses. In order
to improve the signal-to-background ratio one can make use of the final-state
topology of the events ($H^0\gamma \to b\bar{b}\gamma$). Since only two- and three-jet topologies
can simulate the Higgs channel, the single-quark decay mode ($\sim t\bar{t}$) can be
efficiently eliminated. The two-jet topologies are characterized by angular
collimation of high-energy particles so that a conservative angular cut (e.g.
200 mrad for a 10 GeV particle) should remove more than 90% of the background.
Finally, in the three-jet cases, the γ background will also emerge from a
cluster of collimated particles. It is thus possible to require an isolation
criterion in order to reduce this background. Although no detailed simulation
yet exists, our present guess is a reduction of the order of 10. These
improvements would allow the limit on $m_H{}^0$ to be increased by about 5 GeV.

In addition to the inclusive photon peak, a Higgs signal would be charac-
terized by the presence of b$\bar{b}$ jets. The microvertex detectors can provide this
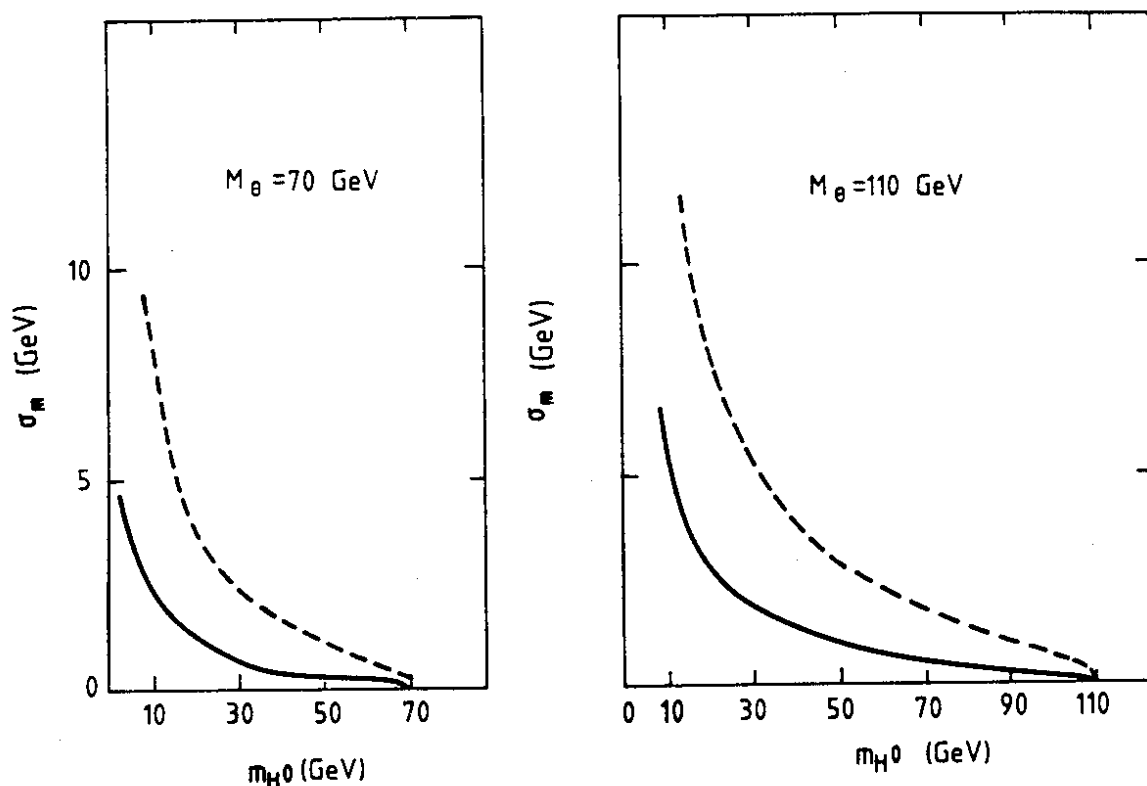
Fig. 5.5 Uncertainty in the Higgs mass determination (per event) as a function of m_H^0 for a BGO detector (full line) and a gaseous detector (dashed line)

very useful signature since they have a good tagging efficiency ($\geq$ 50%, to be compared with the semileptonic decay method), with low contamination (typically 25% from $c\bar{c}$ pairs when keeping 75% of $b\bar{b}$ events).

With these various requirements, running for less than one year will allow the mass limit on H^0 to be pushed up to typical values of 65, 80, and 85 GeV for m_θ = 70, 90, and 110 GeV, respectively.

The precision on the H^0 mass per event is indicated in Fig. 5.5 for two types of electromagnetic detectors. It differs typically by a factor of 3-5, and in both cases the precision improves when the H^0 mass increases. Obviously the precision of the final determination of the Higgs mass has to include the statistical and systematic errors.

Figure 5.6a shows, as a function of m_θ, the H^0 mass region that can be investigated at LEP with the reaction $\theta \to H^0\gamma$. The contour of the domain is fixed by m_θ > 44 GeV, m_θ > m_H^0, and the rate limit below which this reaction is meaningless. This rate limit has been determined using the parameters of LEP given in Ref. [38], and the luminosity growth was assumed to be linear in energy for beam energies above 60 GeV. It has been taken arbitrarily as 0.1 event per 'day' ($\simeq$ 10 events per year). As already mentioned, the two-jet background is unimportant unless $m_H^0 \sim m_\theta$ (close to the diagonal of the plot), in which case
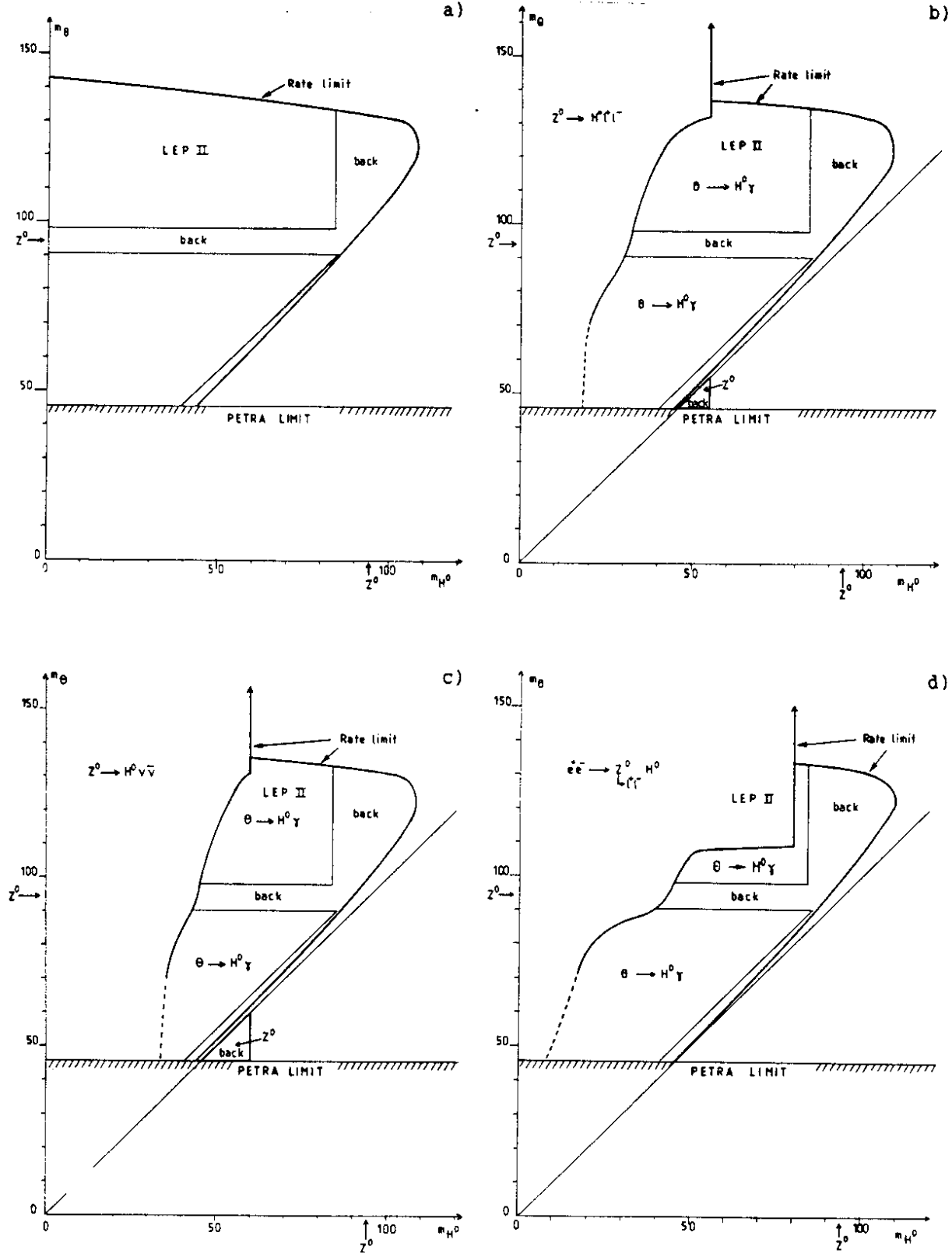
Fig. 5.6 a) Accessible range of Higgs masses (abscissa) for given toponium mass (ordinate); in the 'back' regions the Higgs search is more difficult owing to background. b-d) Comparison of Higgs search in θ and Z^0 decays. The indicated process has a higher rate.

the limit depends on the details of the topological cuts and on the properties of the detector.

5.2.2 Radiative contaminations

Two difficult regions are indicated as 'back' in Fig. 5.6a. They occur in the following two cases:

a) $m_\theta \sim m_Z0$

In this case the radiative process $Z^0 \rightarrow q\bar{q}\gamma$ has a very high rate. Owing to the strong dependence of the cross-section on the initial energy, only radiation in the final state is contributing. Asking for a minimal angle θ between the quark and the photon of momentum k, the following radiation probability is obtained:

$$P_R = \frac{2\bar{\alpha}}{\pi} \log \frac{1 + \cos \theta}{1 - \cos \theta} \frac{\Delta k}{k} F \left(\frac{k}{E}\right) , \qquad (5.3)$$

where

F(k/E) is close to 1 when k/E is not too large (otherwise, QED and QCD corrections should be introduced);

$\bar{\alpha} = 0.225 \, \alpha_{em}$ if $\sin^2 \theta_w = 0.215$ [*] ;

$\Delta k/k$ is fixed by the energy resolution of the electromagnetic calorimeter. Now we can estimate the signal-to-background ratio

$$\frac{S}{B} = \frac{R^{H^0 \gamma}}{R^{Z^0} \cdot P_R} \approx \begin{cases} 2/3, & \text{BGO detector ,} \\ \\ 1/6, & \text{gaseous detector .} \end{cases} \qquad (5.4)$$

Given that the $H^0\gamma$ rate is $\simeq 2$ per day, the 3σ level will be reached in 7 (27) days with a BGO (gaseous) detector. The ability to detect H^0 in this region will be very much detector-dependent, the situation becoming very difficult anyway when $m_\theta \simeq m_H0$.

b) $m_\theta > m_Z0$ and $m_H0 \simeq m_Z0$

In this case the reaction $e^+e^- \rightarrow \theta \rightarrow H^0\gamma$ will produce a photon which has the same energy as that of the radiative process $e^+e^- \rightarrow Z^0\gamma$.

Requiring a minimum angle β of the photon with respect to the beam direction, one obtains the following probability for a photon to fall in the peak region, diluted by the Breit-Wigner of the Z^0:

---

[*] $\bar{\alpha}$ is the electromagnetic fine-structure constant weighted by the charges of the various flavours times the branching ratios at Z^0.

$$P_R = \frac{\log\left[(1 + \cos\,\beta)/(1 - \cos\,\beta)\right]}{2\left(\log\frac{2E}{m_e} - \frac{1}{2}\right)} \frac{\Delta E_\gamma}{\Gamma} \simeq 0.2\,\frac{\Delta E_\gamma}{\Gamma}\ , \qquad (5.5)$$

where ΔE_γ is the energy resolution of the detector and Γ is the Z^0 width. Owing to the very large rate of the radiative Z^0 events compared with the $\theta \to H^0\gamma$ (see Fig. 2.16 and Table 5.2), one finds that $S/B \leq 1/100$, and we conclude that the search for H^0 through toponium seems difficult if $|m_{H^0} - m_{Z^0}| < 10$ GeV.

5.2.3 Comparison with other processes

Finally, in order to evaluate the quality of the toponium decay method, we compare it with other processes that are considered more frequently [62].

a) $Z^0 \to H^0 l^+ l^-$

This process will probably be the first one to give information on the H^0 mass, since LEP will certainly start to run for a significant length of time on the Z^0 pole. The rate limit of 0.1 event per day is reached for $m_{H^0} = 55$ GeV (straight vertical line in Fig. 5.6b when e^+e^- and $\mu^+\mu^-$ modes are added).

Taking into account the LEP machine parameters, one can compare, for the accessible mass domain previously defined, the rate given by toponium and the rate given by $H^0 l^+ l^-$. The border line given in Fig. 5.6b corresponds to equal rates. From this curve one concludes that, on the average, toponium wins when $m_{H^0} > 30$ GeV.

Remarks

- The main background to $H^0 l^+ l^-$ comes from

$$Z^0 \to t \qquad\qquad \bar{t}$$
$$\ \vdash\!\!\to l^+ + X\ \vdash\!\!\to l^- + X\ .$$
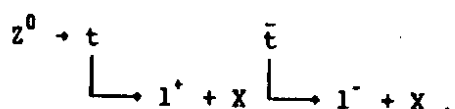
  This background is concentrated at large Higgs masses, which confirms the advantage of toponium in the search for heavy Higgs scalars.
- A very peculiar situation occurs when $m_\theta < m_{H^0}$ with $m_{H^0} < 55$ GeV, in which case only the $H^0 l^+ l^-$ process is operative.

b) $Z^0 \to \nu\bar{\nu}H^0$

This process has a higher rate than the previous one but is much less constrained and requires specific cuts to eliminate the background. The H^0 mass can be obtained by combining the information from the central detector and from the electromagnetic and hadronic calorimeters. One expects then a resolution of the order of $0.8/\sqrt{m_{H^0}}$ (FWHM), i.e. $\Delta m_{H^0}/m_{H^0} \simeq 0.15$ for $m_{H^0} = 30$ GeV.

Here as well the main background originates from $t\bar{t}$ decays, and it is also concentrated at large Higgs masses. The comparison with the $\theta \rightarrow H^0\gamma$ method is made in Fig. 5.6c.

c) $e^+e^- \rightarrow Z^0 + H^0$ $(Z^0 \rightarrow \mu^+\mu^-, e^+e^-)$

It has been shown [62] that this process is efficient as long as the condition $W \gtrsim m_{Z^0} + \sqrt{2}m_{H^0}$ is fulfilled, i.e. for $m_{H^0} < 80$ GeV at maximal LEP II energy. This limit is shown in Fig. 5.6d, where the rate comparison with the $\theta \rightarrow H^0\gamma$ method is also made. In this figure we show the border, on the left-hand side of which the reaction $e^+e^- \rightarrow Z^0 + H^0 (Z^0 \rightarrow l^+l^-)$ produces more events. One sees that here also, for $m_\theta \lesssim 110$ GeV, the $\theta \rightarrow H^0\gamma$ process will be more efficient for producing large H^0 masses.

5.3 Summary and conclusions

After a careful estimate of signal and background rates, we have found that toponium is an excellent place to search for heavy Higgs-like scalar particles.

Charged Higgs particles with masses less than the mass of the top quark $(m_{H^\pm} < m_t)$ will be easy to find if ξ_{Htb}, which represents the unknown (tb) mixing angle, is not too small.

Using the $\theta \rightarrow H^0\gamma$ toponium decay channel, it appears possible to discover neutral Higgs scalar particles with masses $m_{H^0} < (0.7-0.9)m_\theta$ (depending on the θ mass) within a reasonable running time. The missing-mass technique will allow the H^0 mass to be determined with a precision of less than one GeV. We have also shown that this method compares favourably with other reactions for 30 GeV $< m_{H^0} < 85$ GeV. In particular, if the toponium mass is in the LEP I energy range, the process $\theta \rightarrow H^0\gamma$ will allow H^0 mass values to be reached, which are only achievable in the LEP II range through the reaction $e^+e^- \rightarrow Z^0H^0$.

6. SUPERSYMMETRY AND TOPONIUM DECAYS

A number of toponium decays have been proposed which could allow some of the particles predicted by supersymmetry[*] to be detected and their masses to be determined. The drastically different scenarios which are summarized in Tables 6.1 and 6.2 depend on the choice of the unknown masses of the t-quark and of the various postulated new particles. Various supersymmetric models make specific predictions for relations between different masses. Nevertheless, considering the large variety of models, we will consider the masses as free parameters, solely constrained by the available experimental information.

---

*) For recent reviews, see Refs. [67], [68] and, especially, [69].

Table 6.1

Toponium decays in supersymmetric models

with $m_t > m_{\tilde{t}} + m_{\tilde{\gamma}}$, $m_{\tilde{g}} > m_{\tilde{\gamma}}$

Assume $m_{\tilde{g}} > m_{\tilde{\gamma}}$ and ignore nearly degenerate mass assignments where allowed modes are drastically phase-space suppressed

---

Top heavier than lightest SUSY particle

No → SUSY irrelevant for toponium

Yes ↓

$m_t > m_{\tilde{t}} + m$ (gaugino)

No → Only SUSY anni-hilation decays. Standard decays of open top! See Table 6.2.

Yes ↓

Supersymm. SQDs are dominant! Toponium decays are drastically modified! Also, open top decays into $\tilde{t}$ + gaugino   1)

$m_t > m_{\tilde{t}} + m_{\tilde{g}}$

Yes ←   → No

Yes: Extremely large decay rates for $(t\bar{t}) \rightarrow (\tilde{t} + \tilde{g} + \bar{t})$ or c.c. $\Gamma_{tot} \gtrsim 1$ GeV $> m(2S) - m(1S)$! No individual resonances.

No: $m_t > m_{\tilde{t}} + m_{\tilde{\gamma}}$, $(t\bar{t}) \rightarrow (\tilde{t} + \tilde{\gamma} + \bar{t})$ or c.c. allowed and dominant! $\Gamma_{tot} \sim 100$ MeV. Individual resonances remain distinguishable.

↕ Denotes cases where the appearance of toponium is drastically changed.

1) Probably excluded by the observation of semileptonic top decays at the collider.

Table 6.2

Toponium decays in supersymmetric models

with $m_t < m_{\tilde{t}} + m_{\tilde{\gamma}}$, $m_{\tilde{g}} > m_{\tilde{\gamma}}$

Supersymmetric annihilation decays for different mass assignments

---

$m_t > m_{\tilde{g}}$ and $m_t < m_{\tilde{t}}$
→ decays into gluino pairs
are possible (evtl. + anything)

$m_t \ll m_{\tilde{t}}$

Yes:

Production of gluinos through intermediate gluons!
→ α_s corrections to ordinary hadronic decays. For example,

$Br[1^{--} \rightarrow g + g + \tilde{g} + \tilde{g})] \sim 1\%$

$Br[2S \rightarrow \gamma + {}^3P_J (\rightarrow g + \tilde{g} + \tilde{g})] \sim 0.1\%$

$Br[1^{--} \rightarrow \gamma + (\tilde{g}\tilde{g})] \sim 10^{-3}$ (for Υ)
$\sim 10^{-3}$ (for 60 GeV) $^{4)}$

No:

$m_t \lesssim m_{\tilde{t}}$
Gluino pair production through $\tilde{t}$ exchange

$m(\tilde{t}_R) = m(\tilde{t}_L)$

Yes:

P and C conserved.
$1^{--} \rightarrow \tilde{g} + \tilde{g}$ forbidden.
${}^3P_J \rightarrow \tilde{g} + \tilde{g}$ allowed and
for 1^{++} dominant.
$1^{--} \rightarrow \tilde{g} + \tilde{g} + \gamma$ and $\tilde{g}\tilde{g}\gamma$
allowed. $^{3)}$

No:

$1^{--} \rightarrow \tilde{g}\tilde{g}$ allowed and for
nearly all masses dominant.
${}^3P_J \rightarrow \tilde{g}\tilde{g}$ allowed, but
negligible $Br(2S \rightarrow {}^3P_J + \gamma)$.

$m_t > m_{\tilde{g}}$ and $m_t > m_{\tilde{t}}$
→ complicated mixture of → $\tilde{g} + g + g$
and → $\tilde{t} + \tilde{t}$

$m_t > m_{\tilde{t}}$ and
$m_t < m_{\tilde{g}}$ $^{1)}$

$m_t \lesssim m_{\tilde{g}}$

Yes:

$(t\bar{t}) \rightarrow \tilde{t}\tilde{\bar{t}}$
through $\tilde{t}$ exchange
dominant.

No →

$m_t < m_{\tilde{t}}$ and $m_t < m_{\tilde{g}}$
$m_t > m_{\tilde{\gamma}}$

$(t\bar{t}) \rightarrow \tilde{\gamma} + \tilde{\gamma}$ like $\rightarrow \nu + \bar{\nu}$
$Br(\rightarrow \tilde{\gamma} + \tilde{\gamma})$ several %.
$(t\bar{t}) \rightarrow \tilde{g} + \tilde{\gamma} + g$ access to
large gluino masses. $^{2,3)}$ *

→ $\tilde{g}$ far heavier than t
$(m_{\tilde{g}} \gtrsim 3m_t)$
Gluino exchange suppressed!
Photino exchange allowed!
Small, but not unreasonable
rates for
$(t\bar{t}) \rightarrow \tilde{t} + \tilde{t}$ and
$\rightarrow \tilde{\gamma} + \tilde{\gamma}$ $^{1)}$

↙↘ Denotes cases where the appearance of toponium is drastically changed.

* Denotes cases that are consistent with semileptonic decays of open top and with currently favoured mass assignments.

1) Note that this scenario is only allowed for $m_t < m_{\tilde{t}} < m_{\tilde{t}} + m_{\tilde{\gamma}}$ in order to avoid the supersymmetric SQD. Since $m_{\tilde{\gamma}}$ is normally assumed to be small, this can occur only for a very restricted mass range.

2) This mode is of interest, since it gives access to very heavy gluinos.

3) If kinematically allowed, the supersymmetric analogue of Wilczek's decay could be of interest

4) This situation would be characteristic for light gluinos in Υ decays.

In toponium decays we have to consider two fundamentally different classes of processes: The first class, which is summarized in Table 6.1, consists of single-quark decays into supersymmetric (SUSY) particles. These decays are only possible if $m_t > m_{\tilde{t}} + m_{gaugino}$. If it were kinematically allowed, they would dominate the weak decays of open top by a large factor and completely change the appearance of both toponium and open-top mesons. Since open top is expected to be discovered and studied before the toponium search is started, the dramatic change of toponium properties would be anticipated.

The second class of decay modes, summarized in Table 6.2, are annihilation decays. Depending on the masses of the various SUSY particles, the resulting rates will dominate toponium decays in some of the cases; in other cases they might only appear with tiny branching ratios.

In the following we will first present the theoretical framework together with the relevant formulae. We will then present two more specific case studies, based on detailed Monte Carlo calculations. The first one will be a study of $\theta \to \tilde{g}\tilde{g}$. It will be demonstrated that this decay mode would be an ideal place for a rather accurate gluino mass determination. The second example will be an analysis of $\theta \to \tilde{g}\gamma g$ for a massive gluino. This will serve to demonstrate that rather high gluino masses could be probed in toponium decays.

6.1 Supersymmetric single-quark decays

The mass assignment $m_{\tilde{t}} < m_t$ has been favoured by a number of currently discussed models. If $m_t > m_{\tilde{t}} + m_{\tilde{g}}$ (or $m_{\tilde{\gamma}}$) toponium could drastically alter its appearance or even cease to exist as a well-defined resonance. Although these scenarios are already ruled out if the semileptonic top decays observed by the UA1 Collaboration [4] are taken at their face value, we nevertheless mention them for completeness.

Single-quark decays into a scalar quark and a light gaugino (Fig. 6.1)--if kinematically allowed--can have an extremely high rate [70]. The rate for the hadronic decay is given by

$$\Gamma[(t\bar{t}) \to \tilde{t}\tilde{g}\bar{t} + t\bar{t}^*\tilde{g}] = 2\,\frac{2}{3}\,\alpha_s m_t\,\left(\frac{2\,\vec{p}_{\tilde{g}}}{m_t}\right)^2 . \tag{6.1}$$

If not severely suppressed by phase space, the resulting width exceeds 1 GeV and is thus larger than the toponium level spacing. Obviously no $(t\bar{t})$ resonances
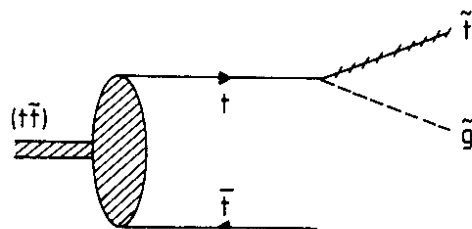
Fig. 6.1 Diagram for the decay of a bound t-quark into scalar quark plus gluino

exist in this case and one will only observe open-top production with a 'smeared' threshold region.

This situation can be described in the following (semiclassical) space-time picture: the constituents' characteristic time of revolution would be large compared with their lifetime, and the notion of a bound state becomes meaningless.

Even if this hadronic mode is kinematically forbidden the corresponding electromagnetic decay mode into a scalar quark and a photino could still proceed at an appreciable rate:

$$\Gamma[(t\bar{t}) \rightarrow \tilde{t}\gamma\bar{t} + t\tilde{t}^*\tilde{\gamma}] = 2\,\frac{1}{2}\,\alpha_{em}e_t^2\,m_t\left(\frac{2\,\vec{p}_{\tilde{\gamma}}}{m_t}\right)^2 \ . \tag{6.2}$$

It would still dominate, by far, all other channels; however, its rate of ~ 100-200 MeV would not be sufficient to wipe out the lowest-lying toponium resonances. A determination of the fundamental potential-model parameters E(2S)-E(1S), Γ_{ee}(1S), and Γ_{ee}(2S) would be feasible.

However, it must again be stressed that if semileptonic top decays are observed at the $p\bar{p}$ Collider or on top of the Z^0 in e^+e^- machines, SUSY-induced SQDs are ruled out for toponium.

6.2 Annihilation decays

As shown in Table 6.2, a large variety of annihilation decays is possible, depending on the masses of the various postulated particles. In all these cases the properties of open top would be unaffected and only those of toponium would be changed--eventually in a rather drastic manner. In the following we will not try to be completely general and cover all possibilities, but rather we will discuss a few of the more promising choices.

6.2.1 Gluino production through virtual gluons

Toponium (and Y) decays as a means of searching for gluinos have already been proposed some time ago [71]. Being electrically neutral, gluinos are hard to produce in e^+e^- collisions. However, as colour octets they may be pair-produced either in hadronic collisions or in toponium decays through the processes indicated in Fig. 6.2. Evidently the rate for these processes depends
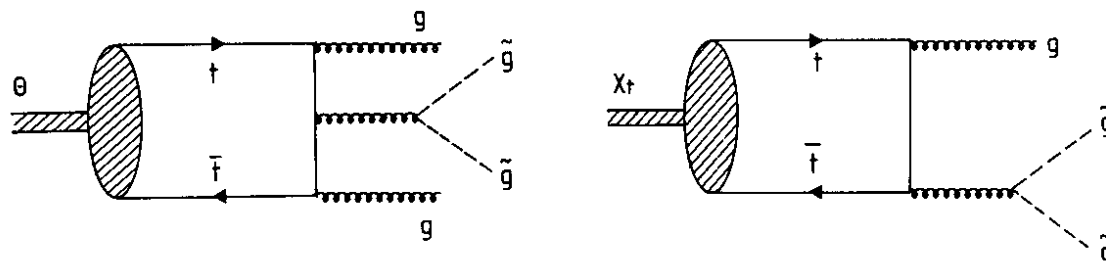

Fig. 6.2 Lowest-order diagrams for gluino production in toponium decays through virtual gluons
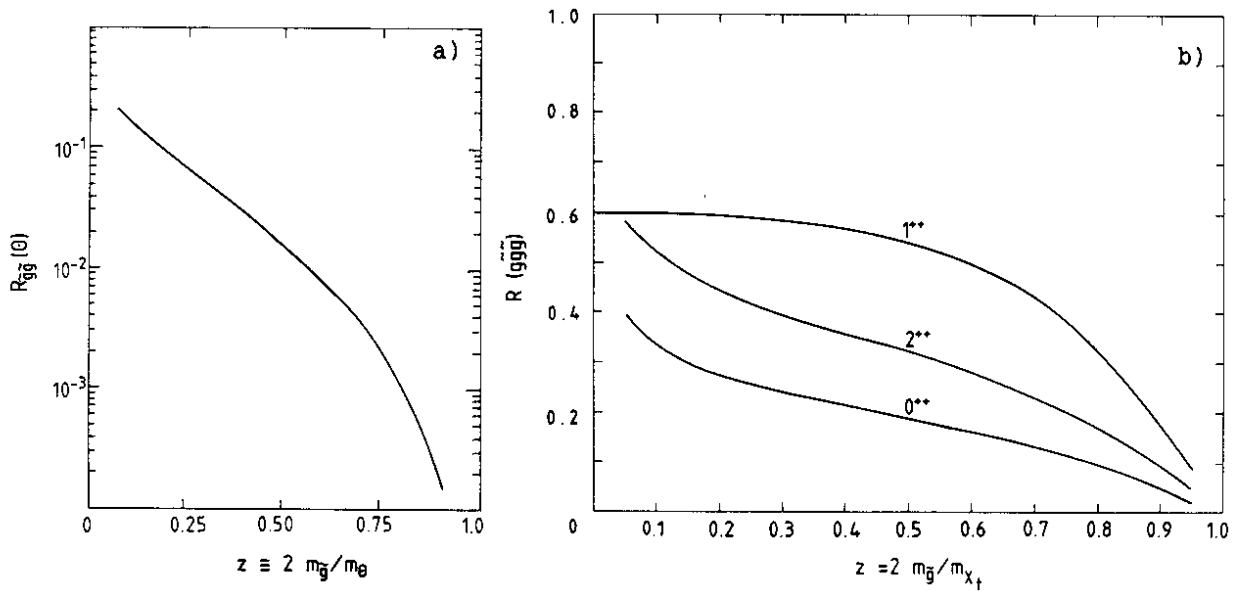
Fig. 6.3 Decay rates for toponium states into gluinos and gluons, relative to their dominant conventional hadronic decay rates as defined in Eqs. (6.3); a) $^3S_1$ decays (from Ref. [71]); b) ^3P_J decays (from Ref. [69]).

on the gluino mass only and is independent of all other SUSY parameters--quite in contrast with the reactions to be discussed later. Compared with the production of heavy quarks (charm, bottom) the rates are enhanced by a factor $1/2 \; \Sigma \; f^2_{abc}/\Sigma(\lambda^a_{ij}/2)^2 = 3$. In Fig. 6.3a we show the rates for $^3S_1$-states and in Fig. 6.3b those for P-states as a function of $m_{\tilde{g}}$ normalized to their dominant conventional hadronic decay rate

$$R(^3S_1) \equiv \Gamma(gg\tilde{g}\tilde{g})/\Gamma(ggg) \; , \tag{6.3a}$$

$$R(^3P_0, ^3P_2) \equiv \Gamma(g\tilde{g}\tilde{g})/\Gamma(gg) \; , \tag{6.3b}$$

$$R(^3P_1) = \Gamma(g\tilde{g}\tilde{g})/\Gamma(gq\bar{q}) \; , \tag{6.3c}$$

for fixed m_θ = 80 GeV and a binding energy of 1.5 GeV for the P-states ($\alpha_s \equiv 0.15$). [We used the analytic forms given in Ref. [72] for heavy-quark production.] For light gluinos these ratios can become quite sizeable: up to 20% for S-states and even up to 60% for P-states. However, as discussed in Ref. [25], the hadronic branching ratios themselves become relatively small for a heavy toponium P-state. As a specific example, let us consider m_θ = 80 GeV. To obtain the overall branching ratio, the ratio $R(^3S_1)$ has to be multiplied by ~ 0.1, and the P-state ratios $R(^3P_J)$ by 0.20, 0.03, and 0.07 for J = 0, 1, 2. Furthermore, taking the branching ratio for dipole transitions into account, one finds at best ($m_{\tilde{g}}$ = 5 GeV),

$$BR(1^3S_1 \rightarrow gg\tilde{g}\tilde{g}) \approx 10^{-2} ,$$

$$\sum_J BR[2^3S_1 \rightarrow \gamma + {}^3P_J(\rightarrow g\tilde{g}\tilde{g})] \approx 10^{-3} .$$

(6.4)

The rates are higher by a factor of ~ 3 for ${}^3S_1$ and by a factor of ~ 10 for P-states, if $m_\theta = 70$ GeV, but the experimental verification still looks quite difficult. For heavier gluinos these branching ratios rapidly become worse. Since we suspect that the detection of light gluinos on top of the Z^0 is more favourable, we have not studied this scenario further.

6.2.2 Gluino production through virtual scalar quark exchange

A number of authors [70, 73] have speculated that the scalar partner of top could be the lightest of all scalar quarks with a mass comparable to m_t. This would lead to sizeable branching ratios for toponium decays into gluino pairs through scalar quark exchange (Fig. 6.4). The rate would be proportional to α_s^2 and could thus even dominate in some cases. Since this mode also leads to a rather clean signature (two-body decay into energetic gluinos!) it is quite a promising candidate for gluino searches.
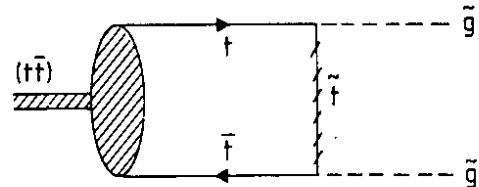

Fig. 6.4 Diagram for gluino-pair production in toponium decays through scalar t-quark exchange

To understand the relevance of this channel for the various $(t\bar{t})$ states, we first discuss the selection rules for decays into two Majorana fermions. The quantum numbers of a fermion-antifermion system are given by

$$P = -(-)^L , \qquad C = (-)^{L+S} .$$

(6.5)

This result holds true also for Majorana particles. From the requirement of antisymmetric wave functions for identical fermions, one derives, in addition,

$$L \text{ even }, \quad \text{for } S = 0$$
$$L \text{ odd }, \quad \text{for } S = 1 .$$

(6.6)

This implies that two Majorana particles can only have the following quantum numbers: 0^{-+}; 0^{++}, 1^{++}, 2^{++}; 2^{-+}; ... . Hence, if charge conjugation is conserved ${}^3S_1(1^{--}) \rightarrow \tilde{g}\tilde{g}$ is forbidden, and ${}^1S_0(0^{-+}) \rightarrow \tilde{g}\tilde{g}$ and ${}^3P_J(J^{++}) \rightarrow \tilde{g}\tilde{g}$ are allowed. In

general, however, the scalar partners of right- and left-handed quarks are expected to have different masses; parity and charge conjugation symmetry are violated; and $^3S_1 \to \tilde{g}\tilde{g}$ is allowed [70, 73, 74] and is usually even dominant. For completeness we list all relevant decay rates:

$$\Gamma(0^{-+} \to \tilde{g}\tilde{g}) = \frac{2}{3} 2^6 \alpha_s^2 \left[\frac{R(0)}{m}\right]^2 a_s^2 \left(\frac{m_{\tilde{g}}}{M}\right)^2 \beta \ , \tag{6.7a}$$

$$\Gamma(1^{--} \to \tilde{g}\tilde{g}) = \frac{2}{3} \frac{2^5}{3} \alpha_s^2 \left[\frac{R(0)}{m}\right]^2 a_1^2 \beta^3 \ , \tag{6.7b}$$

$$\Gamma(1^{+-} \to \tilde{g}\tilde{g}) = 0 \ , \tag{6.7c}$$

$$\Gamma(J^{++} \to \tilde{g}\tilde{g}) = \frac{2}{3} 2^{10} \alpha_s^2 \left[\frac{R'(0)}{m^2}\right]^2 \begin{cases} b_1^2 \left(\dfrac{m_{\tilde{g}}}{m}\right)^2 \beta^3 & , \ J = 0 \ , \\[2ex] (a_5 - b_1)^2 \beta & , \ J = 1 \ , \\[2ex] b_1^2 \dfrac{1}{5}\left(\dfrac{3}{4} + \dfrac{2m_{\tilde{g}}^2}{m^2}\right)\beta^3 , & J = 2 \ , \end{cases} \tag{6.7d}$$

where

$$\beta \equiv \left(1 - 4\, m_{\tilde{g}}^2/m^2\right)^{1/2} \ ,$$

$$a_{1,5} \equiv \frac{1}{2}\left(\frac{m_t^2}{-m_t^2 - m_R^2 + m_{\tilde{g}}^2} \mp \frac{m_t^2}{-m_t^2 - m_L^2 + m_{\tilde{g}}^2}\right) \ ,$$

$$b_{1,5} \equiv \frac{1}{2}\left[\frac{m_t^4}{(-m_t^2 - m_R^2 + m_{\tilde{g}}^2)^2} \pm \frac{m_t^4}{(-m_t^2 - m_L^2 + m_{\tilde{g}}^2)^2}\right] \ ;$$

m denotes the mass of the respective bound states and $m_{R,L}$ are the masses of the scalar t-quarks. In the extreme case where $m_L \approx m_t$, $m_R \gg m_L$, and $\beta \approx 1$, this mode would dominate all $^3S_1$ decays up to $m_\theta \approx 110$ GeV (excluding the tiny region $m_Z \pm 5$ GeV), but also for less extreme choices it would still be the dominant channel. Since this holds true also for radial excitations, decays into P-states would be quite suppressed.

Apart from the determination of Γ_{ee} and the level spacings, none of the standard toponium topics (electroweak interferences and decays, gluon properties, Higgs search, ...) would be accessible. However, toponium would then be an excellent place to study a rather clean sample of events with only two gluinos in

the final state. In subsection 6.3 we show that the mass of gluinos could be measured in this case with an uncertainty of less than 0.5 GeV.

If parity and charge conjugation were conserved ($m_L = m_R$), gluino decays could be important for P-state decays. In this case, dipole transitions from n^3S_1 to $\gamma + {}^3P_J$ would proceed with normal strength, and P-states could subsequently decay into gluino pairs [74]. In Fig. 6.5 we therefore compare the corresponding rates for decays of 1^{++} and 2^{++} states with their conventional modes. If not suppressed by phase space, ${}^3P_1$ annihilation into $\tilde{g}\tilde{g}$ would even dominate the ${}^3P_1 \rightarrow {}^3S_1 + \gamma$ dipole transition, and one of the three two-photon cascades would be absent in this peculiar scenario. However, the energy difference between photons from transitions to the various P-states will only amount to a few MeV, so that even a BGO detector will be unable to observe the lines separately. One might try to tag the events with their combined branching ratio of roughly 1% by requiring missing energy from the gluino decay. However, in this case one has to face a 10% contamination from semileptonic SQDs, in particular from t → bvτ (→ hadrons + v). These could be removed to some extent if one is able to reject B mesons with the microvertex detector and thus achieve another factor of 10 in rejection rate. Alternatively, one could gain a comparable factor by requiring a photon of the (already measured) energy E_γ = M(2S) - M(1P)
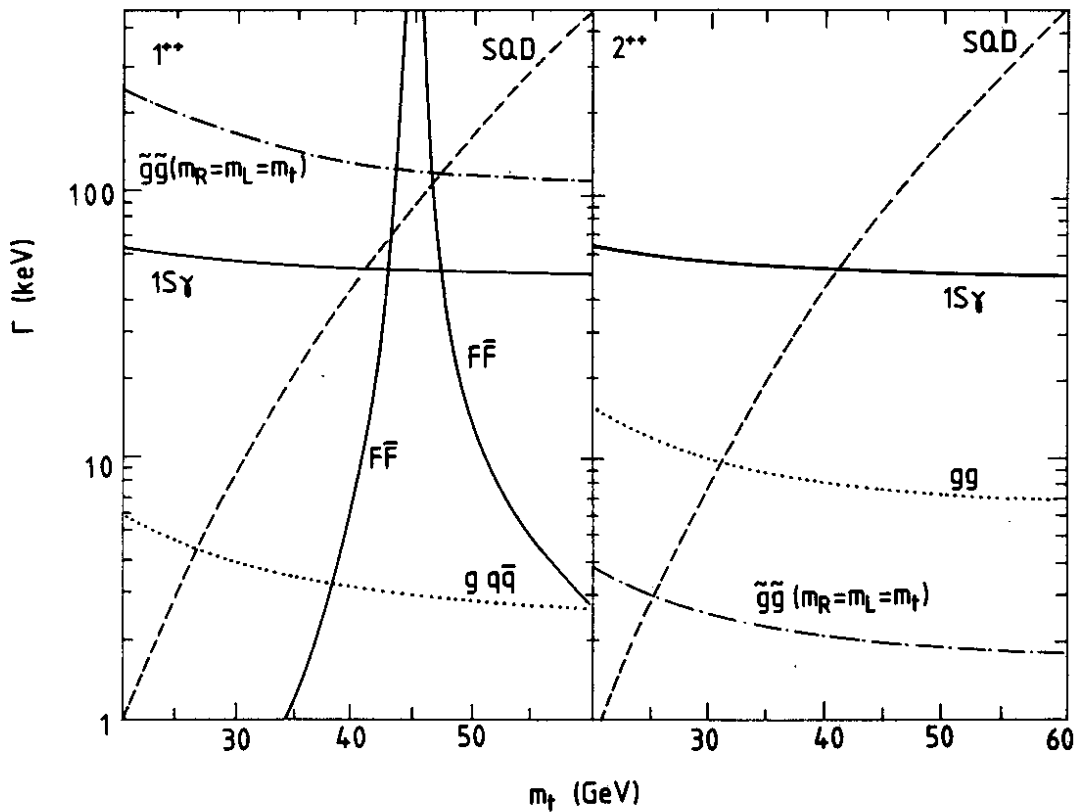

Fig. 6.5 Conventional decay rates of 1^{++} and 2^{++} χ_t states, compared with their decay rates into two gluinos through scalar quark exchange. From Ref. [74].

with the BGO detector. Even then it would be barely possible to identify $2S \rightarrow \gamma + 1P(\rightarrow \tilde{g}\tilde{g})$.

It should be noted that instead of gluinos, also two photinos could be produced, and all previous formulae apply after the substitution $\alpha_s^2 \rightarrow 9/2 \, \alpha^2 e_t^4$. The branching ratio for $1^3S_1 \rightarrow \tilde{\gamma}\tilde{\gamma}$ is comparable to the one for e^+e^- decays and is thus non-negligible if decays into a gluino pair are kinematically forbidden. Since the decay products are invisible, this would effectively only reduce the visible cross-section by at most 10%, and thus this decay mode would remain unnoticed. Tagging the invisible channel through $2^3S_1 \rightarrow \pi\pi + 1^3S_1$ or $2^3S_1 \rightarrow \tilde{\gamma}\tilde{\gamma} + 1^3S_1$ is possible, in principle; in practice, however, the combined branching ratios are rather low ($\lesssim 10^{-3}$).

If the photino is relatively light and the masses of top and scalar top are comparable, one may have access to high gluino masses through the mode [75]

$$\theta \rightarrow \tilde{g}\tilde{g}\tilde{\gamma} \, , \tag{6.8}$$

mediated by scalar top exchange. For $m_L = m_R = \tilde{m}$, the differential rate is given by

$$\frac{d\Gamma(\tilde{g}\tilde{g}\tilde{\gamma})}{\Gamma(gg\gamma)} = \frac{dy \; dz}{(\pi^2-9)z^2(x+h)^2\left(y+h+\frac{1}{2}n^2\right)^2}$$

$$\cdot \left\{ [2(x-y)^2 h - 4h - 2 + 2z - z^2 - 2xy](1-z) + 4xyh + 2h^2 + (2xy - h^2 - zh^2)(x^2 + y^2) + R \right\} \, , \tag{6.9a}$$

$$R = (n^2/64)[2n^4(3 + 8x - 4y - 2xy - 2x^2) + 16h^2(x-y)(2+z) - n^2(n^4 + 4n^2 h + 8h^2)$$

$$+ \; 16hn^2(1 - y + 3x - xy - x^2) + 4n^2(18 - 16y + 12xy + y^2 + 4x^2 y - 21x^2 + 4x^3)$$

$$+ \; 32h(6 - 4y - 2xy - 7x^2 - y^2 + 3x^2 y + 2xy^2 + 2x^3 + y^3)$$

$$+ \; 16(12z - 14 - 2x^2 + 4y^2 + 24xy - 13x^2 y - 3xy^2 + 5x^3 - y^3 - 4xyz + xyz^2)] \, , \tag{6.9b}$$

where

$$x = E_{\tilde{g}}/m \, , \qquad\qquad n = m_{\tilde{g}}/m \, ,$$

$$y = E_{\tilde{\gamma}}/m \, , \qquad\qquad h = (\tilde{m}^2/m^2 - 1 - n^2)/2 \, ,$$

$$z = 2 - x - y \, .$$

In subsection 6.4 we study this case in more detail. As a representative example, we have chosen for the masses $m_\theta = 80$ GeV, $m_{\tilde{g}} = 60$ GeV, and $m_{\tilde{\gamma}} = 0$. Although the branching ratio is rather small, we still find that this decay mode can be separated from the conventional decays but with some effort. It should

be stressed that detection of gluinos on top of the Z would be difficult for the
masses chosen in our example.

An amusing borderline case would be the mass assignment $m_{\tilde{t}} + m_{\tilde{\gamma}} > m_t > m_{\tilde{t}}$.
In this case $\theta \rightarrow \tilde{t} + \tilde{t}^*$ mediated by gluino exchange could play the dominant role
[70]. For completeness we should mention that also $\theta \rightarrow \tilde{H} + \tilde{\gamma}$ and $\tilde{Z} + \tilde{\gamma}$ have been
discussed in the literature [73].

A completely different supersymmetric model has been proposed by Samuel
and Wess [76]. In this model, supersymmetry is realized in a non-linear form.
In the context of quarkonium physics it would lead to the decays $\theta \rightarrow \gamma\lambda\lambda$ and
$^3P_{1,2} \rightarrow \lambda\lambda$, where λ denotes the weakly interacting Goldstone fermion [77, 69].
Experimental observation of the channel $2S \rightarrow \gamma + 1P(\rightarrow \lambda\lambda)$ seems difficult.

6.3   Gluino-mass determination from the decay $\theta \rightarrow \tilde{g}\tilde{g}$

6.3.1   Assumptions

As discussed in the previous subsection, toponium annihilation into a pair
of gluinos could dominate all other channels if $m_{\tilde{g}} < m_t$ and if $\tilde{m}_R \neq \tilde{m}_L$. In this
case it would be possible to study a rather clean sample of gluino pairs. We
shall use this to demonstrate that a study of this decay would allow the gluino
mass to be measured with high accuracy. We base this case study on the follow-
ing assumptions:

- m_θ = 80 GeV, $m_{\tilde{g}}$ = 35 GeV , $m_{\tilde{\gamma}}$ = 0 ,

- BR($\theta \rightarrow \tilde{g}\tilde{g}$)   dominant ,

- $\tilde{g} \rightarrow q\bar{q}\tilde{\gamma}$ generated with the squared matrix element

$$|A|^2 \propto (P_{\tilde{g}}P_{\bar{q}}) \cdot (P_{\tilde{\gamma}}P_q) + (P_{\bar{q}}P_{\tilde{\gamma}}) \cdot (P_{\tilde{g}}P_q) , \qquad (6.10)$$

- $q\bar{q}$ = $u\bar{u}$, $d\bar{d}$, $c\bar{c}$, and $b\bar{b}$ generated with equal probability.

6.3.2   Missing-energy distribution

Figure 6.6a shows the total missing energy due to $\tilde{\gamma}$ for $m_{\tilde{g}}$ = 35 GeV.
Figures 6.6b-d show how this distribution varies with $m_{\tilde{g}}$ (25, 30 and 40 GeV).
Such variations suggest that $m_{\tilde{g}}$ be estimated from the width of the missing-
energy distribution.

Figure 6.7 displays the dependence of $m_{\tilde{g}}$ versus the standard deviation
σ for these distributions. With 1000 events, we can in principle measure $m_{\tilde{g}}$
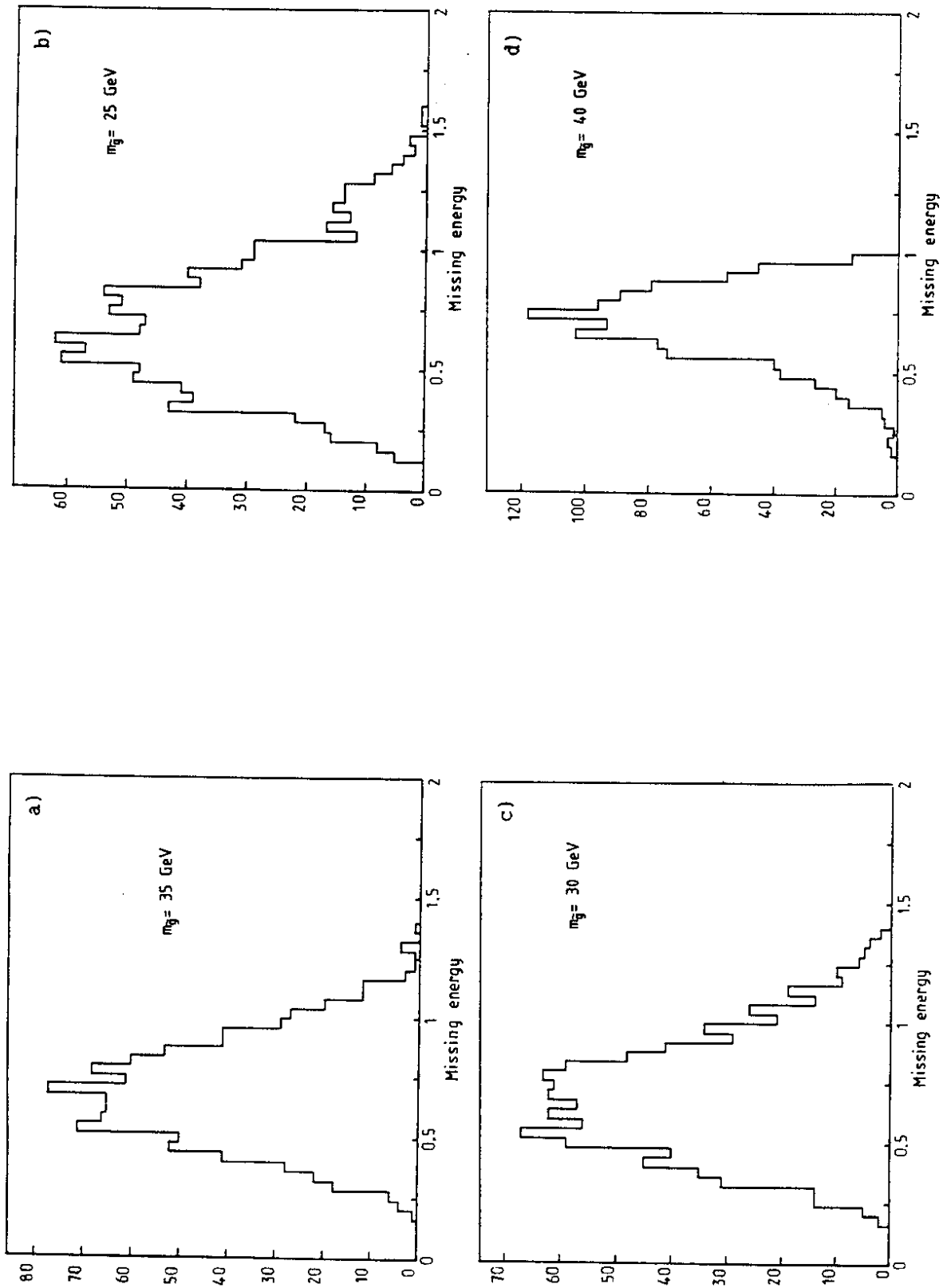to better than 500 MeV.

Fig. 6.6 Distribution of the energy carried by the two photinos in the decay $\theta \rightarrow g\tilde{g}$, $\tilde{g} \rightarrow q\bar{q}\tilde{\gamma}$ with $m_\theta = 80$ GeV, $m_{\tilde{\gamma}} = 0$. The energy is normalized to the beam energy. a) $m_{\tilde{g}} = 35$ GeV, b) $m_{\tilde{g}} = 25$ GeV, c) $m_{\tilde{g}} = 30$ GeV, d) $m_{\tilde{g}} = 40$ GeV.
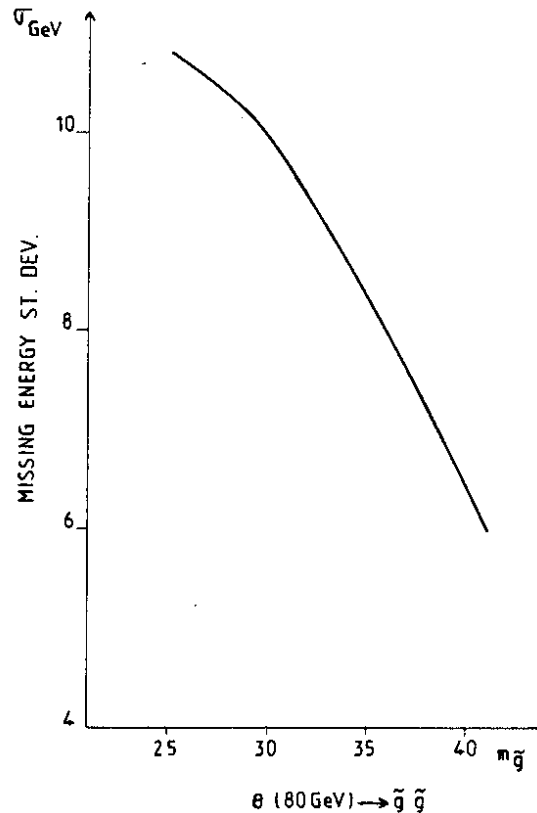
Fig. 6.7 Missing-energy dispersion
[standard deviation of the distri-
butions (6.6)] versus $m_{\tilde{g}}$

$e\ (80\,GeV) \longrightarrow \tilde{g}\ \tilde{g}$

Remarks:

i) This figure does not include effects due to possible contaminations
coming from energy leaks (apparatus).

ii) The missing-energy distribution (Figs. 6.6b-d) can be modified if one
takes into account semileptonic decays from heavy flavours coming from
gluino decays. This can be vetoed (except τ's) by eliminating events
with e (μ) in the final state.

6.3.3 Estimating the mass of the gluino

In the following, the gluino fragmentation is assumed to be $\delta(1-z)$.

i) One method has already been described above.

ii) It is expected that the sphericity of the events will also vary with $m_{\tilde{g}}$.
To study this problem we need a hadronization scheme. Since the $\tilde{g}$ lifetime
is long compared with typical hadronization schemes (as for $t\bar{t}$ decays), we
assume that $\tilde{g}$ dresses up into colour-neutral hadrons G ($g\tilde{g}$) or ($\tilde{g}q\bar{q}$) before
decaying.

The Lund Monte Carlo was used to produce the final hadrons.

Figure 6.8 shows how the sphericity S varies with $m_{\tilde{g}}$. Error bars cor-
respond to the accuracy on $\langle S \rangle$ for 1000 events. Again we find that the mass
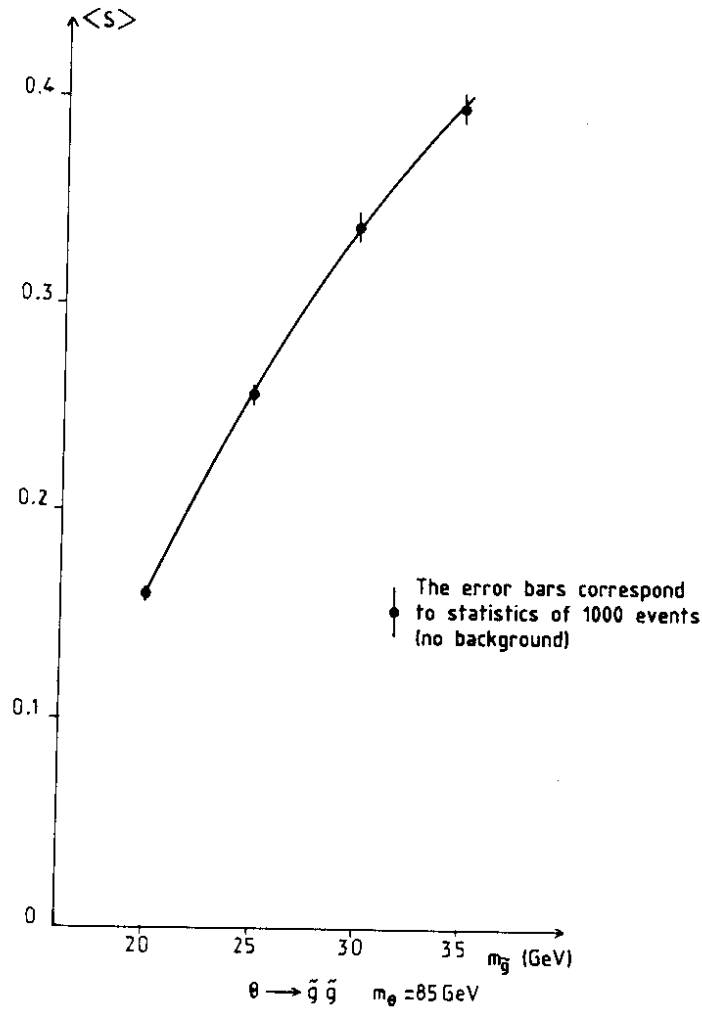estimate can be better than 1 GeV.

Fig. 6.8 Sphericity S versus $m_{\tilde{g}}$ for $\theta \rightarrow \tilde{g}\tilde{g}$ with m_θ = 80 GeV. the hadroni-
zation scheme is described in the text. Error bars correspond to the statistical
accuracy on S for 1000 events.

iii) Finally, we describe a method which gives direct evidence for a mass peak
related to the gluino mass.

Even when the mass of the $\tilde{g}$ is fixed, a full reconstruction of the event is
not possible since one constraint is missing. However, as shown in Ref. [78]
for a similar case, a Jacobian peak method can be used to fix the unknown mass.

To see this we use the centre-of-mass system for the two $\tilde{\gamma}$'s. In this
system (see Fig. 6.9), hadron jets (four jets) are associated with two sub-
systems, called A and B, related to the two gluinos $\tilde{g}_1$ and $\tilde{g}_2$. The energy of
the $\tilde{\gamma}$ is known (= missing energy/2 in this system). The angle α between $\tilde{\gamma}_1$ and
A is fixed once the mass of $\tilde{g}_1$ is fixed.

What remains arbitrary is the choice of the azimuth of $\tilde{\gamma}_1$. The mass of $\tilde{g}_2$
will clearly depend on the choice of this azimuth φ. It turns out that $m_{\tilde{g}2}$ is
stationary with respect to φ when $\tilde{\gamma}$ belongs to the plane defined by $\vec{p}_A$ and $\vec{p}_B$.

Fig. 6.9   Kinematics in the missing-energy frame $(\vec{P}_{\gamma 1} + \vec{P}_{\gamma 2} = 0)$ for $\theta \to \tilde{g}_1 \tilde{g}_2$ with $\tilde{g}_1 \to \gamma_1 A$ and $\tilde{g}_2 \to \gamma_2 B$; α is the angle between $\vec{P}_{\gamma 1}$ and $\vec{P}_A$, β the angle between $\vec{P}_B$ and $\vec{P}_{\gamma 2}$; φ is the azimuthal angle describing the position of $\vec{P}_\gamma$ on the cone with $\vec{P}_A$ axis. The origin for φ is defined by the P_A, P_B plane.
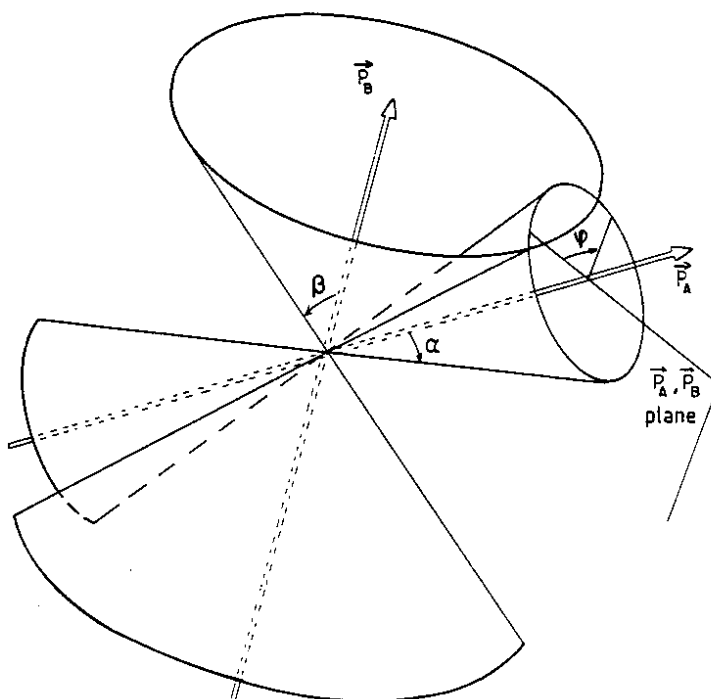
Reference [78] shows that the mass $m_{\tilde{g}2}$ reconstructed with the two possible φ values $(0, \pi)$ shows a peak reflecting this Jacobian effect.

This method has been tried at the parton level and shows the expected peak (Fig. 6.10a).

After hadronization is introduced, the peak is still present (Fig. 6.10b).

Figures 6.10 have been obtained at $m_{\tilde{g}} = 25$ GeV. If we increase $m_{\tilde{g}}$, the peak appears less clearly.
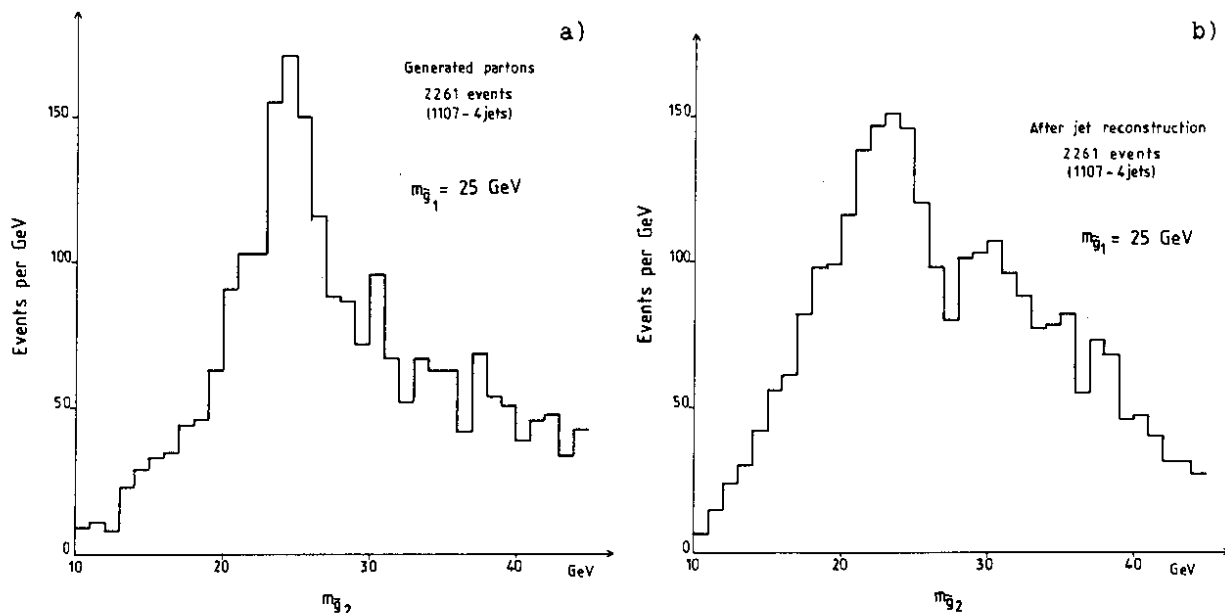

Fig. 6.10 a) Distribution at the parton level of the mass of the $\tilde{g}_2$ system when $m_{\tilde{g}1}$ is fixed at its nominal value of 25 GeV; b) Same as (a) introducing hadronization.
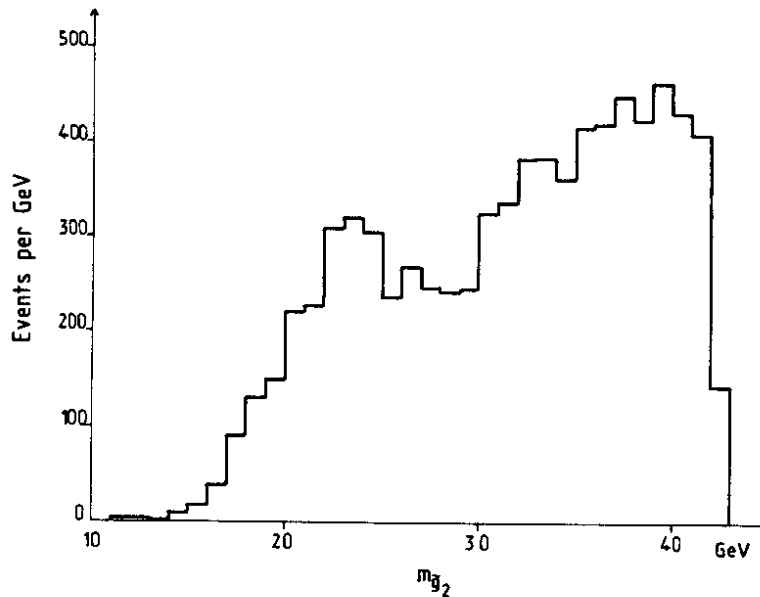
Fig. 6.11 Distribution of $m_{\tilde{g}_2}$ imposing the equality between $m_{\tilde{g}_1}$ and $m_{\tilde{g}_2}$: $|m_{\tilde{g}_1} - m_{\tilde{g}_2}| \leq 2$ GeV. A peak appears at 25 GeV, the generated value.

As the gluino mass is the quantity we want to measure, we have considered for $m_{\tilde{g}_1}$ all the possibilities between 10 GeV and $m_\theta/2$. Figure 6.11 shows the distribution for $m_{\tilde{g}_2}$ with the condition that $|m_{\tilde{g}_1} - m_{\tilde{g}_2}| \leq 2$ GeV. A peak for $m_{\tilde{g}_2}$ appears, centred around the generated mass of 25 GeV.

6.3.4 Conclusion

Using three independent methods, we arrive at the conclusion that $m_{\tilde{g}}$ can be measured to an accuracy of better than 1 GeV.

Most backgrounds to the $\tilde{g}\tilde{g}$ channel can be efficiently eliminated.

6.4 Search for heavy gluinos in the decay $\theta \to \tilde{g}\tilde{g}\gamma$

6.4.1 Assumptions

As discussed in subsection 6.2, toponium decays could give access to very heavy gluinos through the decay $\theta \to \tilde{g}\tilde{g}\gamma$. We shall substantiate this claim by a detailed analysis based on the following assumptions on the masses:

$$m_\theta = 80 \text{ GeV}, \quad m_{\tilde{g}} = 60 \text{ GeV}, \quad m_{\tilde{\gamma}} = 0, \quad m_R = m_L = m_t.$$

We use the distributions from Ref. [75] for the energy distributions [see Eq. (6.9)] and the gluino decay as specified in subsection 6.3. For our choice of masses we derive BR($\tilde{g}\tilde{g}\gamma$) = 0.5%. Figure 6.12a shows the energy distribution of the gluino for our mass assignment, compared with the case $m_{\tilde{g}} = 0$.

a)

b)

c)

d)
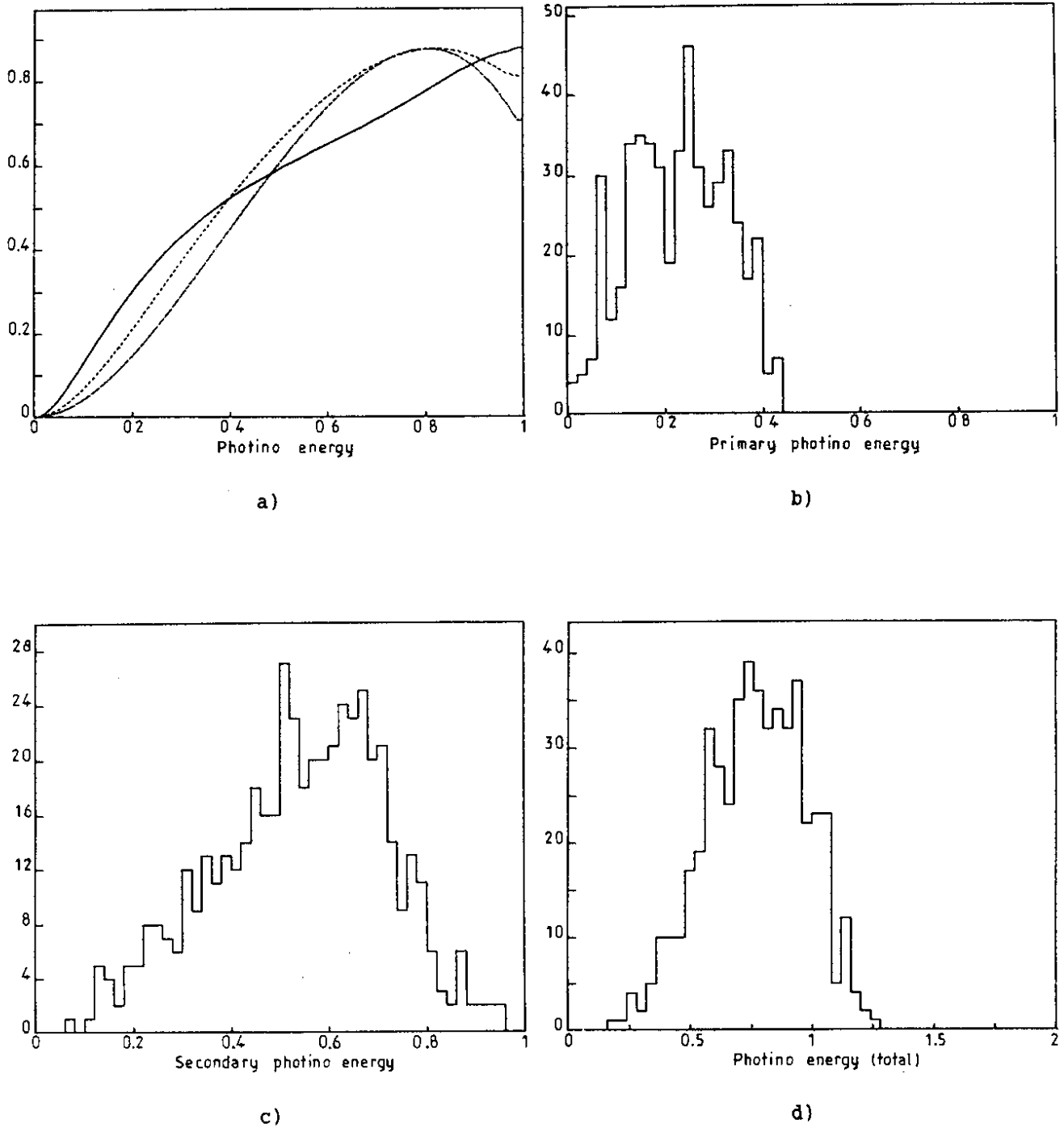
Fig. 6.12 a) Energy distribution of the $\tilde{\gamma}$ (in $\to \tilde{g}\tilde{\gamma}g$) measured in the rest frame of toponium as obtained from Ref. [75]. The energy is normalized to the top mass m_t. The mass of $\tilde{\gamma}$ and $\tilde{g}$ are assumed negligible. The full curve corresponds to $m_{\tilde{t}} = 1.2 m_t$, the dashed curve to $m_{\tilde{t}} = 1.5 m_t$, the dash-dotted curve to $m_{\tilde{t}} = 2 m_t$, where $\tilde{t}$ stands for the scalar partner of top (right- and left-handed scalar quarks are assumed to have equal mass). b) The energy distribution of $\tilde{\gamma}$ with the mass assignments: $m_t = m_{\tilde{t}} = 40$ GeV; $m_{\tilde{\gamma}} = 0$, $m_{\tilde{g}} = 60$ GeV. c) With the same hypotheses as (b), energy distribution of $\tilde{\gamma}$ from $\tilde{g}$ decays with the same normalization. d) With hypotheses of (b), total energy carried by the two photinos $\tilde{\gamma}$ and $\tilde{\gamma}'$ produced in $\theta \to \tilde{g}\tilde{\gamma}g$ ($\tilde{g} \to q\bar{q}\tilde{\gamma}'$) normalized to the top mass.

6.4.2 Missing-energy distributions

Figure 6.12b shows the contribution from the direct $\tilde{\gamma}$, Fig. 6.12c from the secondary $\tilde{\gamma}$. Figure 6.12d gives the total contribution. [*Note:* All energy distributions are normalized to the beam energy (40 GeV).]

6.4.3 Contaminations

i) Single-quark decays from θ give the largest missing energy. These decays can be identified since they are necessarily accompanied by at least one charged lepton (except for $\tau\nu$). The probability of missing this lepton should be kept at the percent level in order to reach a reasonable signal-to-background ratio. We cannot expect topological cuts to help significantly (four jets instead of three). To improve the situation, one could require a missing energy greater than 20 GeV, the maximum value allowed for semi-leptonic decay. This would force double semileptonic decay and increase the probability of detecting at least one lepton. [Not operative for $\tau\nu(\tau \rightarrow \nu + \text{hadrons})$.] The SQD jets cannot exceed the same limit, which means that at least *two energetic hadrons* have to be lost in order to simulate more than 20 GeV missing energy.

From Fig. 6.12d we find that 20% of the good events are rejected by this cut.

Figure 6.13a gives the distribution of missing energy versus the energy of the most energetic lepton for two primary $(t \rightarrow be\nu)$ semileptonic

a)   b)

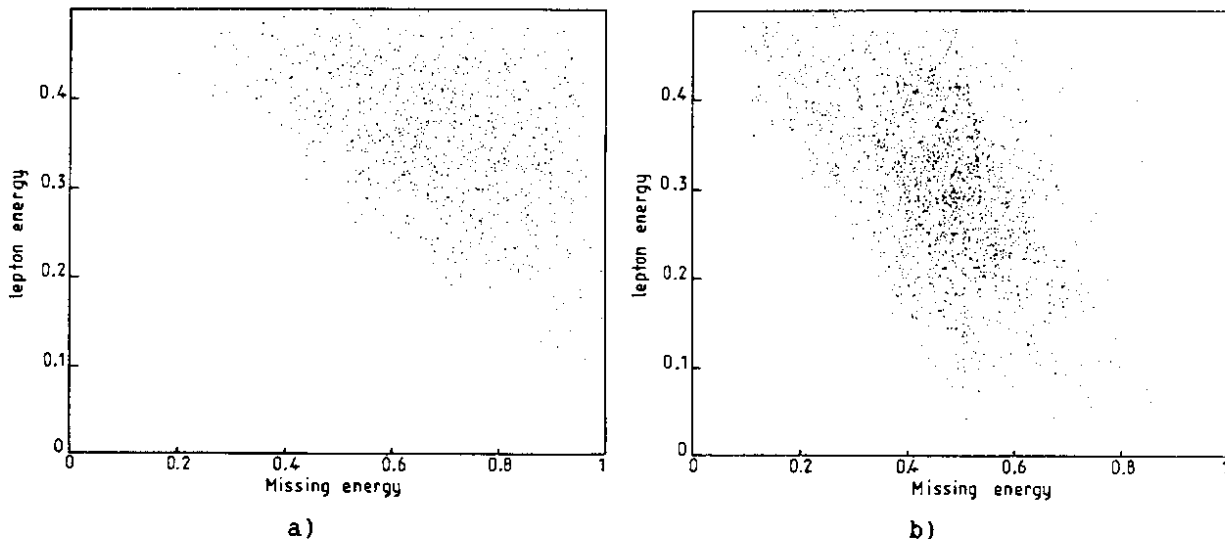Fig. 6.13 a) Assuming $\theta \rightarrow bl^{+}\nu\ b\bar{l}^{-}\bar{\nu}$ through single-quark decay, the energy carried by the two neutrinos normalized to the beam energy is the abscissa, the energy of the most energetic lepton is the ordinate with the same normalization. b) Assuming $\theta \rightarrow bl^{+}\nu b\bar{q}q$ with one of the b decaying semileptonically, the same distribution as in (a) is shown.

decays. Keeping lepton candidates with energy below 3 GeV so as to avoid random vetoes, we reject all these events ($\leq 10^{-3}$ contamination).

Figure 6.13b gives the same plot for one primary decay followed by a secondary decay (b → cev). With the 3 GeV cut, we retain 1% of these candidates.

Taking into account branching ratios, we are left with 5×10^{-4} contamination (normalized to the number of θ events). We have neglected ternary (c → sev) decays.

ii) The background coming from light quarks can be eliminated by cutting on coplanarity (Fig. 6.14). With this cut, 70% of the good events are kept, whilst 93% of the background is rejected.

The missing-energy criterion (25 GeV) gives a 10^3 rejection factor (assuming that only neutrinos give missing energy, i.e. ignoring effects from the apparatus).

Vetoing against charged leptons above 3 GeV leads us finally to a rejection factor of 10^5 (total).

iii) The most serious background comes from

$$t \xrightarrow{\text{(SQD)}} \tau\nu b$$

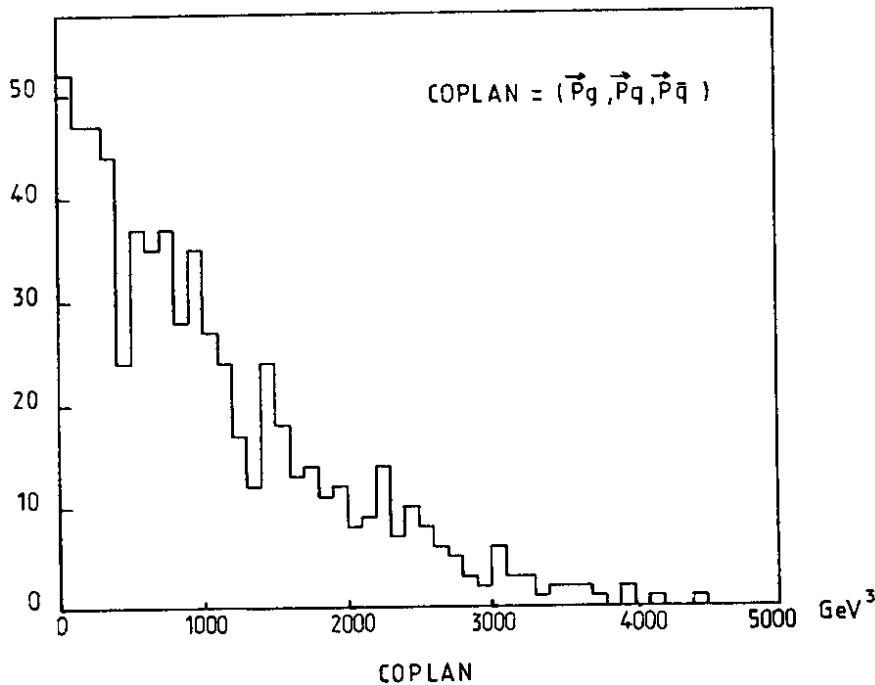$$\phantom{t \xrightarrow{\text{(SQD)}} \tau\nu}\downarrow \rightarrow \text{had} + \nu \; .$$

(6.11)

Fig. 6.14 Coplanarity ($\vec{P}_q$, $\vec{P}_{q\bar{q}}$; $\vec{P}_g$) distributions of light (≠ top) quark decays for 3-jet events
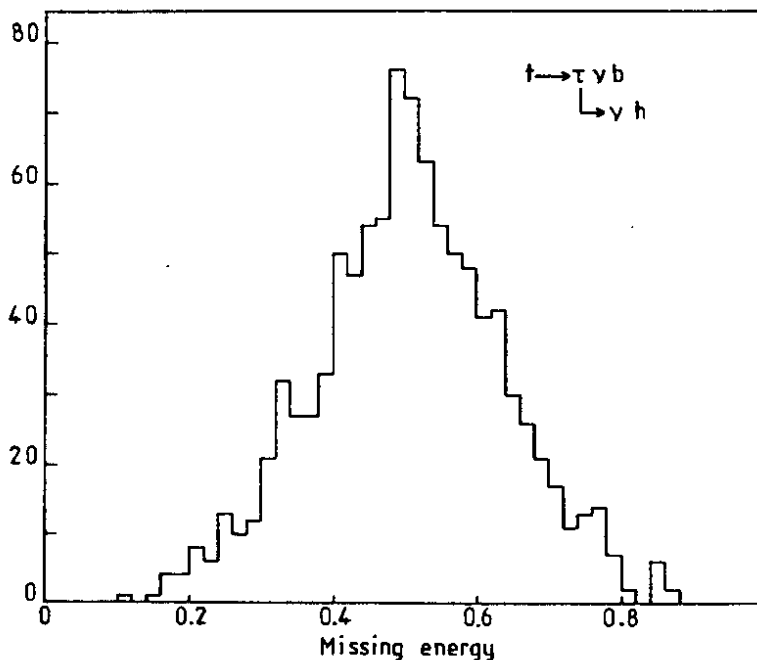
Fig. 6.15 Assuming θ → τ vb + X with τ → hadrons + v, the distribution of the energy carried by the two neutrinos normalized to the beam energy is shown

The missing-energy criterion (> 25 GeV) keeps 28% of these events, as shown in Fig. 6.15.

Vetoing against leptons gives only an additional factor of 2 (decays from accompanying heavy quarks).

Finally we are left with a signal-to-background ratio of ~ 0.7 due primarily to this channel.

6.4.4 Losses

i) Our cut on missing energy rejects 20% of the good events.

ii) Ten percent of the gluino decays are lost by vetoes on charged leptons
$(\tilde{g} \to b\bar{b}\tilde{\gamma}$ or $c\bar{c}\tilde{\gamma})$.

iii) Coplanarity cuts remove ~ 30% of the good events.

6.4.5 Conclusions

After applying the cuts discussed above, 40 signal events and 60 background events would be kept for an integrated luminosity of 150 pb^{-1}. The background events are mainly from t → τvb. We therefore believe that further analysis based, for example, on B-meson rejection through microvertex detectors or on topological cuts to reject low-multiplicity jets from τ → hadrons + v could reduce this background even more. The identification of θ → g$\tilde{g}\tilde{\gamma}$ is thus difficult but feasible.

7. THE ROLE OF THE ENERGY SPREAD

All our figures have been based on the LEP 13 (3 mA) luminosity [38]

$$L = (0.8-2.1) \times 10^{31} \text{ cm}^{-2} \text{ s}^{-1} , \qquad (7.1)$$

and a centre-of-mass energy spread [see Eq. (2.36)],

$$\delta W \text{ (MeV)} = \frac{0.443 \times 10^{-2} \text{ W}^2 \text{ (GeV}^2)}{[1 - 0.41 \times 10^{-6} \text{ W}^3 \text{ (GeV}^3)]^{1/2}} .$$

The LEP machine can be operated in different modes [38], maximizing L, 1/δW, or L/δW (Fig. 7.1). Depending on the signal-to-background ratio, different measurements can be performed in a more efficient way by choosing the appropriate operating mode.

As an example we can study the total time required for the scan of a 2 GeV interval. From formula (3.11) this time is

$$T = \frac{1}{L} n^2 \frac{(\sigma_S + \sigma_B)}{\sigma_S^2} \frac{2 \text{ GeV}}{2\delta W} . \qquad (7.2)$$
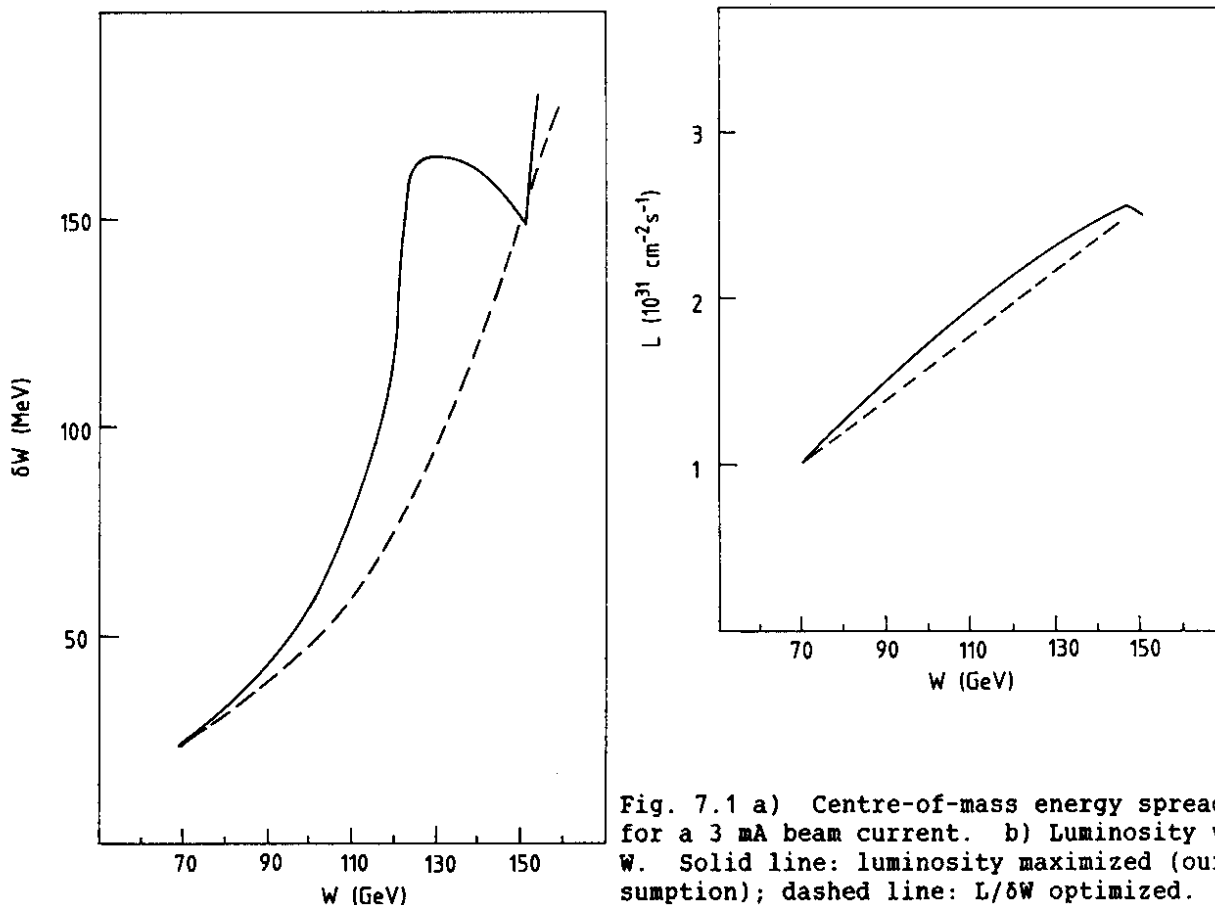

Fig. 7.1 a) Centre-of-mass energy spread δW for a 3 mA beam current. b) Luminosity vs. W. Solid line: luminosity maximized (our assumption); dashed line: L/δW optimized.

Table 7.1
Comparison of different assumptions
on energy spread and luminosity

	Our assumptions			L/δW optimized		
W	δW (MeV)	L (10^{31} cm^{-2} s^{-1})	δW/L	δW (MeV)	L (10^{31} cm^{-2} s^{-1})	δW/L
70	23	0.79	29.1	23.3	1.04	22.4
80	32	1.09	29.3	30.8	1.46	24.4
90	42	1.35	31.1	38.3	1.49	25.7
100	58	1.60	36.2	47.8	1.69	28.3
110	79	1.83	43.1	59.5	1.91	31.2
120	117	2.05	57.1	74.8	2.10	35.6

Since $\sigma_S \propto 1/\delta W$, we notice that T is proportional to $\delta W/L$ if $\sigma_S \ll \sigma_B$. In the other extreme case when $\sigma_B \ll \sigma_S$, T is simply proportional to $1/L$.

For toponium search above Z^0 it will be convenient to maximize $L/\delta W$; in the 70 GeV region it is better to maximize L. Table 7.1 shows a comparison between our 'assumed' operating mode and the $L/\delta W$ optimized mode [38].

The optimal mode is different for measurements on the resonance. As an example, we can consider the time required to measure the α_{RL}^{on} asymmetry with an error Δ. From Eq. (4.9) one finds

$$T = \frac{1}{\Delta^2} \frac{1 + \eta}{L\sigma_S} \left[1 - \langle\alpha_{RL}\rangle^2 + \eta^2 (\langle\alpha_{RL}\rangle - \alpha_{RL}^{off})^2 \right] , \qquad (7.3)$$

where $\eta = \sigma_B/\sigma_S$.

Under the condition of severe background ($\eta \gg 1$) T is proportional to $(1/L)(\sigma_B/\sigma_S^2)$. In this case the quantity to optimize is $L/(\delta W)^2$. In the other extreme case ($\eta \ll 1$) it is more appropriate to optimize $L/\delta W$.

It has been suggested in various papers on e^+e^- machine physics [79] that it is possible (at least in principle) to substantially reduce the spread in the energy of e^+e^- collisions. A study is at present being made to see whether such schemes could be implemented at LEP and a factor of 4 reduction in δW might be possible [80]. We would like to emphasize that such a reduction would not only lead to substantial reductions in the running time and/or improvements in stat-istical accuracy but it would also give access to new questions of physics. As
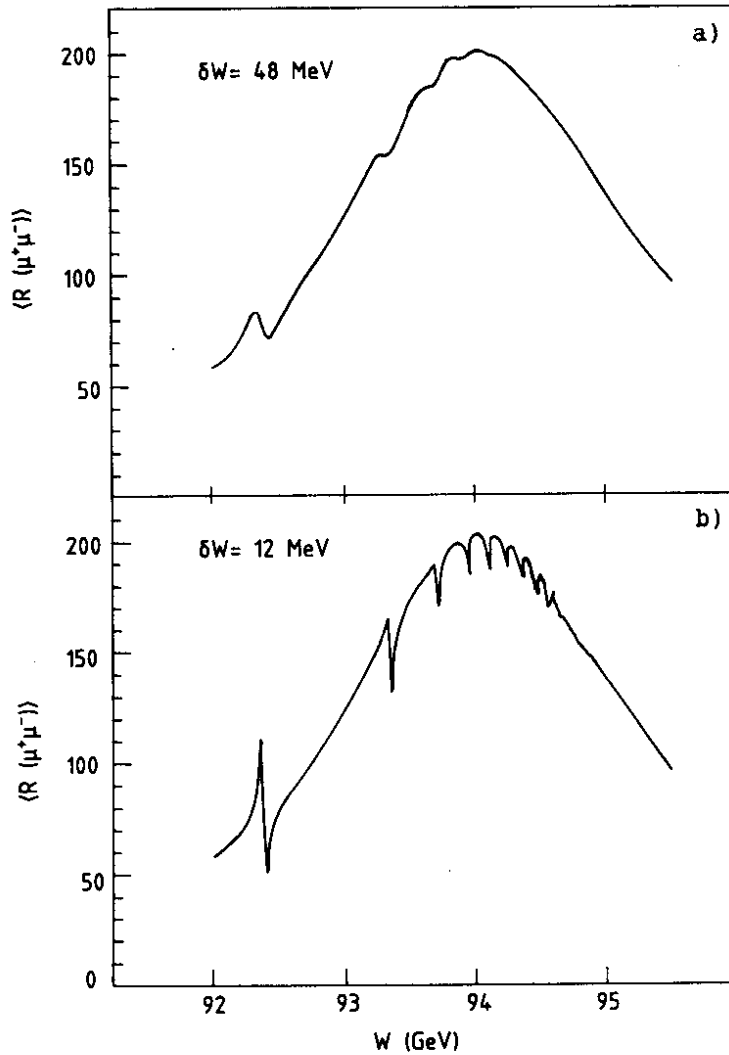
Fig. 7.2 $\sigma(\mu^+\mu^-)/\sigma_{pt}$ in the toponium region, assuming $m_Z = 94$ GeV, $m_t = 47$ GeV and $\delta W = 48$ MeV (a) and 12 MeV (b)

an illustration, we show in Fig. 7.2 the μ-pair cross-section in the toponium region for two choices of energy spread, $\delta W = 48$ MeV and 12 MeV, in the toponium region assuming a t-quark mass of 47 GeV. Evidently, resonance and interference effects are strongly enhanced for $\delta W = 12$ MeV. We expect that the second choice of 12 MeV would allow a rather accurate determination of $\sin^2 \theta_W$ through the polarization and asymmetry measurements discussed in Section 4. In particular one might exploit the fact that the relative importance of the photon and Z^0 contributions to the amplitude are different on the top and in the wing of the resonance [24].

Another instructive example is provided by the direct formation of axial-vector resonances through the neutral current [81]. The following estimate for the production of a 1^3P_1-state with a mass of 80 GeV is based on the wave functions calculated for Richardson's potential. One finds

$$\Gamma(1P \rightarrow e^+e^-) = \frac{3}{4\pi^2} [1 + (1 - 4 \sin^2 \theta_w)^2] \frac{G_F^2 m_Z^4}{(m^2 - m_Z^2)^2 + \Gamma_Z^2 m_Z^2} R'(0)^2 \approx 0.1 \text{ keV} .$$

$$(7.4)$$

A similar result has previously been obtained by Gatto, based on a scaling law for a power potential [82].

This leads to a small resonance enhancement above the large continuum background from $q\bar{q}$ production plus a small contribution from the radiative tail of 1S:

$$R_{1P} = 0.2 ; \quad R_{q\bar{q}} = 2.0 ; \quad R_{rad} = 0.2 .$$

$$(7.5)$$

The $^3P_1$ resonance decays mainly through SQD [BR(SQD) $\approx$ 0.5] or through dipole transitions into 1S [BR(γ+1S) $\approx$ 0.5]. It is thus favourable to use the topology cuts discussed in subsection 3.2 which select SQDs. These cuts reduce the 1P, the $q\bar{q}$, and the 1S event rates by the factors 0.6, 0.05, and 0.4, respectively, which gives

$$R_{1P}^{cut} \approx 0.12 , \quad R_{q\bar{q}}^{cut} \approx 0.1 , \quad R_{rad}^{cut} = 0.08 .$$

$$(7.6)$$

To establish the resonance as a 2σ effect with the unmodified resolution would require an integrated luminosity of 25 pb^{-1}. If, furthermore, one wants to measure three points on and off the resonance, a total of 75 pb^{-1}, corresponding to more than 80 days (maximal luminosity, 24 hours), would be required. (Selecting semileptonic SQDs would reduce these numbers by a factor of $\approx$ 2.)

However, if the energy spread could be reduced by a factor of 5, the luminosity per point would be reduced to 1.2 pb^{-1} and a scanning region of 20 MeV (the estimated uncertainty of model predictions) could be covered, with an integrated luminosity of 4 pb^{-1}.

8. **SUMMARY AND CONCLUSIONS**

In the previous sections we have described the theoretical predictions for quark-antiquark bound states at LEP energies, and we have analysed which aspects of toponium physics appear experimentally feasible given the luminosity and beam spread of LEP. When we began our studies it was clear that toponium was an ideal laboratory for the standard model, which could probe strong *and* electro-weak interactions at a comparable strength. It was not clear, however, whether toponium physics could be realistically carried out at LEP. Indeed, as one sees from Fig. 2.16, a toponium mass around 80 GeV appears at first sight as the precise prediction of a pessimist: the background is about twice as large as the
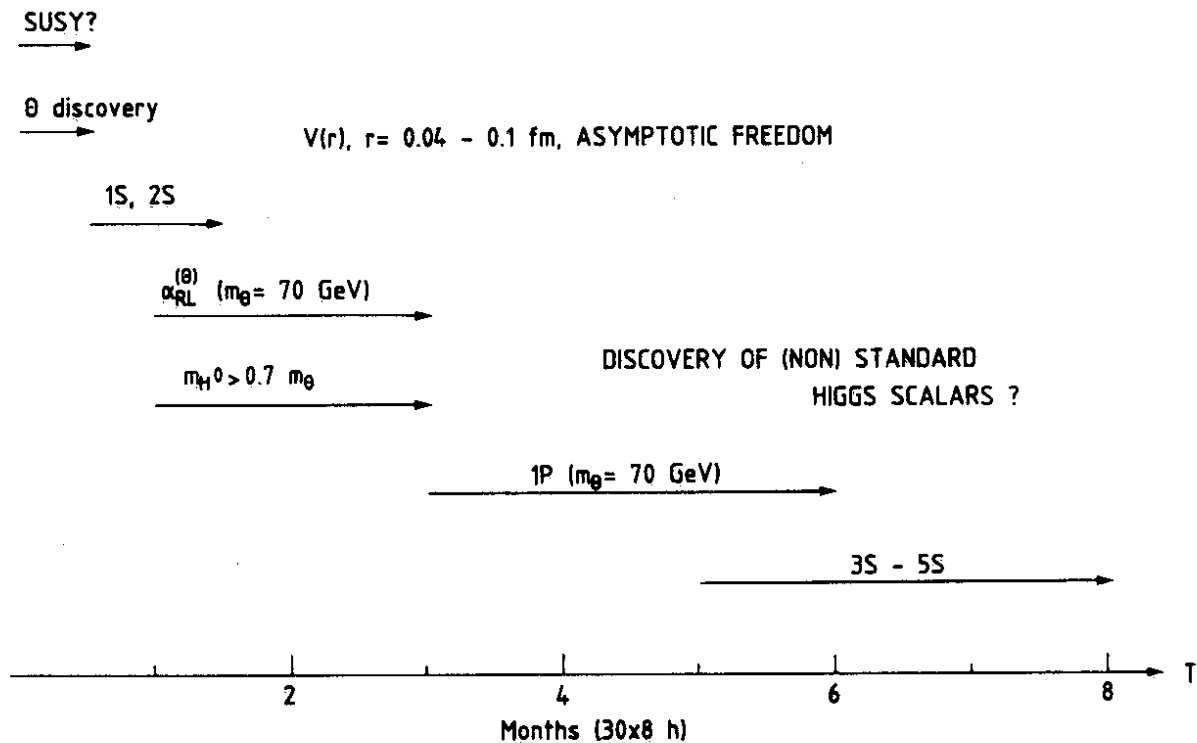
Fig. 8.1 Perspectives for toponium physics at LEP with $m_\theta < m_Z$

signal and the event rates are low. The main result of our quantitative invest-
igation is, however, that an interesting toponium physics program can be carried
out in the whole mass range up to the W-pair threshold.

As discussed in Section 2, a distinction has to be made between three
different regions for the toponium mass m_θ. For $m_\theta \approx m_Z$ the toponium-Z system
with all its interferences has to be treated as a whole, i.e. toponium physics
and Z physics are the same subject. For the case where $m_\theta < m_Z$, our results are
summarized in Fig. 8.1. We expect that Z decays into $t\bar{t}$ pairs will allow a
determination of the t-quark mass with an accuracy of about 500 MeV which would
restrict the size of the scanning interval in the toponium search to approxi-
mately 2 GeV. The toponium ground state could then be established as a 3σ
effect within two weeks. A further month would be required to determine the
1S-2S mass difference and the 1S and 2S leptonic widths (Section 3). These
measurements will determine the quark-antiquark potential down to a distance of
0.04 fm, which should provide direct evidence of asymptotic freedom. The
measurement of the single-quark decay rate will lead to a determination of the
top-quark lifetime. The observation of higher radial excitations and P-states
is more difficult. The determination of the 3S- to 5S-states and of the
1P-states will require about three months each for $m_\theta \approx 70$ GeV (Section 3).

Heavy-quark states are particularly well suited to the search for Higgs particles. One month of running time on the 1S-state is expected to yield a lower bound on the Higgs mass of $m_H^0 > 0.7m_\theta$ (Section 5), or the discovery of the standard Higgs scalar or of a non-standard one. Within a second month the mass bound could be improved by 5 GeV. Two months are also required in order to measure the polarization asymmetry $\alpha_{RL}^{(\theta)}$ with an uncertainty of 0.1 (Section 4). An interesting candidate for 'new physics' is supersymmetry. If the mass spectrum of the new SUSY particles is such that a two-body decay into two scalar t-quarks or two gluinos is kinematically allowed, the discovery of toponium will simultaneously provide evidence of supersymmetry owing to the qualitative change in the decay branching ratios. If two-body SUSY decays are forbidden, the search for SUSY particles, such as a heavy gluino, in toponium decays will be difficult although not impossible (Section 6).

In the case $m_\theta > m_Z$, toponium physics will be more difficult owing to the decrease of the production cross-section and the increase of the energy spread; yet it appears feasible up to about 150 GeV. For $m_\theta = 130$ GeV, for instance, our results are shown in Fig. 8.2. We expect that the scan for the ground state and the determination of the parameters of the 1S- and 2S-states will require two and three months respectively (Section 3). A lower bound on the Higgs mass of 80 GeV can presumably be achieved within five months (Section 5). We emphasize

SUMMARY, $m_\theta \sim 130$ GeV

SUSY?

V(r), r= 0.04 - 0.1 fm,
ASYMPTOTIC FREEDOM

θ discovery

1S, 2S

DISCOVERY OF (NON) STANDARD

HIGGS SCALARS ?

Higgs search, $m_H^0 < 80$ GeV

2   4   6   8   10
Months (30x8 h)

Fig. 8.2 Perspectives for toponium physics at LEP with $m_\theta \approx 130$ GeV

that the main goals of toponium physics--the test of asymptotic freedom, the efficient search for Higgs scalars, and the measurement of the electroweak couplings of t-quarks--can still be achieved.

Our discussion in Sections 3 to 6 has been based on the current estimates of luminosity and beam spread at LEP. As illustrated in Section 7, a decrease of the energy spread or the optimization of the luminosity/beam-spread ratio would be of great value for toponium physics.

Toponium physics at LEP energies is complementary to Z^0 physics. The toponium spectroscopy will test the idea of asymptotic freedom, and toponium decays are the best way to search for Higgs scalars. Both goals can be achieved at LEP for toponium masses below and above the Z^0 mass.

Acknowledgements

REFERENCES

[1] J.J. Aubert et al., Phys. Rev. Lett. **33** (1974) 1404.
   J.-E. Augustin et al., ibid., 1406.
   G.S. Abrams et al., ibid., 1453.

[2] S.W. Herb et al., Phys. Rev. Lett. **39** (1977) 252.
   W.R. Innes et al., ibid, 1240.

[3] P. Schacht, Proc. 22nd Int. Conf. on High-Energy Physics, Leipzig, 1984, eds. A. Meyer and E. Wieczorek (Inst. f. Hochenergiephysik, Berlin-Zeuthen, DDR, 1984), p. 196.

[4] G. Arnison et al., Phys. Lett. **147B** (1984) 493.

[5] J. Ellis and M.K. Gaillard, CERN 76-18 (1976) and 79-01 (1979).

[6] J.H. Kühn, Acta Phys. Polon. **B12** (1981) 347.

[7] W. Buchmüller, Proc. Cornell Z^0 Theory Workshop, 1981, eds. M.E. Peskin and S.-H.H. Tye (CLNS 81-485, Cornell, 1981), p. 210.

[8] J.P. Leveille, ibid, p. 241.

[9] J.H. Kühn, Acta Phys. Austriaca, Suppl. **XXIV**, 23 (1982).

[10] J.D. Jackson, S. Olsen and S.-H.H. Tye, Proc. 1982 Summer Study on Elementary Particles and Fields, Snowmass, eds. R. Donaldson et al. (Amer. Inst. Phys., New York, 1983), p. 175.

[11] L.M. Sehgal, Aachen preprint PITHA 83-9 (1983).

[12] A. Martin, preprint CERN-TH.4060 (1984).

[13] E. Eichten, Fermilab-Conf.85/29-T (1985).

[14] J.H. Kühn, Proc. 5th Moriond Workshop on Flavour Mixing and CP Violation, La Plagne, 1985, ed. J. Tran Thanh Van (Editions Frontières, Gif-sur-Yvette, 1985), p. 91.

[15] E. Eichten et al., Phys. Rev. D17 (1979) 3090, and D21 (1980) 203.

[16] J.L. Richardson, Phys. Lett. 82B (1979) 272.

[17] H. Krasemann and S. Ono, Nucl. Phys. B154 (1979) 283.

[18] W. Buchmüller, G. Grunberg and S.-H.H. Tye, Phys. Rev. Lett. 45 (1980) 103 and 587 (E).

[19] C. Quigg and J.L. Rosner, Phys. Lett. 71B (1977) 153.

[20] A. Martin, Phys. Lett. 100B (1981) 511.

[21] W. Buchmüller and S.-H.H. Tye, Phys. Rev. D24 (1981) 132.

[22] G. Bhanot and S. Rudaz, Phys. Lett. 78B (1978) 119.

[23] C. Quigg and J.L. Rosner, Phys. Lett. 72B (1978) 462.

[24] S. Güsken, J.H. Kühn and P.M. Zerwas, Nucl. Phys. B262 (1985) 393.

[25] J.H. Kühn and S. Ono, Z. Phys. C21 (1984) 395, and C24 (1984) 404 (E).

[26] D.W. Duke and R.G. Roberts, Phys. Rep. 120 (1985) 275.

[27] For a recent review and references, see: W. Buchmüller, Proc. Int. School of Exotic Atoms: Fundamental interactions in low-energy systems, Erice, 1984, eds. P. Dalpiaz, G. Fiorentini and G. Torelli (Plenum Publishing Corporation, New York, 1985), p. 233.

[28] E. Remiddi, Proc. Workshop on Physics at LEAR, Erice, 1982, eds. U. Gastaldi and R. Klapisch (Plenum Press, Inc., New York, 1984), p. 711.

[29] L.M. Sehgal and P.M. Zerwas, Nucl. Phys. B183 (1981) 417.

[30] Particle Data Group, Review of Particle Properties, Rev. Mod. Phys. 56 (1984) S43.

[31] Y.P. Kuang and T.M. Yan, Proc. Cornell Z^0 Theory Workshop, 1981, eds. M.E. Peskin and S.-H.H. Tye (CLNS 81-485, Cornell, 1981), p. 292.

[32] F.M. Renard, Z. Phys. C1 (1979) 225.

[33] J.H. Kühn and P.M. Zerwas, Phys. Lett. 154B (1985) 448.

[34] P.J. Franzini and F.J. Gilman, Phys. Rev. D32 (1985) 237.

[35] L.J. Hall, S.F. King and S.R. Sharpe, Nucl. Phys. B260 (1985) 510.

[36] A. Martin, Phys. Lett. 156B (1985) 411.

[37] J.D. Jackson and D.L. Scharre, Nucl. Instrum. Methods 128 (1975) 13.

[38] J.M. Jowett, preprint CERN LEP TH 85-04 (1985).

[39] F.A. Berends, R. Kleiss and S. Jadach, Nucl. Phys. B202 (1982) 63; Comput. Phys. Commun. 29 (1983) 185.

[40] A. Ali et al., this report.

[41] S. Güsken, J.H. Kühn and P.M. Zerwas, Phys. Lett. 155B (1985) 185.

[42] A.I. Akhiezer and V.B. Berestetzky, Quantum electrodynamics (Interscience, New York, 1965).

[43] A. Ali, Z. Phys. C1 (1979) 25.

[44] M. Gourdin, Paris preprint LPTHE 78-17 (1978).

[45] J.H. Kühn, Nucl. Phys. B237 (1984) 77.

[46] See, for instance, J.M. Izen, preprint DESY 84-104 (1984).

[47] J.H. Kühn, A. Reiter and P.M. Zerwas, preprint SLAC-PUB-3746 (1985).

[48] G. Goggi and G. Penso, Nucl. Phys. B165 (1980) 429.

[49] S. Brandt et al., Phys. Lett. 12 (1964) 57.
     E. Farhi, Phys. Rev. Lett. 39 (1977) 1587.

[50] D. Barber et al. (Mark J Collaboration), Phys. Rev. Lett. 43 (1979) 830.

[51] For more details, see: D. Boutigny, Annecy thesis (to appear).

[52] L3 report to LEP Committee, 14 June 1982: Answer to question 4.

[53] I.Y. Bigi, J.H. Kühn and H. Schneider, preprint MPI-PAE/PTh 28 (1978).

[54] J. Bernabeu and P. Pascual, Phys. Lett. 87B (1979) 69, and Nucl. Phys. B172 (1980) 93.

[55] R. Koniuk, R. Leroux and N. Isgur, Phys. Rev. D17 (1978) 2915.

[56] R. Budny, Phys. Rev. D20 (1979) 2763.

[57] G. Altarelli et al., this report.

[58] A. Martin, unpublished.

[59] J.H. Kühn and K.H. Streng, Nucl. Phys. B198 (1982) 71.

[60] I.Y. Bigi and H. Krasemann, Z. Phys. C7 (1981) 127.

[61] B. Grzadkowski, P. Krawczyk, J.H. Kühn and R.G. Stuart, preprint CERN-TH.4226 (1985), to be published in Phys. Lett.

[62] G. Barbiellini et al., preprint DESY 79/27 (1979).

[63] For a recent investigation, see J. Ellis et al. (Study group on new particles), this report.

[64] F. Wilczek, Phys. Rev. Lett. 39 (1977) 1304.

[65] M.I. Vysotsky, Phys. Lett. 97B (1980) 159.

[66] J. Ellis et al., preprint CERN-TH 4143/85 (1985).

[67] H.E. Haber and G.L. Kane, Phys. Rep. 117 (1985) 75.

[68] H.P. Nilles, Phys. Rep. 110 (1984) 1.

[69] J.H. Kühn, preprint CERN-TH.4083 (1984), to be published in Acta Phys. Polon.

[70] J. Ellis and S. Rudaz, Phys. Lett. 128B (1983) 248.

[71] B.A. Campbell, J. Ellis and S. Rudaz, Nucl. Phys. B198 (1982) 1.

[72] G. Köpp, J.H. Kühn and P.M. Zerwas, Phys. Lett. 153B (1985) 315.

[73] B.A. Campbell, J.A. Scott and M.K. Sundaresan, Phys. Lett. 131B (1983) 213.

[74] J.H. Kühn, Phys. Lett. 141B (1984) 433.

[75] W.Y. Keung, Phys. Rev. D28 (1983) 1129, and D29 (1984) 1544 (E).

[76] J. Wess, in Quantum Theory of Particles and Fields (Birthday volume
     dedicated to Jan Lopuszanski, eds. B. Jancewiz and J. Lukierski, World
     Scientific Publishers, Singapore, 1983), p. 223.

     S. Samuel and J. Wess, Nucl. Phys. B221 (1983) 153.

[77] O. Nachtmann, A. Reiter and M. Wirbel, Z. Phys. C23 (1984) 85.

[78] G. Fontaine, Thèse d'Etat 1973 (Orsay No. 1110), p. 245.

[79] A. Renieri, Frascati preprint INF-75/6(R) (1975).

     A.A. Avdienko et al., Proc. 12th Int. Conf. on High-Energy Accelerators,
     Batavia, 1983 (FNAL, Batavia, Ill., 1984), p. 186.

     K. Wille and A.W. Chao, preprint SLAC-AP 32 (1984).

[80] LEP Experiments Committee, CERN/LEPC/85-26 (1985); J.M. Jowett, CERN LEP
     Note 544 (1985).

[81] J. Kaplan and J.H. Kühn, Phys. Lett. 78B (1979) 252.

[82] R. Gatto, Proc. General Meeting on LEP, Villars-sur-Ollon, 1981 (ECFA
     81/54, CERN, Geneva, 1981), p. 1.

[83] P.B. Mackenzie and G.P. Lepage, Phys. Rev. Lett. 47 (1981) 1244.

[84] S.J. Brodsky, G.P. Lepage and P.B. Mackenzie, Phys. Rev. D28 (1983) 228.

[85] W. Buchmüller, Y.J. Ng and S.-H.H. Tye, Phys. Rev. D24 (1981) 3003.

[86] R. Barbieri, R. Gatto and E. Remiddi, Phys. Lett. 106B (1981) 497.

[87] S.N. Gupta, S.F. Radford and W.W. Repko, Phys. Rev. D26 (1982) 3305.

<u>APPENDIX</u>

Our calculation of branching ratios of toponium decays was based on the tree-level formulae of Section 2. For ratios of the partial widths of annihilation decays, the first-order QCD radiative corrections have been computed. They read as follows:

Three-gluon decay [see (2.16)] [83, 84]:

$$r_{ggg} = \frac{10(\pi^2-9)}{81\pi} \frac{\alpha^3_{\overline{MS}}(m_\theta)}{\alpha^2_{em} e^2_t} \left\{ 1 + \frac{\alpha_{\overline{MS}}(m_\theta)}{\pi} [2.770(7) \beta_0 - 14.0(5)] + \dots \right\} . \quad (A.1)$$

Two-gluon photon decay [see (2.17)] [83, 84]:

$$r_{gg\gamma} = \frac{8(\pi^2-9)}{9\pi} \frac{\alpha^2_{\overline{MS}}(m_\theta)}{\alpha_{em}} \left\{ 1 + \frac{\alpha_{\overline{MS}}(m_\theta)}{\pi} [2.770(7) \frac{2}{3}\beta_0 - 11.8(4)] + \dots \right\} ; \quad (A.2)$$

$\alpha_{\overline{MS}}(\mu)$ and β_0 depend on the number of light quark flavours:

$$\beta_0 = 11 - \frac{2}{3} n_f , \quad (A.3)$$

$$\alpha_{\overline{MS}}(\mu) = \frac{4\pi}{\beta_0 \ln \mu^2/\Lambda^2_{\overline{MS}}} - \frac{4\pi\beta_1}{\beta^3_0} \frac{\ln \ln (\mu^2/\Lambda^2_{\overline{MS}})}{\ln^2 (\mu^2/\Lambda^2_{\overline{MS}})} , \quad (A.4)$$

$$\beta_1 = 102 - \frac{22}{3} n_f . \quad (A.5)$$

Higgs photon decay [see (2.18)] [65]:

$$r_{H^\theta\gamma} = \frac{1}{2x} \frac{m^2_\theta}{m^2_W} \left(1 - \frac{m^2_{H^0}}{m^2_\theta}\right) \left[1 - \frac{4}{3} \frac{\alpha_s}{\pi} a(\kappa)\right] , \quad x = 4 \sin^{-2} \theta_W , \quad (A.6)$$

$$a(\kappa) = - \frac{\pi^2}{12(1-\kappa)} - \frac{F(1-2\kappa)}{2(1-\kappa)} + \frac{\kappa-1}{1-2\kappa} + \frac{2\kappa(\kappa-2)}{(1-\kappa)^2} [\phi(\kappa) + F(1) - F(-1)]$$

$$+ \left(4 + \frac{4}{\kappa} + \frac{8}{1-\kappa}\right) \left(\frac{\kappa}{1-\kappa}\right)^{1/2} \arctan \left(\frac{\kappa}{1-\kappa}\right)^{1/2}$$

$$+ \left[2 + \frac{4}{1-\kappa} + \frac{\kappa}{(1-2\kappa)^2}\right] \ln 2 + \ln (1-\kappa)] ,$$

where

$$\kappa = \frac{m_H^2 0}{m_\theta^2}$$

$$F(x) = \int_0^x \frac{dy}{y} \ln (1 + y) \, ,$$

$$\phi(\kappa) = \int_0^1 \frac{dy}{y - 1/2 \, \kappa} \ln \frac{1 - 4y \, (1 - y)\kappa}{2y(1 - \kappa)} \; ;$$

the scale of α_s in (A.6) is only determined through the second-order radiative corrections.

The radiative corrections to the hyperfine splitting Δm_{hfs} (2.11) is given by [85-87]:

$$\Delta m_{hfs} (\theta) = \frac{8}{9} \frac{\alpha_{\overline{MS}} (m_t)}{e_t^2 \alpha_{em}^2} \Gamma_0 (\theta)$$

$$\cdot \left[1 + \frac{\alpha_{\overline{MS}} (m_t)}{\pi} \left[- \frac{8}{3} - \frac{3}{4} \ln 2 + \frac{21}{8} \xi + \frac{1}{4} \beta_0 \left(\frac{5}{3} - \xi \right) \right] \right] \, , \quad (A.7)$$

$$\xi = \frac{\langle \ln_t (Q^2/m_t^2) \rangle}{\langle 1 \rangle} \, , \quad \langle 1 \rangle = |\phi\langle 0 \rangle|^2 \; .$$

The expectation values in ξ have to be evaluated with the toponium wave functions.